IMPACT ASSESSMENT OF CLIMATE CHANGE ON GLACIERS AND RUNOFF USING SWAT

A Dissertation

by

NINA OMANI

Submitted to the Office of Graduate and Professional Studies of
Texas A&M University
in partial fulfillment of the requirements for the degree of

DOCTOR OF PHILOSOPHY

Chair of Committee,	Raghavan Srinivasan
Committee Members,	Gerald R. North
	Patricia Smith
	Raghupathy Karthikeyan
Head of Department,	Steve Searcy

August 2014

Major Subject: Biological and Agricultural Engineering

ABSTRACT

A modified incorporated snow algorithm in Soil and Water Assessment Tool (SWAT) was applied to consider spatial variation of associated snow parameters by elevation band for flow simulation of five mountainous river basins with different climatic conditions including the Narayani (Nepal), Vakhsh (Central Asia), Rhone (Switzerland), Mendoza (Central Andes, Argentina), and Central Dry Andes (Chile) with total area of 85,000 km^2. The results by modified snow algorithm implied slight to noticeable improvement in simulation of flow cycles and volume depend on the percentage of glacier area and climatic type of a subbasin.

The ability of model in simulation of glacier mass balance and Equilibrium Line Altitude (ELA) then was evaluated for three reference glaciers and their neighboring glacier ranges across the Europe and central Asia. The modified model successfully simulated the annual glacier loss, mass balance profile and annual ELAs with light calibration efforts and limited data. The results revealed that even very good result in monthly runoff simulation alone does not imply the consistency between simulated and measured mass balances. Calibrating the model versus flow data in combination with data of glaciers considerably reduced the model parameterization uncertainty and enhanced mass balance simulation accuracy.

To assess the range of future climate change impacts on the glacier runoff, we used maximum, minimum air temperature and precipitation projections under two RCPs

(Representative Concentration Pathway) climate change scenarios and six Coupled Model Intercomparison Project-5 (CMIP5) models. Simulations of mean annual and monthly runoff, high (Q5) and low (Q95) monthly runoff and flow duration curves (FDCs) under baseline (1979–2008) and climate change scenarios are presented for all river basins. The variation of ELA related to a moderate climate change scenario then was predicted for a test study area. Therefore, the objectives of this study are:

1. Evaluating SWAT's snow hydrologic component in glaciered basins,
2. Improvement of SWAT snow/ice melt processing,
3. Extending the applied method to macro-scale river basins,
4. Assessing the effect of future climate change on the streamflow volume and seasonal variability with focusing on glaciered areas,
5. Investigating that the global mountainous glaciers will be vanished by 2100.

DEDICATION

This dissertation is dedicated to my parents, Nassrin and Hassan, whose endless love, support and encouragement help me go through difficulties in my life.

ACKNOWLEDGEMENTS

Like virtually all research projects, I would not have been able to finish this work without the help and support of many people. It is also equally true that it is probably not possible to acknowledge every single contribution to this work, but I will do my best to enumerate them.

First, I would like to thank the gentleman who got me started on this work: Dr. Raghavan Srinivasan. He supervised this work and provided much support, ranging from discussion on theory to critiquing the results of the computer simulations to funding.

The other member of my committee, Dr. Raghupathy Karthikeyan from the Department of Biological and Agricultural Engineering, provided me with insightful comments about the methodology. Dr. Gerald R. North and Dr. Patricia Smith were also helpful and particularly generous with their time, and for that I am grateful.

TABLE OF CONTENTS

Page

LIST OF FIGURES

Page

LIST OF TABLES

Page

CHAPTER I

HYDROLOGICAL MODELING OF HIGHLY GLACIERIZED RIVER BASINS

Overview

In this study the physically based hydrologic model, Soil and Water Assessment Tool (SWAT), was used for flow simulation of five river basins that are global in coverage and feature contrasts in climatic conditions. The river basins included the Narayani (Nepal), Vakhsh (Central Asia), Rhone (Switzerland), Mendoza (Central Andes, Argentina), and Central Dry Andes (Chile) with a total area of 85,000 km^2. The model performance was first evaluated for default, non-adjusted melt parameters in the absence of elevation bands. The model took into consideration elevation bands to model precipitation and temperature change with altitude, in the presence and elimination of the glaciers for some of the river basins.

The purpose of this evaluation was to assess the influence of orographic precipitation and temperature lapse rate plus glaciers on flow simulation of river basins under various climatic condition and scale. This also reveals the importance of adjusting the melt parameters with consideration to the hydrologic regime of the ungauged basins. Adding the elevation bands obviously enhanced the model performance in terms of magnitude and variation for Mendoza, Rhone and Nepal, respectively. In absence of elevation bands R^2 range between 0.68 and 0.91 and NSE range from -1.97 to -0.34 for Rhone River Basin, while adding the elevation bands improved the simulation results so

that R^2 and NSE range between 0.78 to 0.95 and -0.19 to 0.93, respectively. PBIAS range also decreased from -62% and -153.6% to -87.7% and -8.2%. The results implied that the model performance in simulation of flow was considerably improved in terms of variation of flow by adding the glacier for all river basins.

Three SWAT snow melt algorithms were then evaluated for melt parameter distribution based on total basin (Method 1), subbasins (Method 2), and subbasin-elevation bands (Method 3) for some of the gauged subbasins. The results by Method3 showed slight to noticeable improvement in simulation of spatial distribution of melt, flow cycles and volume in comparison with Method 2. Method 3 was dependent on the percentage of glacier area, glacier distribution and climatic type of a subbasin. This study is the first to examine the second and third methods of snow melt simulation using the SWAT model.

Introduction

In mountainous regions, snow and glacier melt significantly affect the runoff cycle and volume by storing water over a range of temporal scales (Jansson et al., 2003) and releasing it during dry years. Therefore, the ability of hydrological models to accurately predict runoff from snowy and glaciered watersheds depends on how well the model simulates snow fall, snow/glacier storage and melt. The two basic snow melt approaches generally used in hydrologic modeling are categorized into energy balance models and temperature-index models (Anderson, 1976). Temperature-index models are widely used in hydrological studies due to the models performance, simplicity and

availability of temperature data (Schaper et al., 2000; Moore, 1993; Debele and Srinivasan, 2005).

Despite the simplicity, in temperature-index based runoff models such as SWAT, melt rates only vary as a function of elevation resulting from an air temperature gradient (Hock, 2003). To overcome this weakness, a modified snow process was applied in order to consider spatial variation of snow melt and accumulation parameters by elevation band across each subbasin. In previous studies using SWAT, snow melt and accumulation parameters were held constant for the entire basin (Pradhanang et al., 2011; Wang and Melesse, 2005; Zhang et al., 2008; Stehr et al., 2009; Ahl et al., 2008). Although, this method was successful in simulation of snow melt flow, simulation of runoff from glaciered watersheds demands a distributed model for distinguishing of seasonal snow from glacier.

The new approach allows separating seasonal snow from glaciers based on the vertical (elevation bands) and horizontal variability (subbasins) of associated melt parameters. In this study, three SWAT snow melt algorithms were evaluated based on the degree of melt parameter distribution (basin, subbasin, elevation bands) on a basin scale (Method 1), subbasin scale (Method 2), and subbasin-elevation band scale (Method 3). In Method1, snow melt and accumulation parameters are constant within the basin. In Method 2, snow melt and accumulation parameters are allowed to vary on a subbasin scale. Separating of seasonal snow from glaciers not allowed in this method and it demands very small subbasin divisions to achieve good results. In Method3, snow melt and accumulation parameters are allowed to be spatially variable within the elevation

bands and subbasins; this allowing differentiation between seasonal snow and glaciers. Methods 2 and 3 have not been examined in the previous studies by SWAT.

The three snow process algorithms were examined for their ability to simulate flow in five river basins that provide global assessment and feature contrasts in climatic conditions. The river basins included are the Narayani (Nepal), Vakhsh (Central Asia), Rhone (Switzerland), Mendoza (Central Andes, Argentina), and Central Dry Andes (Chile) with a total area of 85,000 km^2. There is widespread evidence that glaciers are retreating in these regions (Agrawala et al., 2003; Huss et al., 2008; Schäfli et al., 2007; Pellicciotti et al., 2005; Shreshtha and Aryal, 2011; Zemp et al., 2006a; Rafferty, 2011). Major fraction of glacial meltwater is temporarily stored in reservoir lakes and help drive hydropower turbine during dry summers in Rhone River Basin (Schafli et al., 2007). There are some countries, such as Norway and Switzerland that depend almost entirely on hydropower for their various electrical energy needs (Rafferty, 2011). In the Andes, glacial meltwater supports river flow and water supply for tens of millions of people during the long dry season (Pellicciottu et al., 2008). Chile is one of the most urbanized countries in South America and majority of the people lives in central Chile. Increase in the meltwater has already taken place and the glaciers are now in a phase of diminishing contribution to the northern Chilean basins stream flow (Pellicciottu et al., 2008). Nepal also has one of the highest population densities in the world with respect to cultivable land (MOPE 2000). Nepal's economy heavily relies on agricultural products. Nearly 91% of the nation's power comes from hydroelectric power (Agrawala et al., 2003). Any variation in river flow from glacier melt put at risks both hydro power and agriculture.

Therefore, the objectives of this study were to: 1) evaluate SWAT's snow hydrologic component in simulation of streamflow in glaciered basins, 2) improve the model's snow/ice melt processing algorithm, 3) extend the applied method to macro-scale river basins that are global in coverage and vary in climatic condition.

Literature Review

The SWAT model is a semi-distributed, physically based model which was developed to predict the impact of land management practices on water, sediment, and agricultural chemical yields in large complex watersheds (Neitsch et al., 2002). The SWAT model has been applied worldwide, and its hydrologic components have been successfully tested where streamflows were predominantly generated from rainfall events (Arnold et al., 1999; 2000; Di Luzio et al., 2002; Srinivasan et al., 1998).

The model less frequently has been applied in mountainous watersheds and a few recent studies have been conducted to test and improve SWAT's snow hydrology component. Fontaine et al. (2002) incorporated the elevation bands method with the SWAT model's original snowmelt algorithm (temperature-index model), which improved the Nash-Sutcliffe coefficient of monthly runoff simulation from -0.70 to 0.86 in the 4,999 km^2 Rocky Mountain Basin in Wyoming. Debele and Srinivasan (2005) incorporated a modified version of SNOW17 into SWAT and compared its performance with the temperature-index model in three watersheds (ranging from 22.28 to 7,106.82 km^2), the results of which showed that the temperature-index model performed better than the SNOW17 model. Debele et al. (2010) incorporated the distributed process-based energy budget SNOWEB in the pixel and elevation band scales into SWAT and

compared its performance with the temperature-index model. In this method, it was assumed that solar radiation varies not only with latitude and altitude of subbasins, which is applied in the current version of SWAT, but also with land surface inclinations (aspect and slope). The temperature-index based snowmelt computation method had overall model efficiency coefficients ranging from 0.49 to 0.73 in simulation of monthly streamflow while the energy budget based approach had efficiency coefficients ranging from 0.33 to 0.59 only. Zhang et al. (2008) applied SNOW17 in SWAT at the pixel scale. The SWAT model with temperature-index plus elevation bands performed as well as the SWAT model with SNOW17.

One simple and common approach that has been widely used in hydrological models in order to simulate melt water is the Enhanced Temperature-Index Model (ETIM) (Hock, 1999; 2003). This method exhibits significant improvements in model performance when compared with the classical temperature-index approach, with a minimal increase in data requirements (e.g. Hock, 1999; Huss et al., 2008). While distributed, process-based, energy budget models have been tested in SWAT; no studies have been done to incorporate the enhanced temperature-index model to SWAT. This method is advantageous in simulation of melt water from snow and glacier separately when incorporated to a distributed hydrologic model. In this model, spatial and temporal distribution of melt depends on the spatial and temporal variations of the melt factor in terms controlled by solar radiation variations.

Both the SWAT melt model and ETIM simulate the temporal variability of the melt factor. In SWAT, temporal variation of the melt factor is modelled by a sinusoidal

equation and ranges between user defined maximum and minimum melt factor parameters, whereas, in ETIM, the melt factor varies based on the solar radiation variation, which is updated every day.

Solar radiation is spatially varied in the pixel and band scales in recent hydroglacial models (Hock, 2003; Magnusson et al., 2011). The effect of solar radiation variation, with aspect and slope, on snow/glacier driven runoff has been investigated comprehensively in previous studies and no significant improvement was detected in the results (Debele and Srinivasan, 2005; Debele et al., 2010). However, we focused on another component of frequently used glacier/snow melt models. A major difference between SWAT melt processes and the melt routine of hydroglacial models arises from the associated melt parameter distribution (i.e. melt factor). In previous studies using SWAT, associated snow melt parameters were held constant for the entire basin; while, in the hydroglacial models melt factors are spatially variable in pixel or band scales. A common approach is to assign two different melt factors to ice and snow. This enables the user to treat seasonal snow and glaciers separately. It is obvious that there is a range of melt factor values throughout a region depending on snow/ice albedo, density, and climate. Melt factors are generally reported higher for ice (6 to 8) and lower for snow (3 to 5) (Braithwaite, 2008). The approach in this study allows discretization of seasonal snow from glaciers based on vertical (elevation bands) and horizontal (subbasin) variability of the associated melt parameters. The accumulation/melt parameters, including maximum and minimum melt factors, melt lag factor, melt temperature and snow fall temperature can be set for the elevation bands of each subbasin separately.

SWAT's snow hydrology component has been improved in previous studies but no studies have been conducted using macro-scale river basins that are global in coverage while focusing on glaciers. In this study, a modified SWAT model was applied in order to treat the glaciered and unglaciered areas separately.

Methodology

Study Area

This study focuses on areas where climate change has had a strong impact on highly glaciated areas. Five river basins with a total area of 85,000 $km^{2,}$ in the northern and southern hemispheres, for which sufficient information is available, were selected for this study (Figure 1. 1). These river basins have different spatial scale and climatic situations, from extreme maritime to extreme continental climates. They include: Vakhsh in Tajikistan, Narayani in Nepal, Upper Rhone in Switzerland, Mendoza in Argentina, and five individual glaciated watersheds in the central dry Andes of Chile.

Vakhsh River Basin

The Vakhsh, the second largest river in southern Tajikistan, is dominated by the peaks of the Pamir-Alay mountain system and contains numerous glaciers. The largest glacier, the Fedchenko which is northwest of the Pamir Mountains, covers more than 700 km^2 with a mean thickness of 1 km. This is the largest glacier in the world outside of the polar regions. The Vakhsh River Basin contains 2,230 glaciers, according the World Glacier Inventory (WGMS, 1989). The area of the Vakhsh River Basin is 39,100 km^2, located at a height ranging from 1,100 to 7,450 m with a mean elevation of 3,500 m.

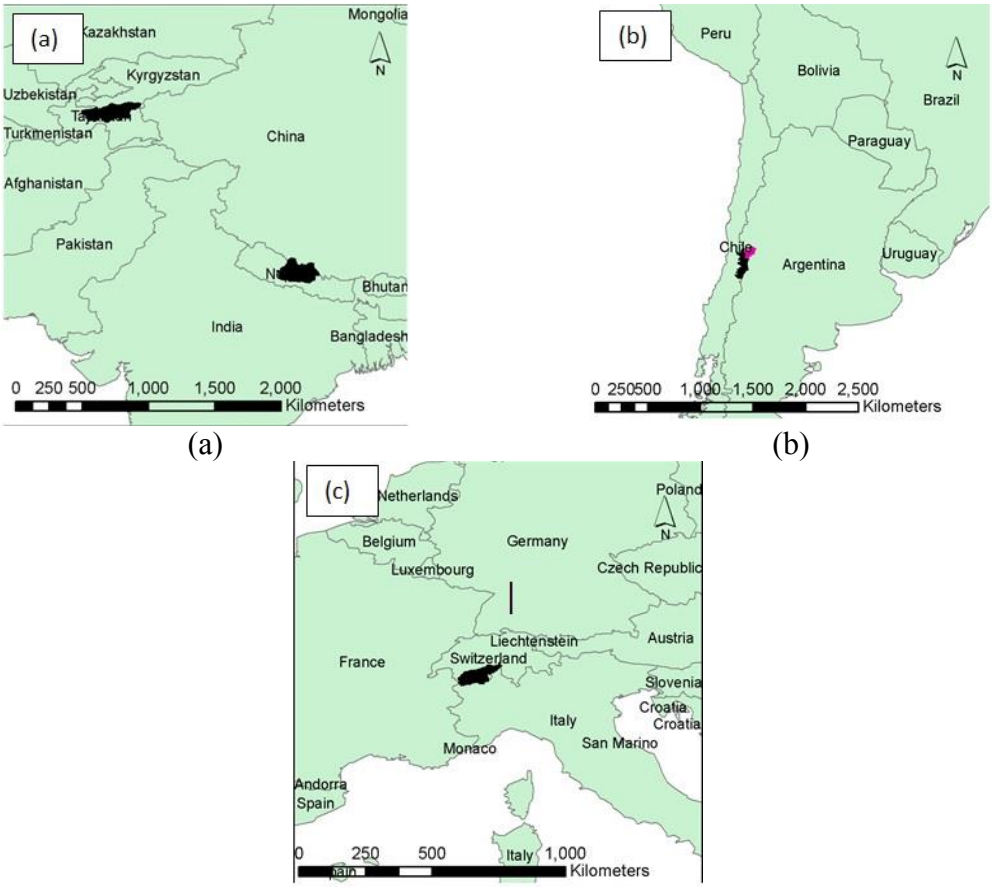

Figure 1. 1. The geographic position of the five river basins used in this study: (a) Vakhsh and Narayani, (b) Mendoza (red) and Central Chile (black) ,(c) Upper Rhone

The climate is continental, with considerable seasonal fluctuations in temperature and precipitation. Monthly average air temperature ranges between -14 °C in January to 7 °C in July, and annual temperature varies between –10 °C in high altitudes to 4 °C at lower altitudes (CFSR/NCEP Reanalysis data from 1979 to 2007). The average annual precipitation ranges between 300 mm at 1500 to 2500 m.s.l. and 1600 mm at 3500-4500 m.s.l. (NCEP, 1979-2007). The heaviest precipitation falls in the south of the river basin

where the Fedchenko glacier is located, while the lightest is in the north and northeast on the border with Kyrgyzstan. Most precipitation occurs in winter and spring.

Measurements at Obikhingou-Tavildara, one of the major glacier-fed tributaries of Vakhsh, indicate that winter flow rates averaged around 25 m^3/s, whereas flow rates during the summer months exceeded 400 m^3/s for available data period (1981 to1985) (Figure 1. 2). The flow rates have great seasonal variability between winter and summer, since the Vakhsh is a snow and glacier-fed river.

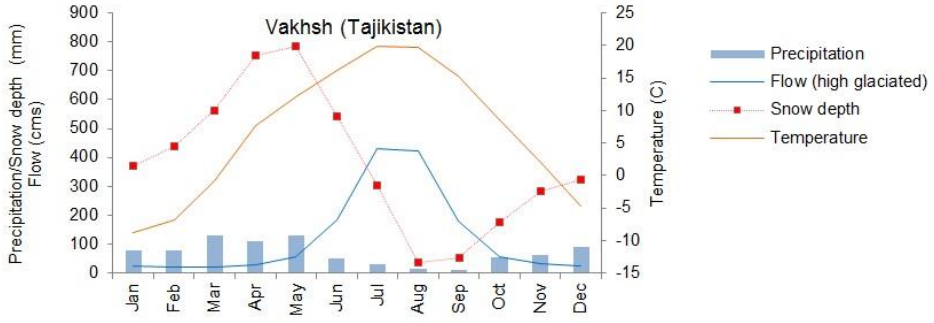

Figure 1. 2. A typical pattern of mean monthly flow (1981-1985), precipitation, temperature and snow depth (1979-2007) at Obikhingou-Tavildara, Vakhsh River Basin.

Narayani River Basin (Nepal)

The Narayani River Basin is the second largest in Nepal. It lies in center of Nepal covering an area of 31,890 km^2 and ranges from the higher Himalayas with at an elevation of 8,143 m to 181 m in the plains.

The climate is alpine and the snowline lies at 5,000 m in the east and at 4,000m in the west. Monthly average air temperature ranged between -18 °C to -14 °C in high

altitudes to 10 °C to 16 °C in low altitudes in January; and 4 °C to 9 °C in high altitudes to 23 °C to 31 °C in low altitudes in July (1979-2007). Annual temperature varies between -7 °C to 0 °C in high altitudes to 18 °C to 26 °C at lower altitudes (1979-2007).

Monsoon precipitation occupies 70 to 85 percent of total precipitation depending on the location (Singh, 1985; Ives and Messerli, 1989). Mean annual precipitation ranges from 2,000-4,000 mm at low altitudes (500-1,500m) and declines to 200-500 mm at high altitudes (3,000 m and higher) (Figure 1. 3). The Himalayan mountain range lies to the northeast and northwest of the river basin and is therefore restricted to monsoon moisture, resulting in a dry climate. Headstreams maintain substantial flows from glacial melt through the hot, droughty spring before the summer monsoon (mid-June to late September).

Summer snow fall in the high altitude plays an important role in the nourishment of glaciers, most of which are of the summer accumulation type in central and eastern Nepal. The timing of maximum runoff coincides closely with the monsoon precipitation with the peak in August and minimum runoff occurs in winter season (Figure 1. 3).

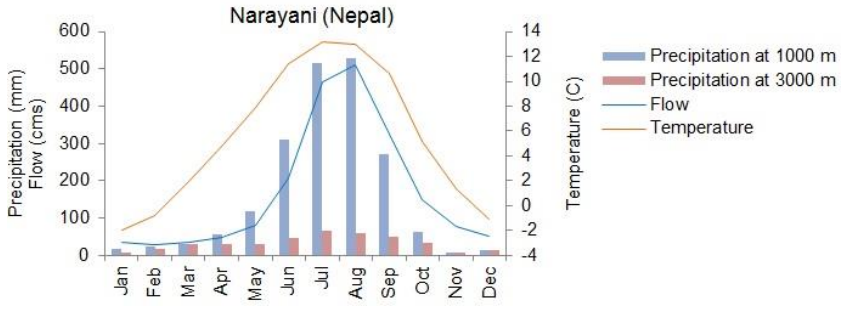

Figure 1. 3. A typical pattern of mean monthly flow (1985-1993), precipitation, temperature (1979-2007) at Narayani River Basin.

Mendoza River Basin (Central Andes - Argentina)

The Mendoza River Basin is located on the eastern slope of the Andes Mountain (-32.2º, -33.4º) and covers 7,090 km^2 with a mean elevation of 3,540 m (ranging between 1,420 m and 6,930 m). Between -28º and -38°, permanent snow and ice occur above 5,500 to 6,000 m. The snow line lies at 4,600 to 4,700 m from higher latitudes and gradually lowers southwards to 3,300 m (Rabassa and Clapperton, 1990). Climate depends on altitude, corresponding to a Tundra climate between 2,700 and 4,100 m.s.l., and to a Polar climate at higher elevations above 4,100 m.s.l. (Moreiras et al., 2012). In high altitudes (over 3,000 m), monthly average air temperature ranges between -6 °C in August to 6 °C in January (NSFR/NCEP Reanalysis data for 1979-2010). Mean annual precipitation reaches about 500 mm in the highest altitudes and less than 200 mm in low altitudes.

Above average winter precipitation anomalies generally coincide with El Niño events, and below-average winter precipitation anomalies are more likely to occur during La Niña years (Vargas and Compagnucci, 1985). The rivers are fed by the melting of snow or glacial ice during the warmer season (December–February) and flow increases with snow melting (Figure 1. 4-a, b). In the figure, the mean monthly precipitation flow and precipitation at the main outlet of the river basin and one of the headwater watersheds (Polvareda) have been presented. These stream flows are sensible to variations of El Niño Southern Oscillation (ENSO) linked to above/below average snow accumulation (Masiokas et al., 2010).

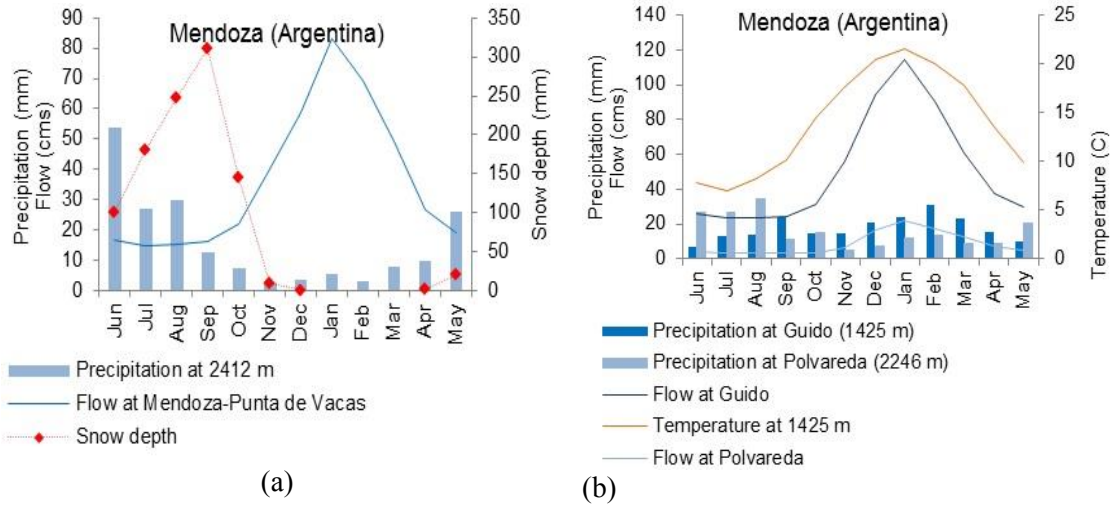

(a) (b)

Figure 1. 4. a) A pattern of mean monthly flow with snow depth changes at Punta de Vacas, Mendoza b) Mean monthly precipitation and flow in Guido in compare of Polvareda.

Central Dry Andes (Chile)

The fourth study area is a 290-km long section of the Chilean Dry Andes and covers 14,342 km^2. The river basins are located on the western slope of the Andes Mountain in southwestern South America (32.4º S, 35.0º S) (Figure 1. 1) with a mean elevation of 2,676 m (ranges between 415 m and 6,560 m). At these latitudes, the existence of numerous peaks at 3,000 to 4,000 m and higher altitudes (0 ºC isotherm) allow the development of important glaciered areas (Rivera et al., 2000).

Mean annual temperature is 15 ºC to 18 ºC in low altitude and decreases to -3 °C at 4,000 m and higher (NSFR/NCEP Reanalysis data from 1979 to 2010). Mean annual precipitation ranges from 200 mm to 600 mm in lower elevations and higher elevations, respectively, in the north (32.4° S) to 500 to 1,000 mm further south at around 35° S (NSFR/NCEP Reanalysis data from 1979 to 2010). The maximum precipitation occurs

in the winter months with a peak in June. In the upper part of the basin above 1,000 m, runoff starts to increase from late October when the snow pack starts to melt and reaches a peak in the summer (Figure 1. 5-a), the time of maximum water demand. This inverse pattern, with maximum runoff corresponding to minimum precipitation is a result of glaciers and snow melt (Figure 1. 5-b).

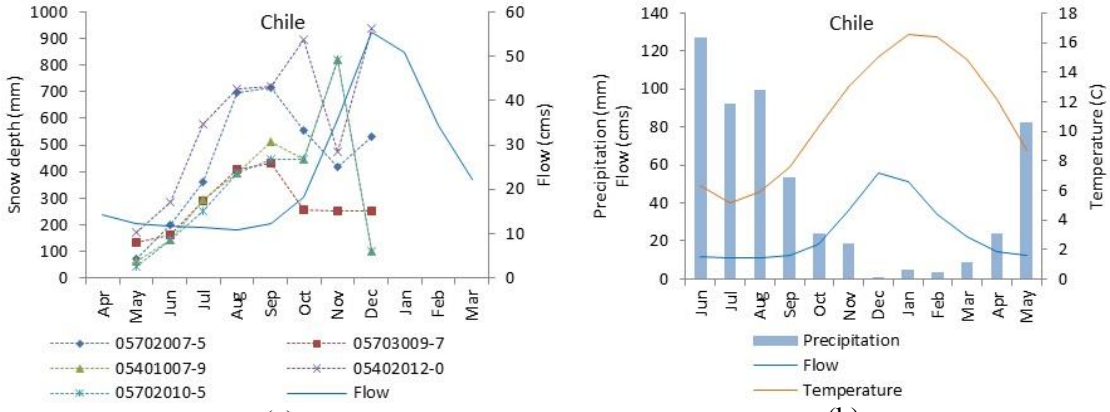

(a) (b)

Figure 1. 5. a) Streamflow starts to increase from late October when the snow pack starts to melt at high altitudes over 1,000 m b) Maximum flow corresponding to minimum precipitation is a result of glaciers and snow melt.

Rhone River Basin

The Upper Rhone River Basin is a highly mountainous area located in central Alps, south of Switzerland, with the drainage area of 3,728 km^2 to the Branson gauge station and altitudes between 440 m to 4,550 m with a mean of 2,196 m. The river basin has a relatively dry continental climate. The glaciers cover about 10 percent of the area and have a significant role in the hydrological regime of the upper Rhone. Mean annual

precipitation varies from less than 600 mm on the plains and to more than 2,500 mm in mountains. The snow-glacial regime is characterized by low discharge in winter and high discharge in summer (Figure 1. 6-a). The importance of the glacier within the basin is high, since in over 50% of the basin, precipitation falls in the form of snow. The glacier melt water postpones the peak flow to late summer, in comparison with maximum peak flow of a glacier free subbasin in late spring (Figure 1. 6-b).

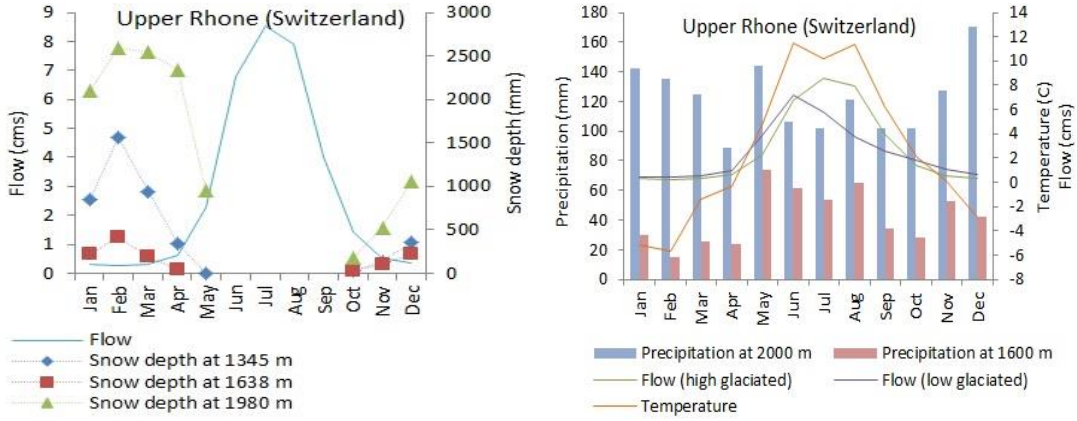

(a) (b)

Figure 1. 6. a) A snow-glacial regime b) The glacier meltwater postpones the peak flow to the late summer in compare with maximum peak flow of glacier free subbasin at late spring.

Data

Glacier Data

Glacier covered areas and thicknesses were extracted from the Global Land Ice Measurements from Space (GLIMS) (Raup et al., 2000; Armstrong et al., 2010) dataset and World Glacier Inventory (WGI). The inventory entries are based upon a single

observation in time. For a few glaciers, mean thickness values are available from extrapolated field measurements. If the GLIMS dataset did not completely cover the entire study area it was complemented with glaciated area by the Moderate Resolution Imaging Spectroradiometer (MODIS) maximum snow extent product (MOD10A2) with 8-day composites at 500-m resolution. The minimum snow cover area at the end of the melting season, from February 2002 to 2010, was considered to be the glacier/permanent snow cover area (Figure 1. 7). Figure 1. 8 a-e show the area of glaciers in this study. The calculated areas of glaciers are presented in Table 1. 1. It is assumed that GLIMS glacier outlines represent the glacial extent at the end of the reference period, as a starting point for the future simulations of glacial extent. From this dataset the thickness of glaciers is also extracted if available.

Table 1. 1. The calculated area of glaciers using GLIMS, MODIS and modeled glaciers area in this study.

	Total area (km^2)	GLIMS	MODIS	Modeled area (This study)
Narayani	31698	9.20	7.32	11
Vakhsh	28907	9.66	13.1	12.3
Upper Rhone	4513	13.61	13.36	14.2
Mendoza	7092	-	4.34	4.25
Central Chile	14342	-	4.35	4.37

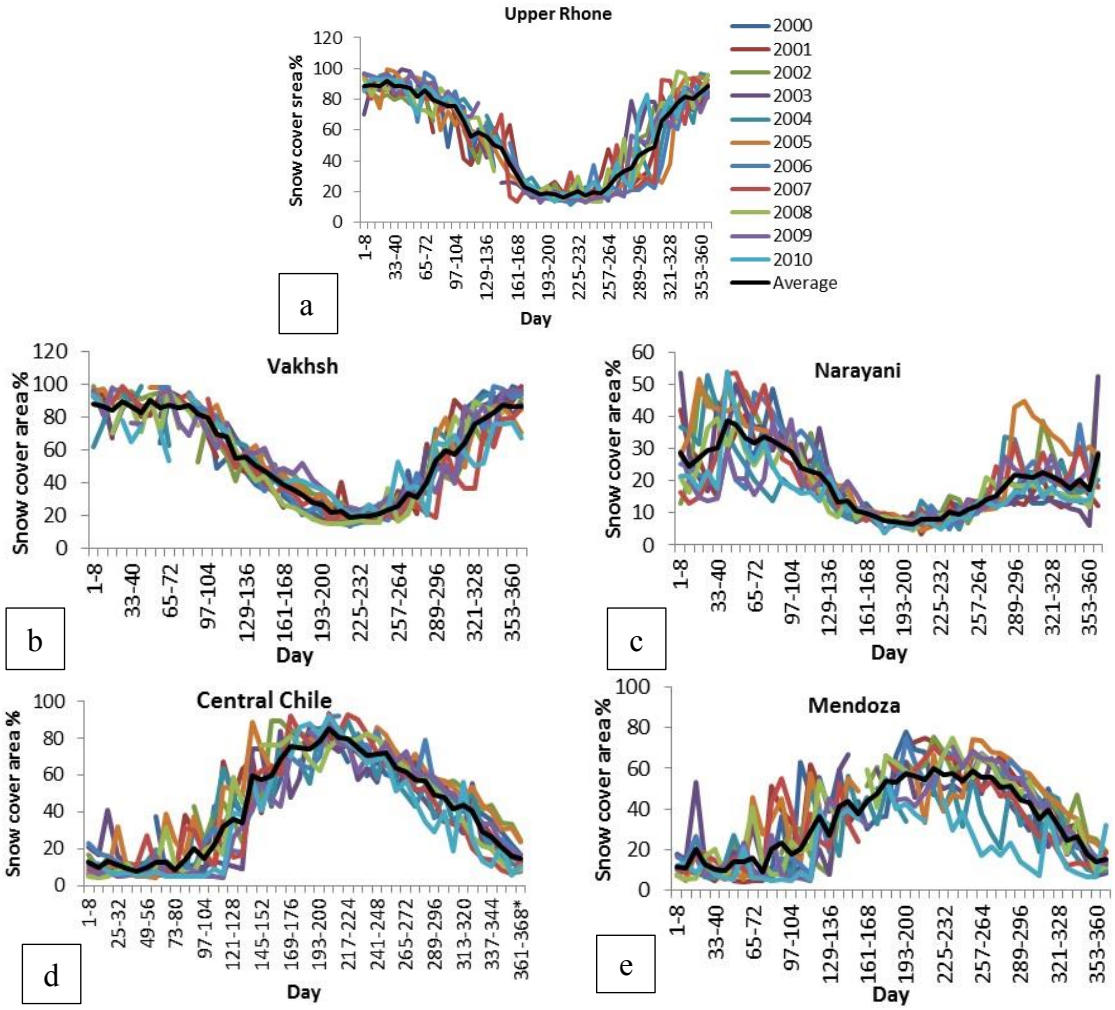

Figure 1. 7. Eight-day snow cover area variations extracted from MODIS products (MOD10A2) from 2000 to 2010 is represented as a percentage of total area of a river basin: a) Upper Rhone b) Vakhsh c) Narayani d) Central Chile e) Mendoza.

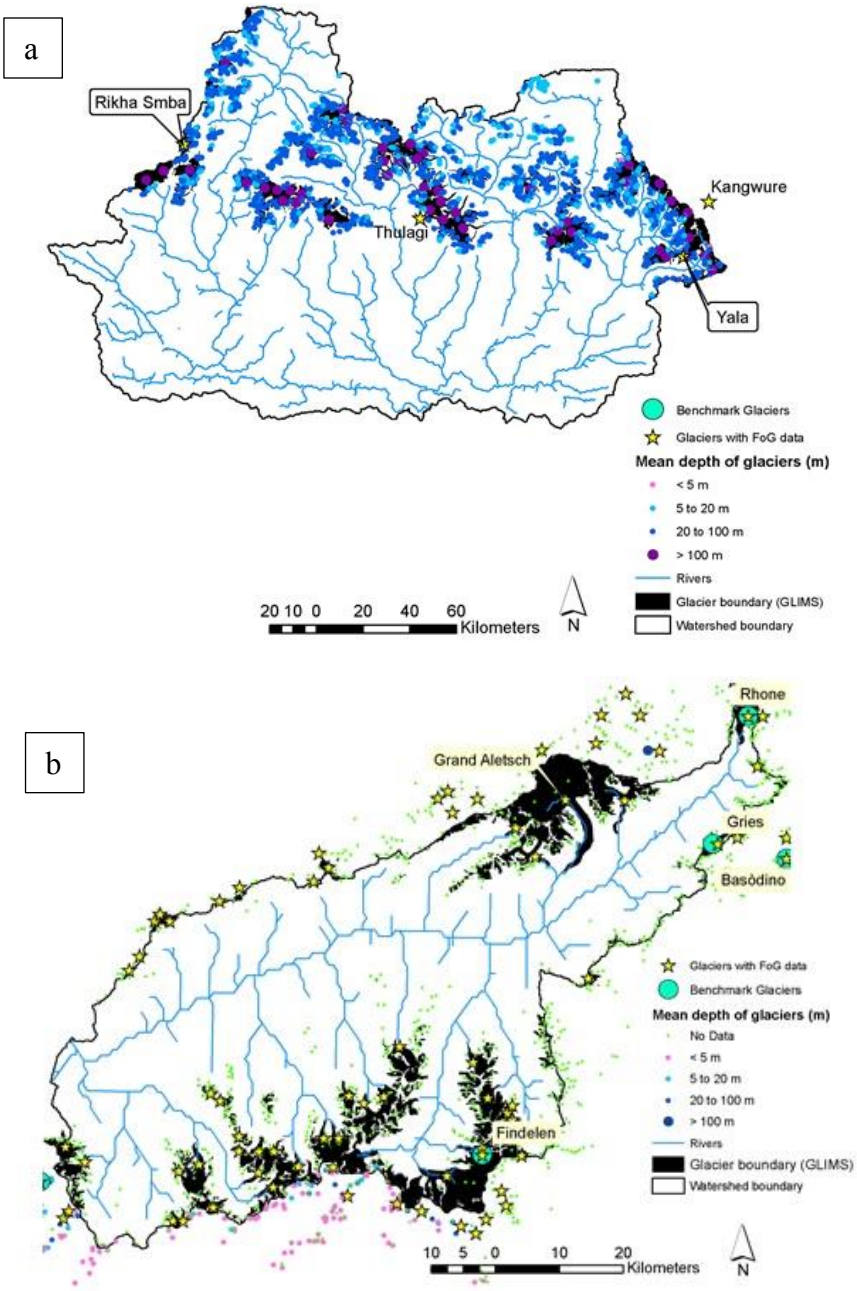

Figure 1. 8. Contribution of glacier snow depth and area; a,b) Glaciers across the Narayani and Rhone River Basins extracted from the GLIMS glacier outlines; c,d,e)The minimum snow cover area from MOD10A2 at end of the melting season from February 2002 to 2010 was considered as glacier/permanent snow cover for Mendoza, Central Chile, and part of Vakhsh River Basins. Green dots show the location of glaciers with no depth information.

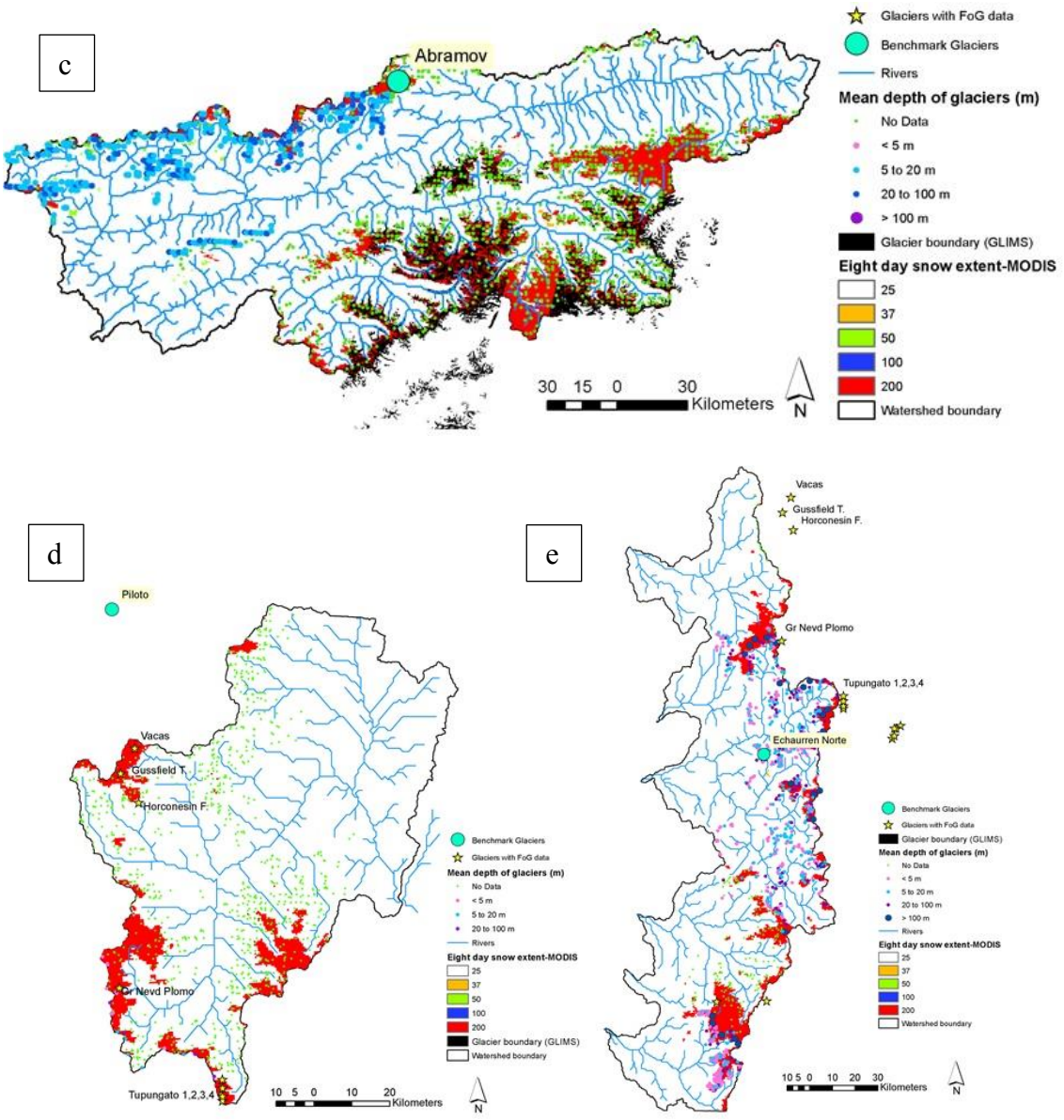

Figure 1. 8. Continued

Digital Elevation Model (DEM)

For this study, 90m Shuttle Radar Topography Mission (SRTM) contributed by USGS/NASA was used as a source for DEM to describe topographic conditions such as

slope and slope length, create flow direction, accumulated flow, and delineate watershed boundaries and channel networks (Neitsch et al., 2002).

Land Use

Land use information was adopted from the USGS Global Land-Cover Characteristics (GLCC). GLCC was developed using satellite data collected from 1992 to 1993 with 1 km spatial resolution for the entire globe (Brown et al., 1993).

Percentages of each land use for total area of watershed and drainage area of gauged subbasins are summarized in Table 1. 2. The dominant land cover in most watersheds is rangeland. In the Vakhsh and Mendoza Watersheds bare land, including glaciers and rock in the upper subbasins is dominant. Forests, which rank second in the Upper Rhone and Narayani, can be found in the mid-altitude areas.

Table 1. 2. Land use categories in each river basin as determined by the USGS.

	Subbasin#	Agricultural	Bare land /glacier/rock	Forest (Deciduous)	Forest (Evergreen)	Forest (Mixed)	Rangeland (brush)	Rangeland (grass)	Water (river & lake)	Pasture	Urban
Vakhsh	72	0.03	75.51	0.00	0.00	0.10	21.62	2.74	0.00	0.00	0.00
	133	12.03	32.66	0.00	0.00	1.46	27.53	26.32	0.00	0.00	0.00
	Basin	12.51	29.95	0.00	0.00	1.07	27.28	29.04	0.15	0.00	0.00
Narayani	123	9.50	19.48	4.87	0.00	11.88	42.75	11.38	0.13	0.00	0.00
	133	11.39	25.21	2.92	0.00	7.70	37.64	14.97	0.17	0.00	0.00
	157	19.69	11.42	8.07	0.00	22.75	29.92	8.08	0.08	0.00	0.00
	159	16.29	14.73	5.28	0.00	19.00	32.68	11.94	0.07	0.00	0.00
	122	3.55	23.52	1.76	0.00	10.08	43.60	17.49	0.00	0.00	0.00
	121	40.28	0.13	8.11	0.00	8.69	22.18	20.61	0.00	0.00	0.00
	96	17.25	17.98	3.61	0.00	6.31	34.45	20.41	0.00	0.00	0.00
	131	40.99	0.00	3.61	0.00	41.02	8.64	5.73	0.00	0.00	0.00
	143	21.43	0.13	11.58	0.00	16.88	25.62	24.36	0.00	0.00	0.00
	Basin	16.29	14.73	5.28	0.00	19.00	32.68	11.94	0.07	0.00	0.00

Table 1. 2. Continued

	Subbasin#	Agricultural	Bare land /glacier/rock	Forest (Deciduous)	Forest (Evergreen)	Forest (Mixed)	Rangeland (brush)	Rangeland (grass)	Water (river & lake)	Pasture	Urban
Rhone	2	0.00	65.59	0.00	0.00	0.00	0.00	16.15	0.00	18.26	0.00
	23	0.00	74.49	0.00	0.32	0.00	0.00	23.66	0.00	1.53	0.00
	14	0.00	51.54	0.93	0.00	0.86	0.00	23.86	0.00	22.81	0.00
	45	0.00	29.22	6.08	13.37	2.12	0.00	23.39	0.34	25.48	0.00
	4	0.00	37.85	0.00	4.41	0.00	0.00	27.24	0.00	30.50	0.00
	78	0.00	36.32	2.31	15.69	0.28	0.00	34.01	0.19	11.20	0.00
	11	0.00	25.68	0.88	6.46	0.29	0.00	24.70	0.00	42.01	0.00
	Basin	0.00	20.76	7.16	21.26	4.10	0.00	24.45	0.27	21.92	0.08
Chile	76	0.00	8.74	0.00	0.00	0.16	35.02	52.71	3.39	0.00	0.00
	66	0.00	15.94	0.00	0.00	0.32	25.53	57.56	0.66	0.00	0.00
	86	0.00	4.25	0.00	0.00	0.32	23.88	68.63	2.91	0.00	0.00
	108	24.27	4.09	0.00	0.00	11.50	40.16	18.45	1.53	0.00	0.00
	59	0.00	7.10	0.00	0.00	0.00	17.23	74.25	1.42	0.00	0.00
	40	1.33	8.29	0.00	0.00	0.27	27.64	61.37	1.10	0.00	0.00
	55	0.59	11.42	0.00	0.00	0.19	25.41	61.53	0.86	0.00	0.00
	37	0.00	1.63	0.00	0.00	0.00	30.80	64.59	2.97	0.00	0.00
	39	0.45	4.40	0.00	0.00	0.24	25.18	68.17	1.56	0.00	0.00
	38	0.00	6.90	0.00	0.00	0.00	14.84	77.68	0.57	0.00	0.00
	25	0.00	0.44	0.00	0.00	0.67	51.57	46.96	0.36	0.00	0.00
	16	0.00	0.00	0.00	0.00	0.10	64.50	34.82	0.58	0.00	0.00
	14	0.00	1.93	0.00	0.00	0.61	35.24	58.63	3.59	0.00	0.00
	9	0.00	1.03	0.00	0.00	0.37	31.54	63.94	3.12	0.00	0.00
	5	0.96	3.01	0.00	0.00	0.65	38.37	55.14	1.87	0.00	0.00
	7	0.00	0.49	0.00	0.00	0.00	30.32	66.42	2.76	0.00	0.00
	6	0.00	4.70	0.00	0.00	0.31	38.07	56.11	0.82	0.00	0.00
	Basin	2.91	4.78	0.00	0.00	1.56	41.44	46.57	2.74	0.00	0.00
Mendoza	79	0.00	18.86	0.10	0.00	0.00	12.57	67.56	0.91	0.00	0.00
	82	0.00	17.41	0.00	0.00	0.00	15.67	66.77	0.15	0.00	0.00
	84	0.05	24.06	0.05	0.03	0.00	21.39	53.51	0.91	0.00	0.00
	90	0.00	24.91	0.00	0.00	0.00	13.59	58.40	3.09	0.00	0.00
	Basin	0.05	24.06	0.05	0.03	0.00	21.39	53.51	0.91	0.00	0.00

Soil

The spatial gridded data with 5 arc-minutes resolution (Ver. 1.2) were taken from ISRIC-WRS (FAO-UNESCO Soil Map of the World, 1971-1981). The soil properties dataset was obtained from the International Soils Reference and Information Center (ISRIC). The soil properties obtained from ISRIC include soil drainage class, organic carbon content, electrical conductivity, particle size distribution (i.e. content of sand, silt and clay), content of coarse fragments (> 2 mm), bulk density, and available water capacity. These estimates are presented by FAO soil unit for fixed depth intervals 20 cm up to 100 cm depth. Soil texture was derived from USDA soil texture classification and particle size distribution information (Baldwin et al., 1938). Saturated soil hydraulic conductivity was estimated based on soil texture by first selecting the bulk density class of low, medium or high, and then using the corresponding textural triangle to select the range of saturated hydraulic conductivity (NRCS/NRCS, 2007). The major soil type in the upper areas of the watersheds is Lithosols which are very shallow, occurring mainly on steep slopes often with exposed rock debris.

Climate Data

Historical weather data for model calibration and validation was obtained from the Climate Forecast System Reanalysis (CFSR) global meteorological dataset (Saha, 2010). CFSR data is available globally since 1979 at a 38-km resolution. Unfortunately, weather stations are often sparsely distributed over mountainous and high altitude regions. The weather data time series at the remote stations is often not enough for the efficient analysis of the entire climate system in a region. In such instances, re-analysis

data such as data from the National Center for Environmental Prediction – National Center for Atmospheric Research (NCEP-NCAR) Global Reanalysis1; National Centers for Environmental Prediction - Climate Forecast System Reanalysis (NCEP-CFSR); and European Centre for Medium-Range Weather Forecasts (ECMWF Interim); was obtained to overcome the data deficit. CFSR is considerably more accurate than the previous global re-analysis made at NCEP in the 1990s. It is more comprehensive because it includes analyses of both the ocean and sea ice, and it has higher resolution in space and time (Saha, 2010). Regardless of the advantages of NCEP-CFSR climate data to other re-analysis datasets, its reliability in watershed modeling should be examined before applying the data due to the climate models shortcomings in predicting the data in remote areas where observational data are absent or atmospheric condition changes abruptly due to the barriers and orography.

Stream Flow

Daily discharge records for model calibration were collected from local hydrologic administrators and online databases. Eighty-three stations for streamflow and their sources are listed in Table 1. 3; although, only 35 stations were used for model calibration. The stations with the most complete records located in high altitude areas were used and those with short data periods, < 3 permanent snow cover, were located on a dammed river were discarded.

Table 1. 3. Available flow gauges with drainage area and data period for each river basins.

	Reach#	River	Station name	Latitude	Longitude	Area (km^2)	Altitude (m)	Period	Missed years
Narayani[1]	122*	BURHI GANDAKI	ARUGHAT	28.04	84.82	4270	485	1964-1985	0
	133*	MARSYANDI	BIMAL NAGAR	27.95	84.43	3850	354	1987-1992	0
	123*	KALI GANDAKI	SETIBENI	28.01	83.60	6630	410	1964-1993	0
	157	KALI GANDAKI	KOTAGAON SHRINGE	27.75	84.35	11400	198	1964-1985	4
	96	SETI	PHOOLBARI	28.23	84.00	582	830	1964-1984	5
	159	NARAYANI GANDAK	DEVGHAT	27.71	84.43	31100	180	1963-1993	19
Vakhsh[1]	72*	MUKSU	DAVSEAR	39.13	71.57	6550	2220	1961-1985	9
	133*	OBIKHINGOU	TAVILDARA	38.70	70.52	5390	1616	1958-1985	0
	109*	VAKHSH	KOMSOMOLABAD	38.87	69.98	29500	1258	1949-1989	45
	85	VAKHSH	GARM	39.00	70.33	20000	1316	1933-1990	8
	40	KIZIL-SU	DOMBRACHI	39.27	71.38	8370	1841	1961-1985	0
Rhone[2]	2*	RHONE	GLETSCH	46.56	8.36	39	1761	1955-2012	
	4*	GONERI	OBERWALD	46.53	8.36	40	1385	1990-2012	
	11*	RHONE	RECKINGEN	46.47	8.25	215	1311	1975-2012	
	23*	MASSA	BLATTENBEI NATERS	46.39	8.01	195	1446	1965-2012	
	60	SALTINA	BRIG	46.32	7.99	78	677	1965-2012	
	45*	RHONE	BRIG	46.32	7.98	913	667	1965-2012	
	78	VISPA	VISP	46.28	7.88	778	659	1903-2012	
	14*	LONZA	BLATTEN	46.42	7.82	78	1520	1955-2012	
	77	SIONNE	SION	46.23	7.37	28	500	2006-2012	
	81	RHONE	SION	46.22	7.36	3373	484	1916-2012	
	99	RHONE	BRANSON	46.13	7.09	3752	457	1967-2012	
	120	DRANCE DE BAGNES	LE CHABLE VILLETTE	46.08	7.21	254	810	1911-2012	
	101	DRANCE	MARTIGNY PONTDE ROSSETTAN	46.10	7.06	672	474	1991-2012	
Central Chile[3]	7*	JUNCAL	EN JUNCAL	-32.85	-70.17		1800		
	14*	BLANCO	EN RIO BLANCO	-32.90	-70.28		1420		
	9*	ACONCAGUA	EN RIO BLANCO	-32.90	-70.30		1420		
	16	ESTERO POCURO	EN EL SIFON	-32.90	-70.53		1000		
	6*	COLORADO	EN COLORADO	-32.85	-70.40		1062		
	5*	ACONCAGUA	EN CHACABUQUITO	-32.85	-70.50		950		
	22	ESTERO ARRAYAN	EN LA MONTOSA	-33.32	-70.45		880		
	25*	ESTERO YERBA	LOCA ANTES J. S. F.	-33.33	-70.35		1350		
	38*	OLIVARES ANTES	JUNTA R. COLORADO	-33.48	-70.13		1500		
	37*	COLORADO ANTES	JUNTA RIO OLIVARES	-33.48	-70.13		1500		
	39*	COLORADO ANTES	JUNTA RIO MAIPO	-33.58	-70.37		890		
	40*	MAIPO	EN EL MANZANO	-33.58	-70.37		850		
	66*	MAIPO	EN LAS HUALTATAS	-33.97	-70.13		1820		
	59*	VOLCAN	EN QUELTEHUES	-33.80	-70.20		1365		

Table 1. 3. Continued

	Reach #	River	Station name	Latitude	Longitude	Area (km^2)	Altitude (m)	Period	Missed years
Central Chile[3]	55*	MAIPO	EN SAN ALFONSO	-33.73	-70.30		1092		
	76*	PANGAL	EN PANGAL	-34.23	-70.32		1500		
	77*	CACHAPOAL	EN PTE TERMAS DE CAUQUENES	-34.25	-70.57		700		
	86*	CACHAPOAL	AGUAS ABAJO	-34.33	-70.37		1127		
	93	CLARO	EN HACIENDA LAS NIEVES J. CORTADERAL	-34.48	-70.70		720		
	100*	TINGUIRIRICA	BAJO LOS BRIONES	-34.72	-70.82		560		
	108*	CLARO	EN EL VALLE	-34.68	-70.87		476		
	30	MAPOCHO	EN LOS ALMENDROS	-33.37	-70.45		966		
	61	MAIPO	EN LAS MELOSAS	-33.83	-70.18		1527		
	106	TINGUIRIRICA AGUAS ABAJO	JUNTA AZUFRE	-34.80	-70.55		1024		
	94	CORTADERAL ANTE	JUNTA CACHAPOAL	-34.37	-70.32		1200		
Mendoza[4]	90*	COLORADO	PUNTA DE VACAS	-32.83	-69.70				
	82*	CUEVAS	PUNTA DE VACAS	-32.87	-69.77				
	86*	MENDOZA	GUIDO	-32.92	-69.24				
	81	MENDOZA	PUNTA DE VACAS	-32.85	-69.77				
	84*	TUPUNGATO	PUNTA DE VACAS	-32.88	-69.77				
	79*	VACAS	PUNTA DE VACAS	-32.85	-69.76				

1) Source: The Global Runoff Data Centre (GRDC)
2) Source: Switzerland Federal Office for the Environment (FOEN)
3) Source: National Water Information System of Argentina
4) Source: Chilean Dirección General de Aguas (DGA)

Dams

Seven grand dams were set up as reservoirs in the modelled river basins (Table 1. 4). Except for the Upper Rhone River Basin, reservoir parameters such as operation starting date, surface area, and volume of water at the principle spillway for all river basins were obtained from the Global Water System Project (GWSP) (Lehner et al., 2011). Considering that all of the gauged subbasins are located at high altitudes, no reservoir dams exist at those areas. Details about hydraulic structures in the Upper Rhone River Basin were collected from the Switzerland Federal Office for the

Environment (FOEN) who manages watersheds and dams on the glacial lakes such as Gries and Bortelsee. All of the gauged subbasins for model calibration purposes in this study were located on upper dam reservoirs.

Table 1. 4. List of the grand dams were set up as reservoir in the modelled river basins.

Dam name	River	Country	Operation year	Hight (m)	Lengt h (m)	Area (km^2)	Capacity (mcm)	Depth (m)	Catchment area (km^2)
Gries	Agene	Switzerland	1965	60	400	0.3	18.6	62.0	7
Zeuzier	Lienne	Switzerland	1957	156	256	0.3	51.0	170.0	13
Moiry	Gougra	Switzerland	1958	148	610	0.7	78.0	111.4	26
Mattmark	Saaser Vispa	Switzerland	1967	120	780	0.8	101.0	126.3	34
Mauvoisin	Drance de Baanes	Switzerland	1957	250	520	1.1	211.5	192.3	110
Les Toules	Drance d'Entre	Switzerland	1963	86	460	0.3	20.1	67.0	37
Yeso	Yeso	Chile	1967	61	350	7.6	250.0	32.9	356

Snow Modeling Components

Initial Snow Storage

Initial snow storage at the beginning of the simulation period can be set in the model for each individual elevation band. This storage can be permanent snow or glaciers at the end of ablation season. The thickness of initial snow is set for each elevation band as its volume of equivalent water; while the lower boundary of the elevation band represents the mean elevation of the snow boundary. This initial storage then is updated on daily basis for accumulation, sublimation and melting of snow.

Snow Pack Storage

SWAT initially stores daily fallen snow in the form of its volume of equivalent water in the snow pack, then updates the snowpack storage with decreasing the snow melt and sublimation or adding snow fall into the storage. The snow pack mass balance for each HRU is

$$SNO_i = SNO_{i-1} + R_{day(i-1)} - E_{sub(i-1)} - SNO_{mlt(i-1)} \quad \text{Eq. 1. 1}$$

where SNO_i is the water content of the snow pack on a given day i (mm H_2O), R_{day} is amount of solid precipitation on a given day, (mm H_2O), E_{sub} is the amount of sublimitation on a given day (mm H_2O), and SNO_{mlt} is the amount of snow melt on a given day (mm H_2O).

Snow Pack Temperature

The snow pack temperature is a function of the mean daily temperature. The equation used to calculate the snow pack temperature is:

$$T_{snow(d_n)} = T_{snow(d_{n-1})} \times (1 - \lambda_{sno}) + \bar{T}_{av} \times \lambda_{sno} \quad \text{Eq. 1. 2}$$

where $T_{snow(d_n)}$ is the snow pack temperature on a given day (℃), $T_{snow(d_{n-1})}$ is the snow pack temperature on the previous day (℃), λ_{sno} is the snow temperature lag factor (TIMP) and ranges between 0 and 1; $\bar{T}_{av}$ is the mean air temperature on the current day (℃). As λ_{sno} approaches 1.0, the mean air temperature on the current day exerts an increasingly greater influence on the snow pack temperature and the snow pack temperature from the previous day exerts less and less influence.

Snow Cover

Snow cover within a watershed is usually non-uniform due to non-climatic factors such as shading, drifting, slope, aspect, shading and land cover. This results in a fraction of the subbasin area that is bare of snow. These non-climatic factors are usually similar from year to year, making it possible to correlate the areal coverage of snow with the amount of snow present in the sub-basin at a given time. This correlation, expressed as an aerial depletion curve, is unique for a watershed. In this study, the seasonal growth and recession of the snow pack was modeled as a function of the amount of snow present in the basin. The areal depletion curve based on a natural logarithm is calculated as:

$$sno_{cov} = \frac{SNO}{SNO_{100}}\left(\frac{SNO}{SNO_{100}} + exp\left(cov_1 - cov_2 \cdot \frac{SNO}{SNO_{100}}\right)\right)^{-1} \qquad \text{Eq. 1. 3}$$

Where sno_{cov} is the fraction of the HRU area covered by snow, SNO is the water content of the snow pack on a given day (mm H_2O), SNO_{100} is the threshold depth of snow at 100 percent coverage and is determined during the model calibration (mm H_2O), cov_1 and cov_2 are coefficients that define the shape of the curve. The values used for cov_1 and cov_2 are determined by solving the equation for two known points: 95 percent coverage at 95 percent SNO_{100}; and 50 percent coverage at a user specified fraction of SNO_{100} ($SNO_{50}CO$).

Areas with a snow depth above SNO_{100}will have permanent snow cover due to the non-climatic factors. Smaller values of SNO_{100} indicate uniform topography and vegetation distribution within the basin and consequently the impact of the areal

depletion curve on snow melt will be minimal. For highly glaciated subbasins with typical permanent snow depths higher than SNO_{100} (SNO_{100} ranges from 0 to 500 (mm H_2O)), the depth of snow over the HRU is assumed to be uniform (i.e. sno_{cov} = 1) and the areal depletion curve of snow does not have any influences on melt.

Snow Accumulation

SWAT classifies precipitation as liquid or solid precipitation by the mean daily air temperature. The user-defined threshold temperature, T_{s-r} (SFTMP), is used to categorize precipitation as rain or snow.

- If $T_{ave} \leq T_{s-r}$ then precipitation = snow fall
- If $T_{ave} > T_{s-r}$ then precipitation = rain fall

If the precipitation is classified as snow then the water equivalent (w.e.) of the snow fall is added to the snow pack in elevation band. The model calculates the temperature and precipitation at each elevation band based on the user-defined temperature and precipitation gradients at a subbasin scale.

Snow Melt

The snowmelt is calculated as a linear function of the difference between the average snow-pack maximum air temperature and the base or threshold temperature for snowmelt (Neitsch et al., 2011):

$$SNO_{mlt} = b_{mlt} \cdot sno_{cov} \cdot \left[\frac{T_{snow} + T_{max}}{2} - T_{mlt}\right] \qquad \text{Eq. 1. 4}$$

where SNO_{mlt} is the amount of snow melt from elevation bands (mm H_2O), b_{mlt} is the melt factor within the basin (mm H_2O /day-℃), sno_{cov} is the fraction of the HRU area

covered by snow, T_{snow} is the snow pack temperature within the basin (°C), T_{max} is the maximum air temperature of a day (°C), and T_{mlt} (SMTMP) is the threshold snow melt temperature within the basin (°C).

The melt factors are spatially constant within a basin but seasonally variable by sinusoidal interpolation between a minimum value on December 21 and a maximum value on June 21:

$$b_{mlt} = \frac{(b_{mlt6} + b_{mlt12})}{2} + \frac{(b_{mlt6} - b_{mlt12})}{2} \cdot sin\left(\frac{2\pi}{365} \cdot (d_n - 81)\right) \qquad \text{Eq. 1. 5}$$

where b_{mlt} is the melt factor for the day (mm H_2O /day-°C), b_{mlt6} (SMFMX) the maximum melt rate for snow during a year (June 21 in the northern hemisphere) (mm H_2O /day-°C), b_{mlt12} (SMFMN) is the minimum snowmelt rate during a year (December 21 in the northern hemisphere) (mm H_2O /day-°C), and d_n is the Julian day number of the year.

To account for orographic effects on both precipitation and temperature, SWAT allows up to 10 elevation bands to be defined in each subbasin. The spatial variation of snow melt/accumulation varies as a function of elevation resulting from orographic precipitation and air temperature lapse rate.

The temperature and precipitation at elevation bands is calculated using:

$$R_{band} = R_{gage} + \left(EL_{band} - EL_{gage}\right) \cdot plaps$$
$$T_{band} = T_{gage} + \left(EL_{band} - EL_{gage}\right) \cdot tlaps \qquad \text{Eq. 1. 6}$$

where T_{band}, is the elevation band mean temperature (°C), T_{gage}, is the temperature recorded at the gage (°C), EL_{band} is the mean elevation of the band (m), EL_{gage} is the

gage elevation (m), R_{band} is the mean precipitation of the band (mm), R_{gage} is the precipitation recorded at the gage (mm H_2O), plaps is the precipitation lapse rate (mm H_2O/m), and tlaps is the temperature lapse rate (°C/m).

Once precipitation and temperature values have been calculated for each elevation band in the subbasin, new weighted average subbasin precipitation and temperature values are calculated using fraction of subbasin within a particular elevation band as the weighting factor.

Modified Snow Hydrology Process

It is obvious that there is a range of melt factor values throughout a region depending on snow/ice albedo, density, and climate. Melt factors are generally reported higher for ice (6 mm /day-°C to 8 mm /day-°C) and lower for snow (3 mm /day-°C to 5 mm /day-°C) (Braithwaite, 2008). The lagging factor, λ reflects the influence of snow pack density, and snow pack depth on snow pack temperature and consequently is highly variable in a basin with shallow seasonal snow cover in lower altitudes, and deep, dense firn and ice in the high altitudes. Anderson (1973) comments on typical values for λ which can theoretically vary between 0 and 1 but commonly is between 0.1 (deep surface layer) and 0.5 (shallow surface layer).

In previous versions of SWAT, spatial variation of snow melt/accumulation only varies as a function of elevation resulting from orographic precipitation and air temperature lapse rate; while, snowmelt parameters are constant within the basin. In the modified snow hydrologic component of SWAT used in this study, the snow melt factors (SMFMX, SMFMN) and other associated parameters, such as temperature lag

factor (TIMP), snow fall temperature (SFTMP), and snow melt temperature (SMTMP) are allowed to be spatially variable within the subbasins and elevation bands.

Many temperature-index based runoff models such as SWAT consider a seasonal variability of melt factor but roughly ignore the spatial variation of melt factor across the basin, which is expected to increase with increasing elevation (Hock, 2003). To overcome this weakness, a modified snow hydrology component of SWAT was applied in order to consider spatial variation of snow melt parameters by elevation band for each subbasin. Hence, not only will melt rates vary as a function of elevation resulting from an air temperature lapse rate across each subbasin, but it also will vary based on ice and snow distribution.

In this study, three SWAT snow melt algorithms have been evaluated based on the degree of parameter distribution on a basin scale, a subbasin scale, and a subbasin/elevation band scale.

1) In the first method, all associated snow melt/accumulation parameters were uniform across the entire basin.
2) In the second method, snow melt parameters were allowed to vary on a subbasin scale. Separation of seasonal snow from permanent snow is not permitted in this method and small subbasins are needed to separate glaciered areas from glacier free areas and consequently achieve good results.
3) In the third method, snow melt parameters were varied based on the elevation bands for each subbasin. This method allows discretization of seasonal snow from glaciers based on vertical (elevation bands) and horizontal (subbasin)

variability of model parameters reflecting the physical properties of ice and snow. In this method, to reflect the influence of density and depth of ice and snow on the vertical temperature profile of the snow pack, the temperature lag factor (TIMP) was determined separately for shallow ice and seasonal snow at lower elevation bands and deep ice at higher elevation bands for each subbasin. Melt factors (SMFMX and SMFMN) were separately determined for glaciered and unglaciered bands.

In general, accumulation depends upon the melt factor for snow and melt depends upon the melt factor for ice (Braithwaite and Raper, 2007). During summer months when snow has largely melted from the glacier surface, the predominant source of melt comes from the ablation of glacier ice; while in winter the snow cover on glaciers and glacier free areas is the main source of melted water. Therefore, the spatial and seasonal variability of melt factors directly affect the accuracy of runoff simulation in glaciered watersheds.

Glacier Modelling

The equilibrium line altitude (ELA) is a theoretical line that determines the boundary of the accumulation zone and ablation zone on a glacier. The ELA, sometimes denoted ELA_0 (the balanced-budget ELA), of a glacier with a climatic mass balance is equal to zero on average over a number of years. The steady-state ELA is difficult to estimate because glaciers are seldom if ever in steady state. It is usually approximated by the balanced-budget ELA (Cogley et al., 2010). So, what is referred to here as steady state ELA (ELA_0) is in fact the balanced-budget ELA assuming that the glacier is in a

steady state during the simulation period. The ELA is determined by climate and the aspect of the glacier. It is not influenced by glacier dynamics, extent and hypsometry, and thus reveals a largely unfiltered climatic signal (Huss et al., 2008). Therefore, it can be a representation of the lowest boundary of climatic glacierization (Zemp et al., 2006b).

Therefore, in this study it was assumed that the ELA0 represent the glacier boundary. The physical boundary of glaciers was then corrected based on the glacier inventory data, GLIMS glacier outlines and MODIS products. Lower elevation bands below the ELA_0, were considered to be seasonal snow cover regardless of extended glacial tongues to lower elevations. A schematic diagram of glacier modeling in SWAT is presented in Figure 1. 9.

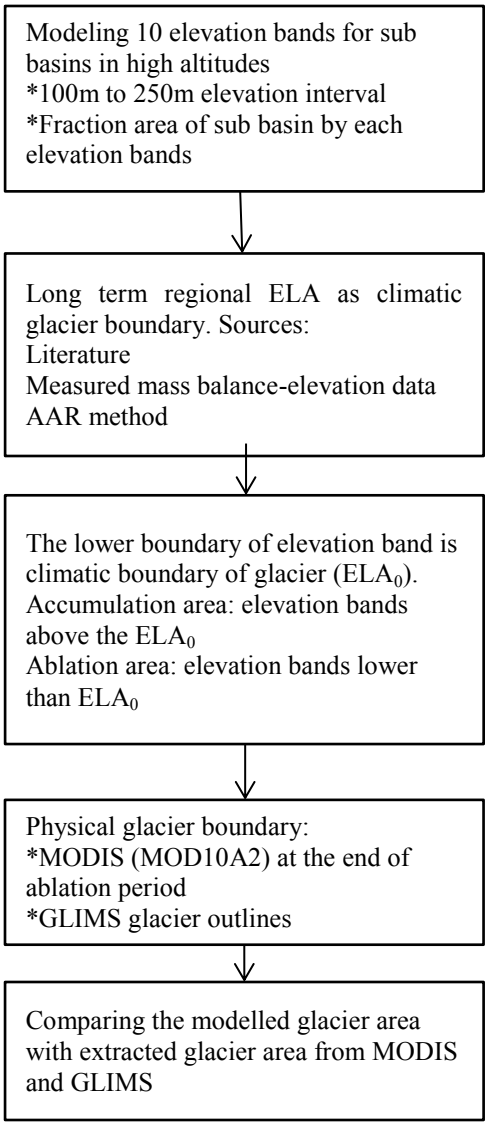

Figure 1. 9. Setting up the glaciered area (accumulation and ablation zones) in elevation bands.

Model Setup

Subbasin Delineation

Flow direction and accumulation were generated using a sink free DEM. A fully connected drainage network was created from flow accumulation grid values higher than a drainage area threshold value. The threshold area, or critical source area, defines the minimum drainage area required to form the origin of a stream.

Next the river basin was automatically delineated into subbasins. The subdivision was determined by the stream links and the value of the drainage area threshold used. Smaller threshold values result in denser networks and larger subbasins. River basins of different sizes can be delineated by applying different threshold values. The watershed boundary of the river basins determined using the automatic delineation procedure is illustrated in Figure 1. 10 to Figure 1. 14.

The drainage area threshold for the river basins was set to a minimum value in order to generate upper tributaries throughout the glacial valleys. When a gauging station was available for calibration, an outlet was inserted manually, splitting the subbasin in two. The upper subbasins were also split into smaller divisions by manually adding an outlet to divide a subbasin into the narrower elevation bands on glaciated areas while the flat subbasins in lower elevations were combined into larger subbasins.

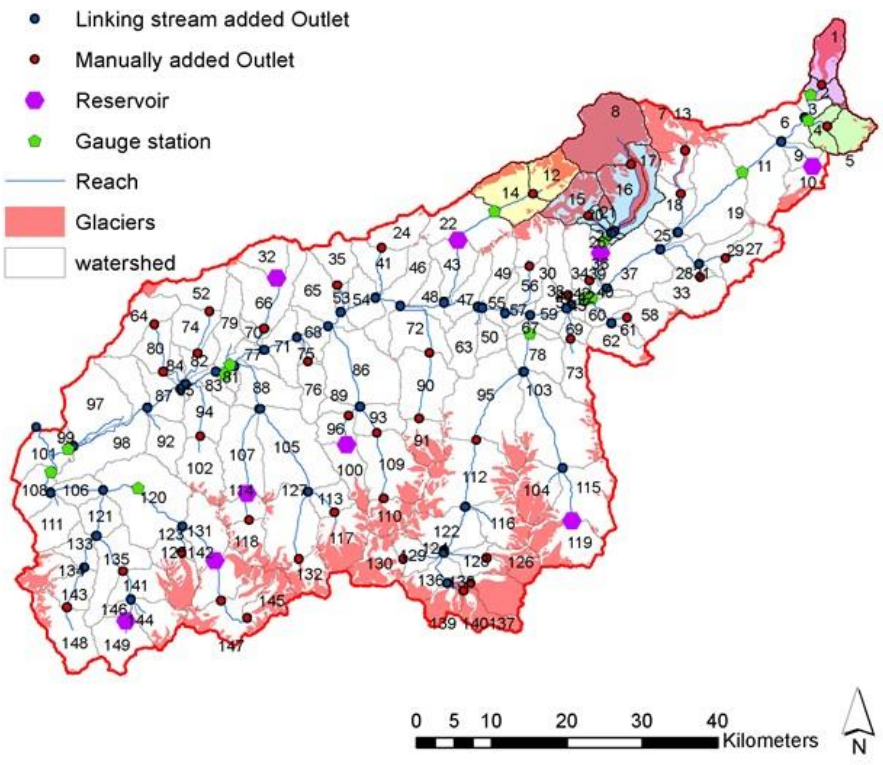

Figure 1. 10. Subbasins delineation, glaciers outlines, and locations of dams and flow gauge stations in Rhone River Basin. The flow data from colored subbasins is used for model calibration.

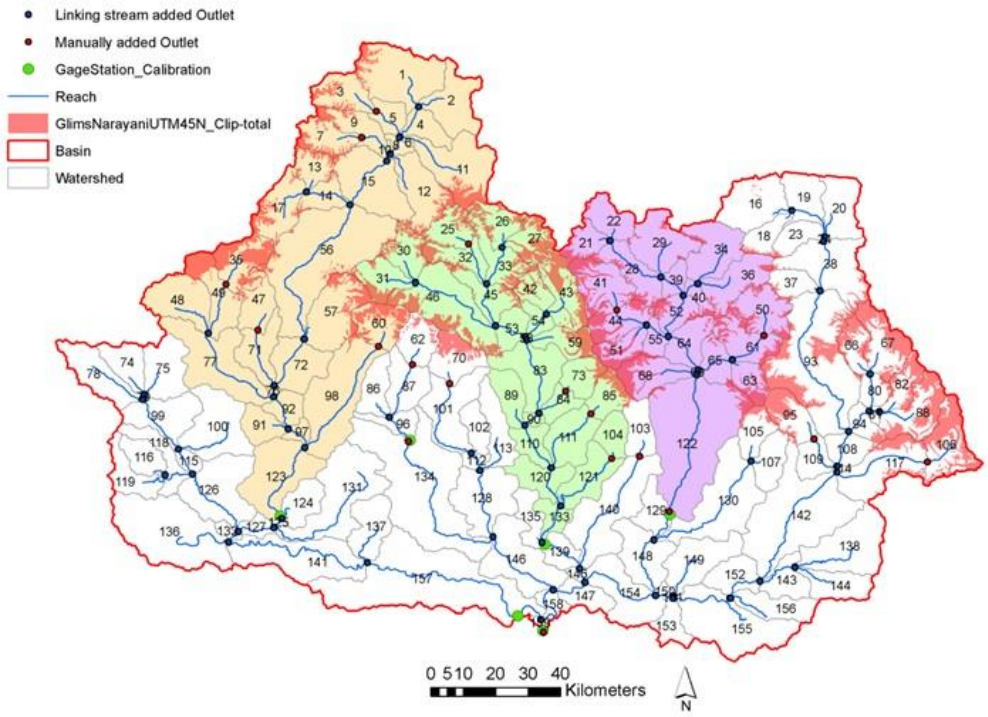

Figure 1. 11. Subbasins delineation, glaciers outlines, and locations of dams and flow gauge stations in Narayani River Basin. The flow data from colored subbasins is used for model calibration.

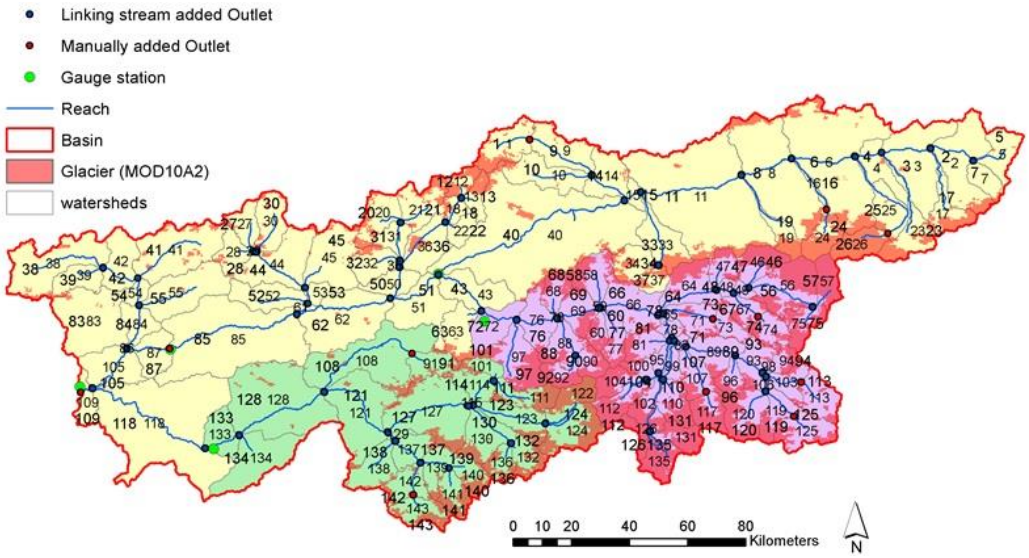

Figure 1. 12. Subbasins delineation, glaciers outlines, and locations of dams and flow gauge stations in Vakhsh River Basin. The flow data from colored subbasins is used for model calibration.

Figure 1. 13. Subbasins delineation, glaciers outlines, and locations of dams and flow gauge stations in Mendoza River Basin. The flow data from colored subbasins is used for model calibration.

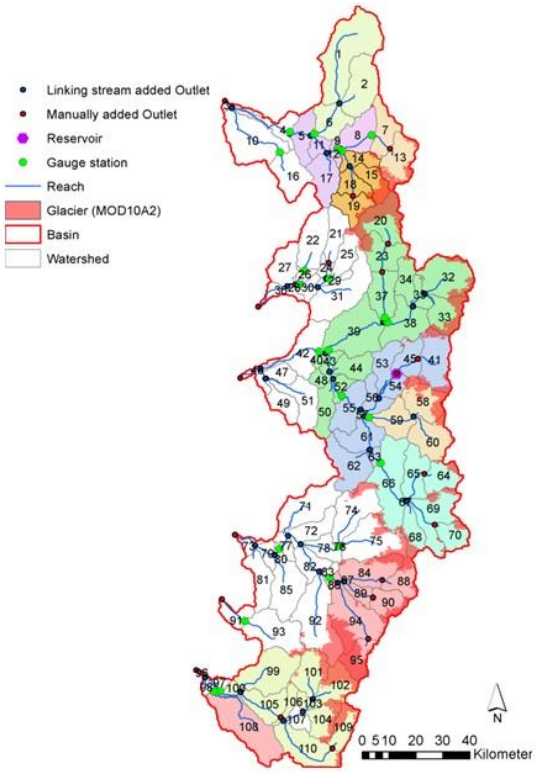

Figure 1. 14. Subbasins delineation, glaciers outlines, and locations of dams and flow gauge stations in Cilean River Basins. The flow data from colored subbasins is used for model calibration.

Hydrological Response Units

SWAT divides each subbasin into more detailed sub divisions called Hydrological Response Units (HRUs). SWAT delineates HRUs with user-defined thresholds represented as percentages of each land use, soil type, and slope. In this study, land use and soil type thresholds were set at 1 percent, meaning that any land use covering more than 1 percent of a subbasin was considered an HRU. From that portion

of land use, any soil type covering more than 1 percent was considered to be an HRU. These thresholds were chosen to avoid creating too many HRUs, which would make analyses too complicated and time-consuming for the modeling process. Based these thresholds a total of 9,878 HRUs were created in the five river basins (Table 1. 5). HRUs in the SWAT model can be defined using an average slope per subbasin or multiple slope categories. To better represent the glaciated HRUs, three slope classes were defined: steep, moderate and gentle, since accumulated permanent snow generally creates flat surfaces with gentle slopes surrounded by steep mountain valleys.

Table 1. 5. Number of subbasins and HRUs for the river basins.

	Subbasins	HRUs
Narayani	159	2913
Vakhsh	143	1658
Upper Rhone	149	2413
Mendoza	114	1224
Central Chile	110	1670

Elevation Bands

Subbasins over 2000 m altitude were divided into 10 elevation bands with 100 to 200 m intervals depending on the elevation range of subbasin. Smaller elevation band intervals enabled SWAT to model the glacier boundaries more accurately. It was assumed that the glacier boundary in a subbasin matched the lowest altitude of the elevation band if more than 50 percent of the elevation band area is covered by glacier.

Glacier Boundary and Thickness

Glacier boundaries were extracted from MODIS products (MOD10A2) and GLIMS. To model the glacier areas, it was assumed that all zones at altitudes higher than ELA_0 were permanent snow/ice and that seasonal snow was located at lower altitudes by default. For all subbasins, the glacier boundaries were modified by MODIS and GLIMS data for the glacier free areas at elevations higher than the steady state equilibrium line altitude (ELA_0), and the areas climatically suited for glacier formation at altitudes lower than ELA_0.

Debris-covered area of glaciers, accumulated wind-blown snow and small isolated glaciers with an area of 0.1 km^2 or less were ignored to estimate the total glaciated area of the river basins. The percentage of the glacier covered area of each river basin by each model, MODIS and GLIMS is presented in Table 1. 1.

ELA_0 values were derived from literature and observed specific net mass balance-ELA data which is only available for benchmark glaciers. The ELA_0 across the Upper Rhone River Basin was calculated from the regression relationship between the specific net balance and the ELA (Østrem, 1975). ELA values outside the glacier altitude range were excluded in the regression analysis. Figure 1. 15 shows an example of the Findelen Glacier in the Southern Rhone River Basin with an ELA_0 of 3,184 m.s.l.

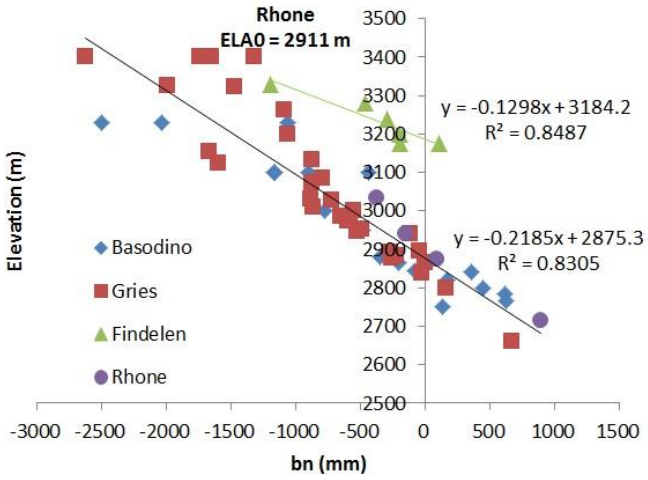

Figure 1. 15. Accumulation area ratio (AAR) and equilibrium line altitude (ELA) versus specific net balance for four glaciers in Rhone River Basin.

The results from regression analysis of the other three glaciers in the northern Rhone River Basin are as follows. Coefficients of determination (R^2) ranged from 0.84 to 0.97, with a mean of 0.83 resulting in an ELA_0 of 2,875 m.s.l which is close to the estimated regional climatic ELA_0 below 2800 m.s.l. in the Rhone River Basin and above the 3,100 m.s.l. determined for the southern basin by Zemp et al. (2007). He derived an empirical relationship between summer temperature and annual precipitation at the ELA_0 (1971-1990) using a geographical information system (GIS) and a digital elevation model. This relationship was then applied over a spatial domain to model the regional climatic ELA_0.

Unfortunately, an observation of the mass balance and ELA from the Nepalese Himalayan glaciers was unavailable. Present ELAs rise from south to north across the Himalayan Range from 5,200 to 5,800 m, as indicated by the altitudes of the lowest cirque glaciers and highest lateral and medial moraines on valley glaciers (Williams

1983). The ELA has also been estimated to be 5,470 m across Ganges River Basin (Savoskul and Smakhtin, 2013).

Various methods were suggested in the literature for estimation of regional ELA_0 such as the Accumulation Area Ratios (AAR) and geodetic method. Braithwaite and Raper (2009) also estimated ELA_0 with an accuracy of about ±100 m for many thousands of glaciers using the median elevation parameter in the World Glacier Inventory.

The AAR is the ratio of the accumulation area to the total glacier area (Meier and Post, 1962). The AAR of a steady-state glacier (AAR_0) is around 0.6-0.7 in humid climates and 0.5-0.6 in continental climates (Kaser and Osmaston, 2002). Gross et al., (1978) suggested an AAR_0 of 0.67 for glaciers in the Alps as an approximation of the ELA_0 and zero mass balance. An AAR_0 value of 0.578 was also reported based on inventory data from over 24,000 Eurasian glaciers by Bahr (1997). Dyurgerov (2009) derived an average value of 58 percent from a sample of 100 glaciers.

In this study, the AAR_0 method was applied to estimate regional ELA_0 of the Narayani and Vakhsh River Basins (Figure 1. 16). Assuming an AAR_0 of 0.58 (Bahr, 1997; Dyurgerov, 2009) the derived ELA_0 values from of 90 m DEM-based hypsometric curve and GLIMS outline glaciers was extracted between 5,000 m in the east to 5,600 m in west across the Narayani River Basin which is in the reported ELA ranges (Williams, 1983; Savoskul and Smakhtin, 2013). A glacier distribution in Narayani is presented in Figure 1. 17.

Average ELA_0 across the Vakhsh River Basin was obtained between 43,00 m in the north to 4,500 m in southern side of the river basin. ELA of glaciers in the central

Chile surpasses 5,000 m in 30º S, and drops to 4,300–4,400 m around 32.5º S to 33.0º S (Hastenrath, 1971; Kull et al., 2002; Lliboutry, 1986, 1999). A profile of glaciation in the Central Andes between 27.0º S and 36° S from Brenning (2005) shows an ELA of 4,500 m at 32.5° S on the western side of the Andes and 4,300 m at 35º S which is in the same elevation of the zero degree isotherm of Central Chile. The ELA value of the Mendoza River Basin in the Eastern Andes is 4,800 m at 33º S while the northern part of the river basin at 32º S is glacier free with a high ELA over 5,000 m.

The mean ice thickness at each elevation band was calculated by averaging the ice thickness values at individual points on Figure 1. 8. Ice thickness was assumed to be 1000 m .w .e when no data was available.

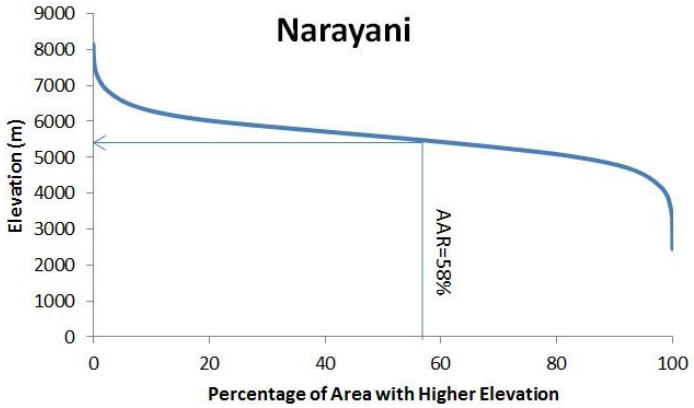

Figure 1. 16. AAR_0 method to estimate regional ELA_0 of Narayani River Basin.

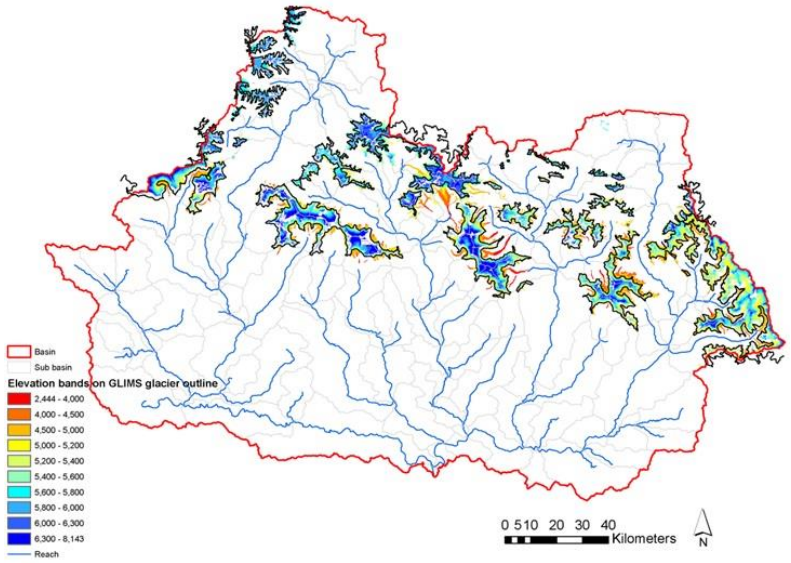

Figure 1. 17. Glacier area from GLIMS and 90m-DEM extracted elevation bands in Narayani River Basin. The thick line shows a boundary of glaciers (ELA_0 line) that has been extracted by AAR_0 method in this study. ELA_0 varies between 5000m (yellow color band) in east to 5600m (cyan color band) in North West. The lower boundary of elevation bands 4 and 7 were considered as a glacier boundary in this study.

Temperature and Precipitation Gradient

Temperature lapse rate and orographic precipitation have been discussed in many studies and the wide range of estimates derived depends on the climate data source. Richard and Tonnel (1985) reported a temperature lapse rate by of -5.3 ºC/km and -5.6 ºC/km across the Swiss pre-Alps and Valais, respectively, while Braithwaite (2008) estimated it as -7 ºC/km for the Upper Rhone. Huss et al. (2008) suggested -5.21 ºC/km across Switzerland. Schaper et al. (1999) reported a temperature lapse rate over the Mass-Blatten located in Upper Rhone, Switzerland of -6.5 ºC/km. Stehr et al. (2009) derived a value of -5 from analyzing the ground station data of Central Chile. Due to the variation in reported lapse rate values using different data sources, this study relied on

the derived lapse rates from NCEP-CFSR 30-year reanalysis data. The estimated lapse rates by temperature-altitude and precipitation-altitude linear regression over a river basin was modified over the gauged subbasins during the calibration iterations. Gradients per 1,000 m are summarized in Table 1. 6 as along with the number of NCEP-CFSR data points for each river basin. Seasonal variation of temperature lapse rate was ignored in this study and it was assumed unchanged over all seasons.

Table 1. 6. Applied precipitation and temperature lapse rates in model set up calculated from NCEP-CFSR 30-year reanalysis data.

	# of data points	Temperature gradient (C)	Precipitation gradient (mm)
Narayani	69	-5.9	-27
Vakhsh	100	-5.3	166
Upper Rhone	34	-3.0	455
Mendoza	30	-4.4	101
Central Chile	45	-4.3	-17

Ice/Snow Melt Factors

A wide range of degree-day factors (DDF) have been reported. In this study, the relevant DDF for ice and snow are primarily derived from the literature (Kotlyakov and Krenke, 1982; Singh and Kumar 1996; Kayastha et al., 2000, 2003; Immerzeel et al., 2011; Lang, 1986; Schaper et al., 1999, 2000; Braithwaite and Zhang, 2000; Braithwaite 2008). It should mentioned that the DDF are not same as melt factors in the temperature index models since the threshold temperature beyond which melt is assumed to occur is not always 0 ºC. However, DDF were used as an initial estimation in model set up.

In glaciered basins, the DDF usually exceed 6 towards the end of summer when ice becomes exposed (Kotlyakov and Krenke, 1982). DDF changes considerably with surface exposure to solar radiation, snow properties such as density and rainfall on snow (Singh and Singh, 2001). Several studies have calculated melt factors for glaciers throughout the Nepalese Himalayan Mountains and central Asia (Singh and Kumar 1996; Kayastha et al., 2000, 2003; Immerzeel et al., 2011), Switzerland Alps (Lang, 1986; Schaper et al., 1999, 2000; Braithwaite and Zhang, 2000; Braithwaite 2008), and Central Andes Chile (Kull et al., 2002). No DDF values from the Central Andes around the study area were found, therefore, the a DDF value of 4.1 mm /day-℃ was used, which is the mean value for winter snow plus summer precipitation at the ELA of 66 glaciers reported by Braithwaite (2008). Results from Braithwaite (2008) reflect different locations (66 glaciers) but also different methods.

Krenke and Khodakov (1966) suggest DDF of 4.5 and 7 mm d^{-1} $^{o}K^{-1}$ for snow and ice, respectively. Hock (2003) suggests DDF of 5.1±2.2 mm /day-℃ for snow on glaciers (18 sites) and 8.9±3.7 mm /day-℃ for ice glaciers (32 sites). Schaper et al. (1999) estimated a DDF value for seasonal snow ranging from 3.5 mm /day-℃ to 5.5 mm /day-℃ during the melt season and 7.5 mm /day-℃ to the end of the snow melt season when glacier ice is melting for Grand Aletsch in the Upper Rhone River Basin. Their method was later extended to the Upper Rhone River Basin and which applied a uniform DDF of 7 mm /day-℃ for exposed ice and gradually substituted new values when new snow temporarily covered the ice. Braitwhite and Zhang (2000) suggested DDF values of 8 mm /day-℃ for the Gries Glacier in Upper Rhone and extended this

value to four other glaciers in the basin. A DDF value of 6 mm /day-℃ has been reported for Himalayan glaciers by Immerzeel et al. (2011). Kayastha et al. (2005) used DDF values of 7.0 mm /day-℃ and 8.0 mm /day-℃ for snow and ice ablations, respectively, at altitudes up to 5000 m.s.l., and 10.5 mm /day-℃ and 9.5 mm /day-℃, respectively above 5000m in the Himalayas. These DDF were preliminarily suggested by Kayastha et al. (2000, 2003) from summer values on Glacier AX010, in east Nepal and the Yala Glacier in the Langtang Valley. DDF are higher in Himalayan glaciers than alpine glaciers in Europe primarily due to ablation attributed to absorbed global radiation at high altitudes where the positive DDF is low because of low summer air temperature (Kayastha et al., 2005).

As a result of the reported DDF in the literature, the SMFMX were set to 6 mm /day-℃ to 8 mm /day-℃ for the elevation bands higher than ELA_0 and lower values for the snow at lower elevation bands (5 mm /day-℃ to 6.5 mm /day-℃). SMFMN were set to lower values for winter melt at higher altitudes (4 mm /day-℃ to 5 mm /day-℃) and lower values for the seasonal snow at lower elevation bands (3 mm /day-℃ to 4.5 mm /day-℃). These parameters were set to higher boundary limits in the Himalayan glaciers and lower boundary limits for the alpine glaciers in the Rhone and Andes.

Model Calibration and Evaluation

The model was calibrated using monthly stream flow at the gauge stations in Table 1. 7 focusing on glaciated subbasins. The model was validated using the monthly stream flow from the Rhone, Mendoza and Chile Watersheds for two periods: recent years from 2008 to 2010 and early years from 1982 to 1992. This was to confirm that the

model works well for different periods and is independent from the time period. For the Vakhsh and Nepal Watersheds model validation periods were selected based on data availability.

Monthly calibration was performed using the SWAT Calibration and Uncertainty Program (SWAT_CUP) (Abbaspour et al., 2007). SWAT-CUP is a generic interface to provide a link between any automatic calibration/uncertainty or sensitivity program and SWAT. Sequential Uncertainty Fitting Version 2 (SUFI2) incorporated in SWAT-CUP allows for calibration and validation of the model at multiple gauging stations and multiple observed datasets simultaneously.

SUFI2 calculates a weighted multi-component objective function (weighted summation of the square errors) based on simulated variables and observed time series of all gauged watersheds, and then minimizes it by searching the Latin Hyperbolic (McKay et al., 1979) generated parameters for the best solution.

In order to perform automatic calibration by SUFI2, the initial parameter values and ranges were determined. A list of the parameters and their ranges (Neitsch et al., 2002) are presented in Table 1. 8. The Groundwater delay (GW-DELAY) and base-flow recession constant (ALPHA-BF) were initially set for simulation of low flow during the winter months. The parameter values then were optimized during the automatic model calibration. The base-flow recession constant is directly proportional to ground-water flow response to changes in recharge.

Table 1. 7. List of the gauge stations applied in model calibration and validation.

	Reach#	Station name	Area (km^2)	Calibration period	Validation period	Warm up period	Glacier MODIS (GLIMS)
Narayani	122	ARUGHAT	4270	1981-1985	-	1979-1980	14.93(10.91)
	133	BIMAL NAGAR	3850	1981-1992	-	1979-1980	16.55(13.16)
	123	SETIBENI	6630	1981-1987	1989-1993	1979-1980	9.77(9.38)
	159	DEVGHAT	31100	1981-1985	1991-1993	1979-1980	9.20
	96	PHOOLBARI	582	1981-1984	-	1979-1980	
Vakhsh	72	DAVSEAR	6550	1981-1985	-	1979-1980	31.00(31.00)
	133	TAVILDARA	5390	1981-1985	-	1979-1980	11.10
	109	KOMSOMOLABAD	29500	1981-1987	1988-1989	1979-1980	9.66
Rhone	2	Gletsch	39	1993-2007	2008-2010,1982-1992	1990-1992	41.00(46.15)
	4	Oberwald	40	1993-2007	2008-2010	1990-1992	0.00(5.1)
	23	Blattenbei Naters	195	1993-2007	2008-2010,1982-1992	1990-1992	62.34(65.10)
	14	Blatten	78	1993-2007	2008-2010,1982-1992	1990-1992	26.46(26.97)
Central Chile	7	EN JUNCAL		1993-2007	2008-2010,1982-1992	1990-1992	15.47
	14	EN RIO BLANCO		1993-2007	2008-2010,1982-1992	1990-1992	16.00
	9	EN RIO BLANCO		1993-2007	2008-2010,1982-1992	1990-1992	12.73
	6	EN COLORADO		1993-2007	2008-2010,1982-1992	1990-1992	0.17
	5	EN CHACABUQUITO		1993-2007	2008-2010,1982-1992	1990-1992	5.70
	25	LOCA ANTES JUNTA SAN FRANCISCO		1993-2007	2008-2010,1982-1992	1990-1992	3.58
	38	JUNTA RIO COLORADO		1993-2007	2008-2010,1982-1992	1990-1992	14.63
	37	JUNTA RIO OLIVARES		1993-2007	2008-2010,1982-1992	1990-1992	27.47
	39	JUNTA RIO MAIPO		1993-2007	2008-2010,1982-1992	1990-1992	15.70
	40	EN EL MANZANO		1993-2007	2008-2010,1982-1992	1990-1992	10.64
	66	EN LAS HUALTATAS		1993-2007	2008-2010,1982-1992	1990-1992	9.68
	59	EN QUELTEHUES		1993-2007	2008-2010,1982-1992	1990-1992	16.89
	55	EN SAN ALFONSO		1993-2007	2008-2010,1982-1992	1990-1992	9.03
	76	EN PANGAL		1993-2007	2008-2010,1982-1992	1990-1992	15.91
	77	EN PTE TERMAS DE CAUQUENES		1993-2007	2008-2010,1982-1992	1990-1992	12.28
	86	AGUAS ABAJO		1993-2007	2008-2010,1982-1992	1990-1992	12.28
	100	BAJO LOS BRIONES		1993-2007	2008-2010,1982-1992	1990-1992	16.35
	108	EN EL VALLE		1993-2007	2008-2010,1982-1992	1990-1992	0.00
Mendoza	90	COLORADO -PUNTA DE VACAS		1993-2007	2008-2010,1982-1992	1990-1992	8.75
	82	CUEVAS -PUNTA DE VACAS		1993-2007	2008-2010,1982-1992	1990-1992	3.21
	86	MENDOZA -GUIDO		1993-2007	2008-2010,1982-1992	1990-1992	4.34
	84	TUPUNGATO -PUNTA DE VACAS		1993-2007	2008-2010,1982-1992	1990-1992	15.00
	79	VACAS -PUNTA DE VACAS		1993-2007	2008-2010,1982-1992	1990-1992	6.00

Table 1. 8. Parameters Selected for SWAT Model Calibration.

Parameter	Description	Default value	Range
TLAPS	Temperature lapse rate [°C/km]	0	-50, +50
PLAPS	Precipitation lapse rate [mm H2O/km]	0	-500, +500
SFTMP	Snowfall temperature[°C]	1	-5, +5
SMTMP	Snow melt base temperature [°C]	0.5	-5, +5
SMFMN	Minimum melt factor on December 21 in Northern Hemesphier(mm H2O/day-°C)	4.5	0, 10
SMFMX	Maximum melt factor on June 21 in Northern Hemesphier (mm H2O/day-°C)	4.5	0, 10
TIMP	Snow temperature lag factor	1	0, 1
SNO50COV	Fraction of snow volume represented by SNO100 that corresponds to 50 snow cover	0.5	0-1
SNOCOVMX	Threshold depth of snow at 100 coverage (mm H2O)	0	0-500
ALPHA-BF	Baseflow recession constant	0.048	0, 1
GW_DELAY	Delay time for aquifer recharge (days)	0	0, 500

After setting the related parameters to adjust low flow, the model was automatically calibrated to determine snow melt parameters at the subbasin scale (Method 2).

The parameters resulting from the automatic calibration were modified on a finer scale for the elevation bands above the $ELA_{0,}$ as an accumulation zone or glacier, and below the ELA_0, as an ablation zone with seasonal snow, separately (Method 3). The melt parameters for the elevation bands were adjusted in order to match the observed and simulated average monthly flow curves and then the parameters were optimized by automatic model calibration using SUFI2. Briefly, model calibration consists of three main steps. First, parameters were automatically calibrated for an entire basin; so that, the snow melt parameters were uniform for all elevation bands and subbasins (Method 1). In the next step, the parameters related to snow/ice melt such as snow melt temperature; maximum melt factor, minimum melt factor, and temperature lag factor

were calibrated automatically for each subbasin (Method 2). In the third step, the results were improved by calibrating the model for snow melt parameters for elevation bands-subbasin (Method 3). Model performance was tested in some of the smaller subbasins first and then extended into the larger subbasins to test the hypothesis that the hydrologic significance of meltwater may be negligible at the macro scale despite the presence of large glaciers in the headwaters area (Immerzeel, 2008; Rees and Collins, 2006).

Calibration and validation were evaluated using the coefficient of determination (R^2), the Nash Sutcliffe Coefficient of Efficiency (NSE) (Nash and Sutcliffe, 1970) and the Percent Bias (PBIAS). R^2 represents the percent of the data that is the closest to the line of best fit. R^2 ranges from 0 to 1.0; higher values indicate better model performance in predicting the variations of observed data. R^2 is computed as shown in equation 1:

$$R^2 = \left(\frac{\sum_{i=1}^{n}(o_i - \bar{o})(p_i - \bar{p})}{\sqrt{\sum_{i=1}^{n}(o_i - \bar{o})^2}\ \sqrt{\sum_{i=1}^{n}(p_i - \bar{p})^2}} \right)^2 \qquad \text{Eq. 1. 7}$$

where o_i is observed data and p_i is simulated variables.

NSE indicates how well the plot of observed versus simulated data fits the 1:1 line. NSE ranges from $-\infty$ to 1.0, where 1.0 indicates a perfect fit and negative values indicate that average values of observed data is more reliable than the model predictions. Positive values show a better match of observed data and predicted values. NSE is calculated with equation 1.8:

$$NSE = 1 - \frac{\sum_{i=1}^{n}(o_i - p_i)^2}{\sum_{i=1}^{n}(o_i - \bar{o})^2} \qquad \text{Eq. 1. 8}$$

PBIAS measures the average tendency of the simulated data to be larger or smaller than their observed counterparts (Gupta et al., 1999). The optimal value of PBIAS is 0.0, with low values indicating accurate model simulation in term of magnitude. Positive values indicate model underestimation bias, and negative values indicate model overestimation bias (Gupta et al., 1999). It is calculated as:

$$PBIAS = \left[\frac{\sum_{i=1}^{n}(o_i - p_i) * 100}{\sum_{i=1}^{n} o_i}\right] \quad \text{Eq. 1. 9}$$

According to Moriasi et al. (2007), model performance in prediction of monthly flow can be classified as satisfactory if $0.5 < NSE \leq 0.65$ and $\pm 15 \leq PBIAS < \pm 25$; good if $0.65 < NSE \leq 0.75$ and $\pm 10 \leq PBIAS < \pm 15$; and very good if $0.75 < NSE \leq 1.00$ and $PBIAS \leq \pm 10$. Model performance is unsatisfactory if $NSE \leq 0.5$ and $PBIAS \geq \pm 25$.

Results and Discussion

Uncalibrated Model

For an initial evaluation of the model performance and to assess the importance of orographic precipitation and temperature in both the presence and absence of glaciers in the basin, SWAT was run without calibration for three scenarios: with elevation bands and glaciers (U-EB-G), without elevation bands but with glaciers (U-NEB-G), and with elevation bands but without glaciers (U-EB-NG) for the Narayani, Rhone, and Mendoza River Basins. While there were considerable differences in model performance among the different scenarios and regions, different degrees of accuracy in predicting the

monthly streamflow were also seen depending on the climate type and hydrologic regime of the river basin.

Overall, U-EB-G showed better results when compared with U-NEB-G with the exception of Narayani River Basin. At gage 159, the main outlet from the watershed in the Narayani River Basin, the R^2 and NSE values dropped from 0.90 and 0.81 for U-NEB-G, to 0.90 and 0.53, for U-EB-G, respectively. However, varying parameters by elevation band improved the prediction of stream flow at the other gauging stations (96, 122 and 123) which were predominantly in mountainous areas.

The SWAT model was originally designed to simulate processes in large-scale ungauged basins with little or no calibration (Arnold et al., 1998). As expected, the uncalibrated model (U-EB-G) showed good performance in simulation of monthly streamflow from Rhone and Narayani River Basins with R^2 over 0.75 and NSE over 0.55 (with exception at Reach 2, Rhone River Basin).

The unsatisfactory monthly flow simulation of Mendoza River Basin could be due to high inter-annual seasonal variability of precipitation in South America under the influence of the Southern Annular Mode (SAM) and El Nino-Southern Oscillation (ENSO) which make it more challenging to predict the monthly streamflow relying on the uncalibrated model (Masiokas et al., 2010).

Higher R^2 values under U-EB-G in compare to of U-EB-NG shows adding the glaciers improved the model performance in simulation of seasonality of monthly flow whereas the volume of monthly flow considerably biased (Table 1. 9). This indicates that glacier ablation in high altitudes has an important effect on runoff regime.

Finally, it can be seen that the uncalibrated model (U-EB-G) had much better performance in simulation of monthly flow from Narayani River Basin in compare to the simulated flow from Mendoza and Rhone River Basins with dry summer and snow/glacier melt dominant summer flow. A possible reason could be dimming the influence of glacier melt on runoff by summer monsoon precipitation in Narayani River Basin which leads to predictable seasonal flow by only rainfall-runoff model.

Table 1. 9. Evaluation coefficients for the default parameters scenarios

	Reach#	U-NEB-G			U-EB-NG			U-EB-G		
		R^2	NSE	PBIAS	R^2	NSE	PBIAS	R^2	NSE	PBIAS
Narayani	96	0.87	0.35	+58.2	0.76	0.72	-19.2	0.78	0.66	-35.0
	122	0.83	0.00	-19.0	0.77	0.54	+39.4	0.85	0.78	+22.6
	123	0.86	0.18	-44.4	0.87	0.84	+16.9	0.90	0.88	+2.8
	159	0.90	0.81	+29.2	0.86	0.51	+45.9	0.90	0.53	+36.3
Rhone	2	0.80	-1.56	-128.5	0. 36	0.32	+12.4	0.87	-0.19	-87.7
	4	0.68	-0.34	-62.0	0.74	0.64	+10.8	0.78	0.55	-15.7
	14	0.82	-0.82	-92.1	0.64	0.61	+0.1	0.89	0.63	-38.3
	23	0.91	-1.97	-153.6	0.87	0.84	+19.9	0.95	0.93	-8.2
Mendoza	84	0.73	-10.85	-191.8	0.36	0.29	+27.5	0.76	0.07	-51.5
	86	0.30	-14.4	-185.1	0.16	-0.36	-2.5	0.42	-1.41	-67.8
	90	0.51	-25.56	-334.4	0.31	-0.23	-3.4	0.61	-4.57	-146.4
	82	0.54	-6.11	-88.9	0.44	0.29	+14.1	0.53	0.17	-31.4
	79	0.46	-10.87	-207.7	0.26	0.20	+14.3	0.31	-3.55	-140.0

Model Calibration and Validation

The calibration process and improvement in model performance under the non-distributed (Method 1) and distributed snow melt methods (Methods 2 and 3) are discussed in detail for gauged subbasins with the largest percentage of glacial area. For all the other gauged subbasins only the statistical results are presented. The non-glaciated and snow free gauged watersheds located at lowlands and glaciated subbasins

with insufficient flow data, as well as dammed subbasins, were ignored in the model calibration. Calibration and validation results for all watersheds are given in Table 1. 10.

Table 1. 10. Evaluation coefficients under the calibration parameters scenario for calibration and validation periods.

		Calibration										Validation			
		R^2			NSE			PBIAS			Performance	R^2	NSE	PBIAS	Performance
	Reach#	1*	2	3	1	2	3	1	2	3	3		3		
Narayani	96	0.81		0.83	0.81		0.83	-6.6		+0.5	Very good				
	122	0.85	0.83	0.83	0.77	0.72	0.73	+10.5	+27.3	+25.0	Satisfactory				
	123	0.88	0.88	0.88	0.85	0.87	0.87	+2.1	+10.1	+8.6	Very good	0.79	0.78	+22.5	Satisfactory
	133			0.80			0.70			+18.0	Good				
	159	0.91		0.89	0.69		0.70	+39.5		+33.8	Unsatisfactory	0.78	0.70	+12.9	Good
Vakhsh	72			0.92			0.80			+2.8	Very good				
	109			0.92			0.72			-7.4	Good	0.89	0.73	-8.15	Good
	133			0.91			0.87			+9.1	Very good				
Rhone	2	0.82	0.88	0.85	0.76	0.75	0.83	-24.7	-20.96	-13.2	Very good	0.86	0.81	-21.6	Satisfactory
	4	0.81	0.81	0.81	0.75	0.74	0.74	2.7	-5.83	+5.5	Very good	0.76	0.61	-9.4	Good
	14	0.86	0.87	0.91	0.85	0.87	0.91	-7.3	-6.61	-1.5	Very good	0.86	0.82	-16.1	Satisfactory
	23	0.95	0.96	0.95	0.86	0.93	0.95	+25.9	-4.61	+2.2	Very good	0.95	0.89	-13.1	Good
Mendoza	84	0.76	0.78	0.78	0.70	0.76	0.77	+22.5	+5.3	+5.0	Very good	0.80	0.71	+6.2	Good
	86	0.72		0.70	0.65		0.56	-2.9		-14.3	Satisfactory	0.69	0.24	-21.7	Unsatisfactory
	90	0.66	0.63	0.65	0.32	0.57	0.59	-15.8	+7.2	+3.6	Satisfactory	0.43	-0.24	+5.8	Unsatisfactory
	82	0.60		0.62	0.52		0.58	+7.2		+7.9	Satisfactory	0.61	0.59	+12.5	Satisfactory
	79	0.45		0.54	0.28		0.50	-17.9		+5.5	Satisfactory	0.57	0.46	-2.1	Unsatisfactory
Chile	6		0.67	0.67		0.66	0.66		+4.2	+3.3	Good	0.44	0.34	+50.0	Unsatisfactory
	66		0.58	0.59		0.43	0.47		+15.3	+8.1	Unsatisfactory	0.45	0.21	-18.7	Unsatisfactory
	5			0.75			0.61			+33	Unsatisfactory	0.58	0.38	+41.0	Unsatisfactory
	7			0.72			0.62			+10.7	Satisfactory	0.60	0.22	+4.7	Unsatisfactory
	9			0.62			0.41			-32.4	Unsatisfactory	0.50	0.31	+40.2	Unsatisfactory
	14			0.71			0.70			+6.7	Satisfactory	0.50	0.21	+51.4	Unsatisfactory
	37			0.43			0.42			+4.3	Unsatisfactory	0.35	0.11	+46.3	Unsatisfactory
	38			0.51			0.29			-42.7	Unsatisfactory	0.30	0.15	+44.0	Unsatisfactory
	39			0.70			0.33			+38	Unsatisfactory	0.51	0.00	+41.2	Unsatisfactory
	40			0.63			0.53			+13.7	Satisfactory	0.55	0.50	+11.0	Satisfactory
	55			0.57			0.50			+18.4	Satisfactory	0.48	0.44	-0.2	Unsatisfactory
	59			0.66			0.55			+36.5	Satisfactory	0.57	0.65	+31.0	Unsatisfactory
	76			0.62			0.33			+8.8	Unsatisfactory	0.30	-0.14	-8.3	Unsatisfactory
	77			0.57			0.41			-6.0	Unsatisfactory				
	86			0.68			0.66			+6.7	Good	0.64	0.57	+2.6	Satisfactory
	100			0.56			0.53			+3.8	Satisfactory	0.57	0.41	-1.8	Unsatisfactory
	108			0.68			0.56			+34.2	Unsatisfactory	0.44	0.41	+39	Unsatisfactory

* 1, 2 and 3 indicates Method 1, Method 2 and Method 3.

Rhone River Basin

SWAT was calibrated with observed monthly stream flow from four gauging stations at Reaches 2, 4, 14, and 23. Table 1. 11 shows calibration parameter values in elevation band scale (Method 3), the value of each parameter at every subbasin, an average value for the parameter and the range of the parameter across all subbasins for 53 calibration parameters, 13 subbasins and 10 elevation bands.

Figure 1. 18 shows the observed and the flows simulated using the three methods described in Section 1.4 at different gauge stations. In the highly glaciated subbasins 2 and 23, Method 1 (snow melt parameters uniform across the basin and elevation bands) resulted in high PBIAS value in compare with the flow from other subbasins. Method 2 shows considerable improvement in predicted flow from Reach 23 while for Reach 2, Method 3 generated the best result (Table 1. 10). It can be justified by different distribution of glaciers in the drainage area of Reach 2 and Reach 23. The glaciers of drainage area of Reach 23 have been dominantly discretized by subbasin boundaries but it was impossible for Reach 2 due to the extended glacier area to the lower elevations. So, it can be concluded that Method2 can be used confidentially while glacier area is discretized from glacier free area by subbasins.

Like Reach 2, Method 3 led to best results for Reach 14 while Method 1 and Method 2 showed similar results to each other (R^2: 0.86 and 0.87, NSE: 0.85 and 0.87 and PBIAS: -6.61 and -7.3). Both R^2 and NSE of Method 3 were improved to 0.91 from 0.87 by Method 2. This can be again justified by the distribution of glacier through the

subbasin which is undividable by subbasins boundary; so, melt parameter distribution by elevation band has a key role in this type of subbasins.

There is no improvement in the simulated flow by Method 1, Method 2 and Method 3 from glacier free drainage area of Reach 4 (R^2=0.81 and NSE=0.74 and PBIAS range of +2.7 to -5.8 for three methods).

Figure 1. 18 shows that the observed mean monthly flow curves of Reach 23 and 14 are matched to the simulated mean monthly flow by Method 3. This degree of accuracy in simulation of the seasonal pattern of monthly flow is only achievable by adjustment of melt parameters based on elevation bands (Method 3). As an example, the variability of monthly flow from Reach 23 (65 percent glaciered area) changes with a change in SMFMX from 2 to 8 mm/d-1 ºC-1, in the upper elevation bands. Additionally, SMFMX in lower elevation bands had more influence on the rising limb of the flow curve whereas the descending limb was more sensitive to SMFMX changes in the higher elevation bands (Figure 1. 19). This indicates that the late spring flow is under the influence of snow melt at lower elevations and late summer flow is controlled by glacier melt at higher elevations. This can also be investigated by analyzing the melting lag time at the elevation bands. Seasonal melting from October 1998 to October 1999 from each of the elevation bands of Subbasin 12 as an example of a typical subbasin with a wide range of elevation and 10 elevation bands is presented in Figure 1. 20-a, for glacier free elevation bands with seasonal snow cover; and in Figure 1. 20-b for high elevation bands with permanent snow cover or glacier. In Figure 1. 20-a snowpack in the elevation bands

1, 2, 3, 4 and 5 is completely vanished by mid-August whereas in Figure 1. 20-b the glacier ablation reaches its peak in August and continues through October.

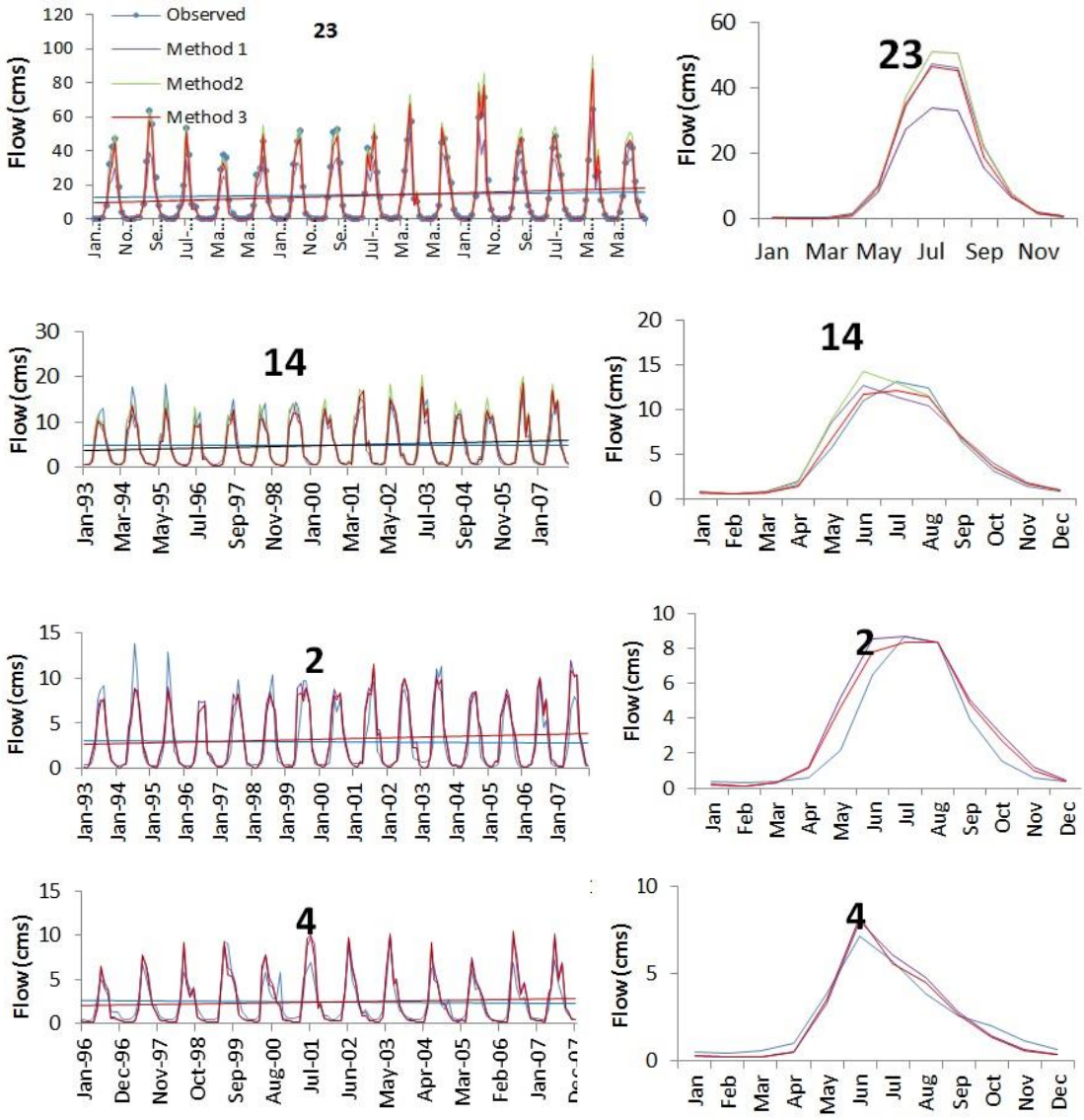

Figure 1. 18. Observed and simulated monthly runoff and mean monthly runoff using SWAT with different melt processes for the calibration period at Rhone River Basin.

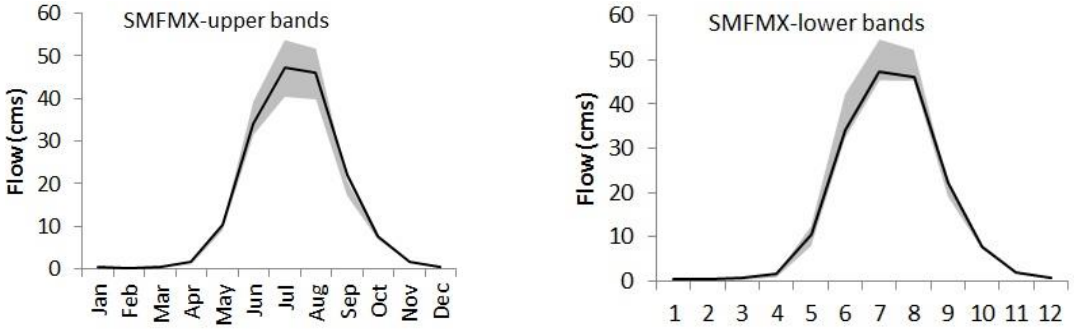

Figure 1. 19. Variability of monthly flow from Reach 23 (65 glaciered area) to SMFMX changes (2 to 8 mm/d^{-1} c^{-1}) in the upper elevation bands and lower elevation bands.

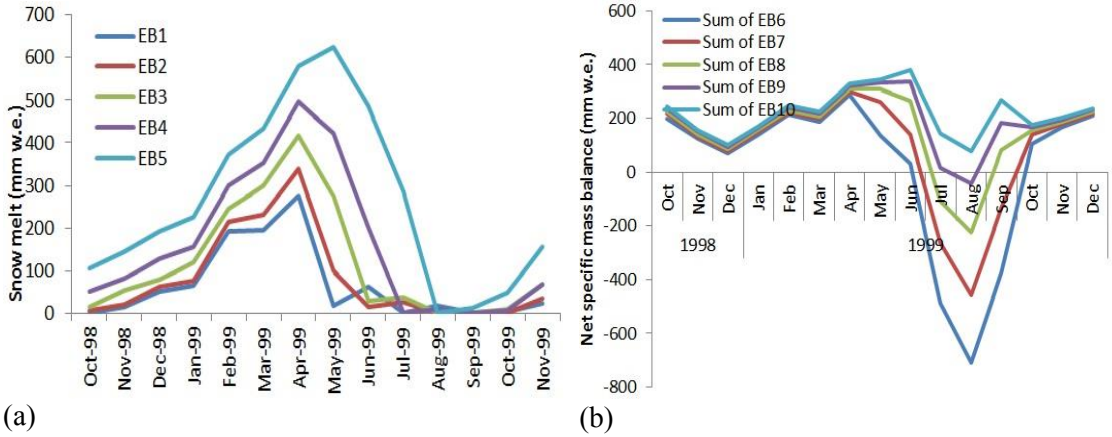

Figure 1. 20. Seasonal melting from the elevation bands of Subbasin 12 from October 1998 to October 1999; a) glacier free elevation bands with seasonal snow cover; b) high elevation bands with permanent snow cover or glacier. In (a) a snowpack in the elevation bands 1, 2, 3, 4 and 5 is completely vanished by mid-August whereas in (b) the glacier ablation reaches the pick at August and continues to October.

Table 1. 11. Calibration parameters for subbasins and elevation bans (Method 3), Rhone River Basin.

Rhone	Subbasin #															
Parameter	1	2	4	5	12	14	8	15	16	17	20	21	23	Ave.	Min.	Max.
SFTMP1	1	-1	0	0	0	0	2	2	2	2	2	2	2	1.08	-1	2
SFTMP2	1	-1	0	0	0	0	2	2	2	2	2	2	2	1.08	-1	2
SFTMP3	1	-1	0	0	0	0	2	2	2	2	2	2	2	1.08	-1	2
SFTMP4	1	0	0	0	0	0	2	2	2	2	2	2	2	1.15	0	2
SFTMP5	1	0	0	0	2	2	2	2	2	2	2	2	2	1.46	0	2
SFTMP6	2	2	1	1	2	2	2	2	2	2	2	2	2	1.85	1	2
SFTMP7	3	2	1	1	2	2	2	2	2	2	2	2	2	1.92	1	3
SFTMP8	3	2	1	1	2	2		2	2	2	2	2		1.91	1	3
SFTMP9	3	2	1	1	2	2			2	2		2		1.89	1	3
SFTMP10	3	2	1	1	2	2			2	2		2		1.89	1	3
SMTMP1	2	0	0	0	2	2	0	0	0	0	0	0	0	0.46	0	2
SMTMP2	2	0	0	0	2	2	0	0	0	0	0	0	0	0.46	0	2
SMTMP3	2	1	0	0	2	2	0.5	0	0	0	0	0	0	0.58	0	2
SMTMP4	2	1	0	0	2	2	0.5	0.5	0	0	0	0	0	0.62	0	2
SMTMP5	2	1	0	0	2	2	0.5	0.5	0	0	0	0	0	0.62	0	2
SMTMP6	3	1	2	2	2	2	0.5	0.5	0.5	0.5	0.5	0.5	0.5	1.19	0.5	3
SMTMP7	3	3	2	2	2	2	0.5	0.5	0.5	0.5	0.5	0.5	0.5	1.35	0.5	3
SMTMP8	3	3	2	2	2	2		0.5	0.5	0.5	0.5	0.5		1.50	0.5	3
SMTMP9	3	3	2	2	2	2			0.5	0.5		0.5		1.72	0.5	3
SMTMP10	3	3	2	2	2	2			0.5	0.5		0.5		1.72	0.5	3
SMFMX1	3	3	3	3	2	2	4	4	4	4	4	4	4	3.38	2	4
SMFMX2	3	3	3	3	2	2	4	4	4	4	4	4	4	3.38	2	4
SMFMX3	3	3	3	3	2	2	6	4	4	4	4	4	4	3.54	2	6
SMFMX4	3	3	3	3	2	2	6	6	4	4	4	4	4	3.69	2	6
SMFMX5	3	3	3	3	2	2	6	6	4	4	4	4	4	3.54	2	6
SMFMX6	5	5	4	4	6	6	6	6	6	6	6	6	6	5.54	4	6
SMFMX7	5	5	4	4	6	6	6	6	6	6	6	6		5.50	4	6
SMFMX8	5	5	4	4	6	6		6	6	6	6	6		5.45	4	6
SMFMX9	5	5	4	4	6	6			6	6		6		5.33	4	6
SMFMX10	5	5	4	4	6	6			6	6		6		5.33	4	6
SMFMN1	1.5	1.5	2	2	1.5	1.5	4	4	4	4	4	4	4	2.92	1.5	4
SMFMN2	1.5	1.5	2	2	1.5	1.5	4	4	4	4	4	4	4	2.92	1.5	4
SMFMN3	1.5	1.5	2	2	1.5	1.5	5	4	4	4	4	4	4	3.00	1.5	5
SMFMN4	1.5	1.5	2	2	1.5	1.5	5	5	4	4	4	4	4	3.08	1.5	5
SMFMN5	1.5	1.5	2	2	1.5	1.5	5	5	4	4	4	4	4	3.08	1.5	5
SMFMN6	2.5	2.5	2.5	2.5	1.5	1.5	5	5	5	5	5	5	5	3.69	1.5	5

Table 1. 11. Continued

	Subbasin #															
Parameter	1	2	4	5	12	14	8	15	16	17	20	21	23	Ave.	Min.	Max.
SMFMN7	2.5	2.5	2.5	2.5	1.5	1.5	5	5	5	5	5	5		3.58	1.5	5
SMFMN8	2.5	2.5	2.5	2.5	1.5	1.5		5	5	5	5	5		3.45	1.5	5
SMFMN9	2.5	2.5	2.5	2.5	1.5	1.5			5	5		5		3.11	1.5	5
SMFMN10	2.5	2.5	2.5	2.5	1.5	1.5			5	5		5		3.11	1.5	5
TIMP1	0.6	0.6	0.5	0.5	0.5	0.5	0.7	0.7	0.7	0.7	0.7	0.7	0.7	0.62	0.5	0.7
TIMP2	0.6	0.6	0.5	0.5	0.5	0.5	0.7	0.7	0.7	0.7	0.7	0.7	0.7	0.62	0.5	0.7
TIMP3	0.6	0.6	0.5	0.5	0.5	0.5	0.05	0.7	0.7	0.7	0.7	0.7	0.7	0.57	0.05	0.7
TIMP4	0.6	0.6	0.5	0.5	0.5	0.5	0.05	0.05	0.7	0.7	0.7	0.7	0.7	0.52	0.05	0.7
TIMP5	0.6	0.6	0.1	0.1	0.5	0.5	0.05	0.05	0.7	0.7	0.7	0.7	0.7	0.46	0.05	0.7
TIMP6	0.01	0.01	0.01	0.01	0.01	0.01	0.05	0.05	0.05	0.05	0.05	0.05	0.05	0.03	0.01	0.05
TIMP7	0.01	0.01	0.01	0.01	0.01	0.01	0.05	0.05	0.05	0.05	0.05	0.05		0.03	0.01	0.05
TIMP8	0.01	0.01	0.01	0.01	0.01	0.01		0.05	0.05	0.05	0.05	0.05		0.03	0.01	0.05
TIMP9	0.01	0.01	0.01	0.01	0.01	0.01			0.05	0.05		0.05		0.02	0.01	0.05
TIMP10	0.01	0.01	0.01	0.01	0.01	0.01			0.05	0.05		0.05		0.02	0.01	0.05
ALPHA_BF	0.048	0.048	0.01	0.01	0.048	0.01	0.01	0.048	0.048	0.048	0.048	0.048	0.048	0.036	0.01	0.48
PLAPS	300	300	0	0	300	400	100	100	100	100	100	100	100	267	0	400
TLAPS	-7	-7	-5	-5	-7	-7	-7	-7	-7	-7	-7	-7	-7	-6.69	-5	-7

Narayani River Basin

SWAT was calibrated using the observed monthly stream flow from four gauging stations at reaches 96, 122, 123, 133 and 159 (main outlet). The data of gauged, non-glaciated and snow free watersheds located in the lowlands were ignored for model calibration. Table A. 1 (Appendix A) shows calibration parameter values in elevation band scale (Method 3) at every subbasin (32 subbasins and 10 elevation bands) for drainage area of Reach 123. Table 1. 12 gives an average value and range for all the parameters across all subbasins for all of the reaches in the watershed, focusing on the calibration reaches.

Figure 1. 21 shows the observed and simulated flows at gauging stations 122, 123 and 133. It can be seen from Table 1. 12 that the average values for SMFMX and SMFMN are larger than the obtained values for Rhone River Basin (Table 1. 10).

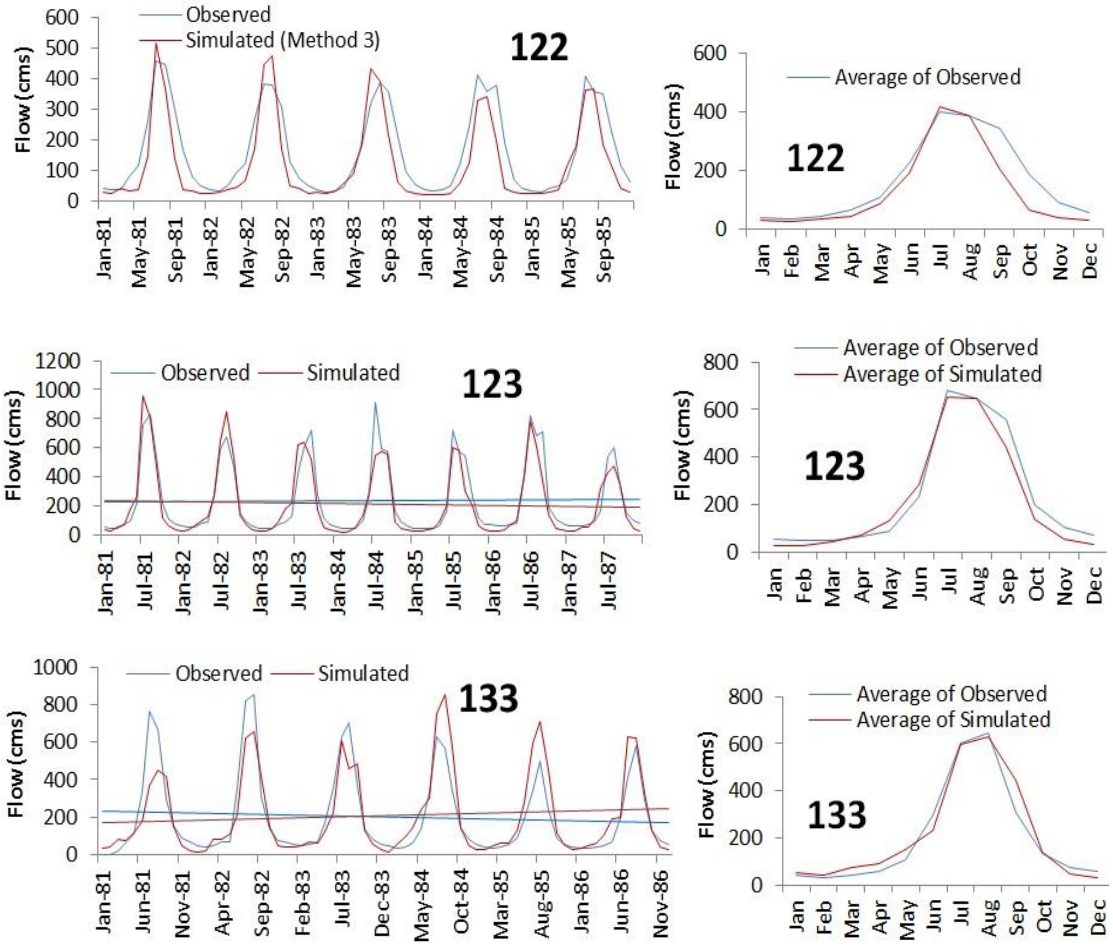

Figure 1. 21. Observed and simulated monthly runoff and mean monthly runoff using SWAT with different melt processes for the calibration period for some of the subbasins of Narayani River Basin.

PBIAS and NSE values in Table 1. 10 indicate same model performance by all three methods based on PBIAS and NSE values. As mentioned in the previous section, a possible reason could be again diminishing the influence of glacier/snow melt on runoff by coincident summer monsoon precipitation in Narayani River Basin which leads to predictable seasonal flow by rainfall-runoff model rather than snow hydrology process. There is although positive biases in predicting the volume of water from all gauge stations which means the model has under-predicted the volume of flow. This systematic bias might be due to underestimated NCEP reanalysis spring/summer precipitation (May-September) in Narayani River basin by 20 percent.

Table 1. 12. Range and mean values of calibration parameters in subbasin-elevation band scale (Method 3), Narayani River Basin

	123			122			133			96			Rest of the basin			Total Basin
Parameter	Ave.	Min.	Max.	Ave.	Min.	Max.	Ave.	Min.	Max.	Ave.	Min.	Max.	Ave.	Min.	Max.	Ave.
SFTMP	2.00	2	2	3.24	2	4	2.04	2	3	1.21	0.28	4	1.98	0.28	4	2.09
SMTMP	0.74	0	2	0.00	0	0	1.58	0	2	0.80	0.5	0.9	1.06	0	2	0.83
SMFMX (1-6)	5.56	5	7	6.62	6	7	4.33	4	6.7	5.15	5	5.6	5.22	4	7	5.38
SMFMX (7-10)	8.03	8	9	9.00	9	9	7.87	6	9	5.88	5	8.5	7.79	5	9	7.71
SMFMN (1-6)	4.04	3.5	6	5.00	5	5	3.96	3	4	4.33	3.8	4.5	4.15	3	6	4.29
SMFMN (7-10)	6.03	6	7	6.76	6	8	5.42	4	7	4.40	4.1	4.5	5.36	4	7	5.59
TIMP(1-6)	0.70	0.7	0.7	0.70	0.7	0.7	0.68	0.27	0.7	0.59	0.5	0.87	0.66	0.27	0.87	0.67
TIMP(7-10)	0.06	0.05	0.06	0.06	0.04	0.2	0.02	0.01	0.04	0.39	0.067	0.5	0.06	0.01	0.5	0.12
ALPHA_BF	0.048	0.048	0.048	0.010	0.010	0.010	0.077	0.048	0.200	0.080	0.037	0.210	0.050	0.048	0.100	0.053
TLAPS								-6.5								
PLAPS		-100			0			-200			-200			-200		

Vakhsh River Basin

SWAT was calibrated with observed monthly stream flow from three gauge stations at Reaches 72, 133 and 109. The data of the gauges at Reach 40 and 85 were ignored during model calibration due to the low quality of the climate data available in the northern part of the basin. Table A. 2 (in Appendix A) shows for each parameter and elevation band combination (Method 3) in subbasin 133, the value of each parameter at every subbasin (26 subbasins and 10 elevation bands). Table 1. 13 gives an average value and range for all the parameters across all subbasins for all of the reaches in the watershed, focusing on the calibration reaches.

The parameter values for Reach 109 (main outlet) do not include the calibration parameters of draining subbasins to Reaches 72 and 133. show the observed and simulated flows at gauges 72, 109 and 133. SMFMX for snow and glacier ranges between 2 to 6 and 4 to 8, respectively. SMFMN ranges between 2 to 5 for snow and 3 to 7 for glaciers. TIMP values were lower in the high elevation bands where the glaciers exist and ranges between 0.036 to 1 with average value between 0.06 for high elevation bands to 0.65 for low elevation bands.

The model had very good performance (Moriasi et al., 2007) in simulation of monthly flow from the glaciered area of the Vakhsh River Basin with PBIAS smaller than 10 percent and NSE greater than 0.72. The major problem in simulation of monthly flow from the Vakhsh River Basin was the lack of data for calibration and the low quality of the climate data, especially in the northern-half part of the river basin. The short calibration period of 2.5 years for Reach 133 was not long enough to capture the

long term variability of the monthly flow. The comparison between observed and simulated monthly flow from the main outlet of the basin (Reach 109) during the validation period indicated that there was good agreement to the observed and simulated streamflow which was verified by PBIAS and NSE -8.15 and 0.73, respectively.

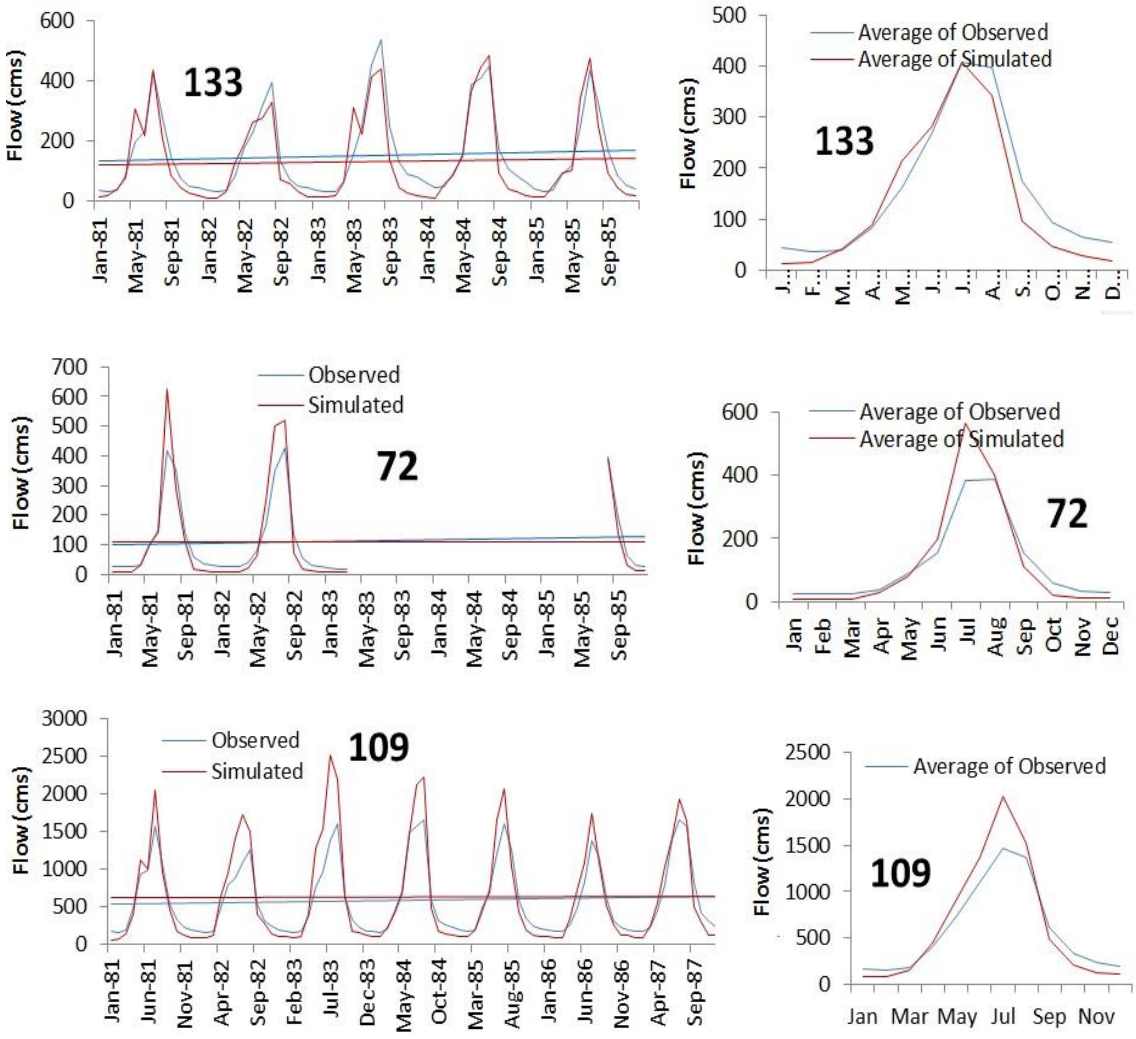

Figure 1. 22. Observed and simulated monthly runoff and mean monthly runoff using SWAT with different melt processes for the calibration period at Vakhsh River Basin

Table 1. 13. Range and mean values of calibration parameters in subbasin-elevation band scale (Method 3), Vakhsh River Basin

Vakhsh	133			72			109			Basin
	Ave.	Min.	Max.	Ave.	Min.	Max.	Ave.	Min.	Max.	Ave.
SFTMP	1.90	1.50	2.00	1.96	1.00	3.00	2.97	1.30	3.00	1.72
SMTMP(1-4)	0.27	0.00	1.00	1.97	0.50	2.00	2.00	2.00	2.00	1.41
SMTMP(5-10)	1.04	0.50	1.50	1.97	0.50	2.00	2.00	2.00	2.00	1.67
SMFMX(1-4)	5.31	5.00	6.00	4.90	4.00	5.00	2.00	2.00	3.00	4.27
SMFMX(5-10)	7.31	7.00	8.00	5.99	4.50	7.00	4.03	4.00	5.50	5.77
SMFMN(1-4)	5.00	5.00	5.00	4.05	4.00	6.00	2.04	2.00	4.00	3.68
SMFMN(5-10)	6.31	6.00	7.00	5.01	4.50	6.00	3.04	3.00	5.00	4.77
TIMP(1-4)	0.54	0.50	0.70	0.71	0.70	1.00	0.70	0.70	0.70	0.65
TIMP(5-10)	0.10	0.03	0.20	0.03	0.01	0.12	0.05	0.05	0.05	0.06
TLAPS	-7.50			-7.80			-7.80			-7.70
PLAPS	500.00			300.00			135.00			312.0
ALPHA_BF	0.020			0.005			0.004			0.01
GW_DELAY	31.00			31.00			60.00			40.7

Mendoza River Basin

SWAT was calibrated with observed monthly stream flow from five gauge stations at reaches 79, 82, 84, 90, and 86. Table A. 3 and Table A. 4 in Appendix A show the calibration parameter values in elevation band scale (Method 3) for drainage area of Reaches 79 and 84. Table 1. 14 gives an average value and range for all the parameters across all subbasins for all of the reaches in the watershed, focusing on the calibration reaches.

SMFMN for snow and glacier ranges between 2 to 3 and 2 to 3.8, respectively. SMFMX ranges between 2 to 4.5 for snow and 2 to 5.4 for glaciers. TIMP values was

higher in the high elevation bands where the glaciers exist and ranges between 0.036 to 1 with average value of 0.005 for high elevation bands and 1 for lower elevation bands.

Model performance for all three snow melt methods are presented in Table 1. 10. Figure 1. 23 shows the observed and simulated flows at the four calibration gauges. Subbasins 84 and 90 were selected to compare the model performance using snow melt Methods 2 and 3. Among the gauged watersheds, the drainage area of Reach 84 has the largest percentage in glaciers. Subbasin 90 is a smaller subbasin and is a good option to show the streamflow response to melt parameter distribution.

There was a negligible improvement in the model performance when using Method 3 over Method 2 in Reach 84 (Figure 1. 23 and Table 1. 10). For Reach 90, the model accuracy was improved 50 percent (PBIAS 3.6 in compare with 7.2) by Method 3. Figure 1. 23 shows that the simulated peaks by Method 3 are match the observed peak flows. This level of accuracy is only achievable by adjusting the melt parameters for seasonal snow and permanent snow for each elevation band since Method 2 was not able to capture the peaks by calibrating the model for many different sets of melt parameters.

Comparison between observed and simulated monthly streamflow during the validation period indicated that the model performance in simulation of monthly flow is unsatisfactory to good by PBIAS values in the range of -2.1 to -12.7 and by NSE values in the range of -0.24 to 0.71.

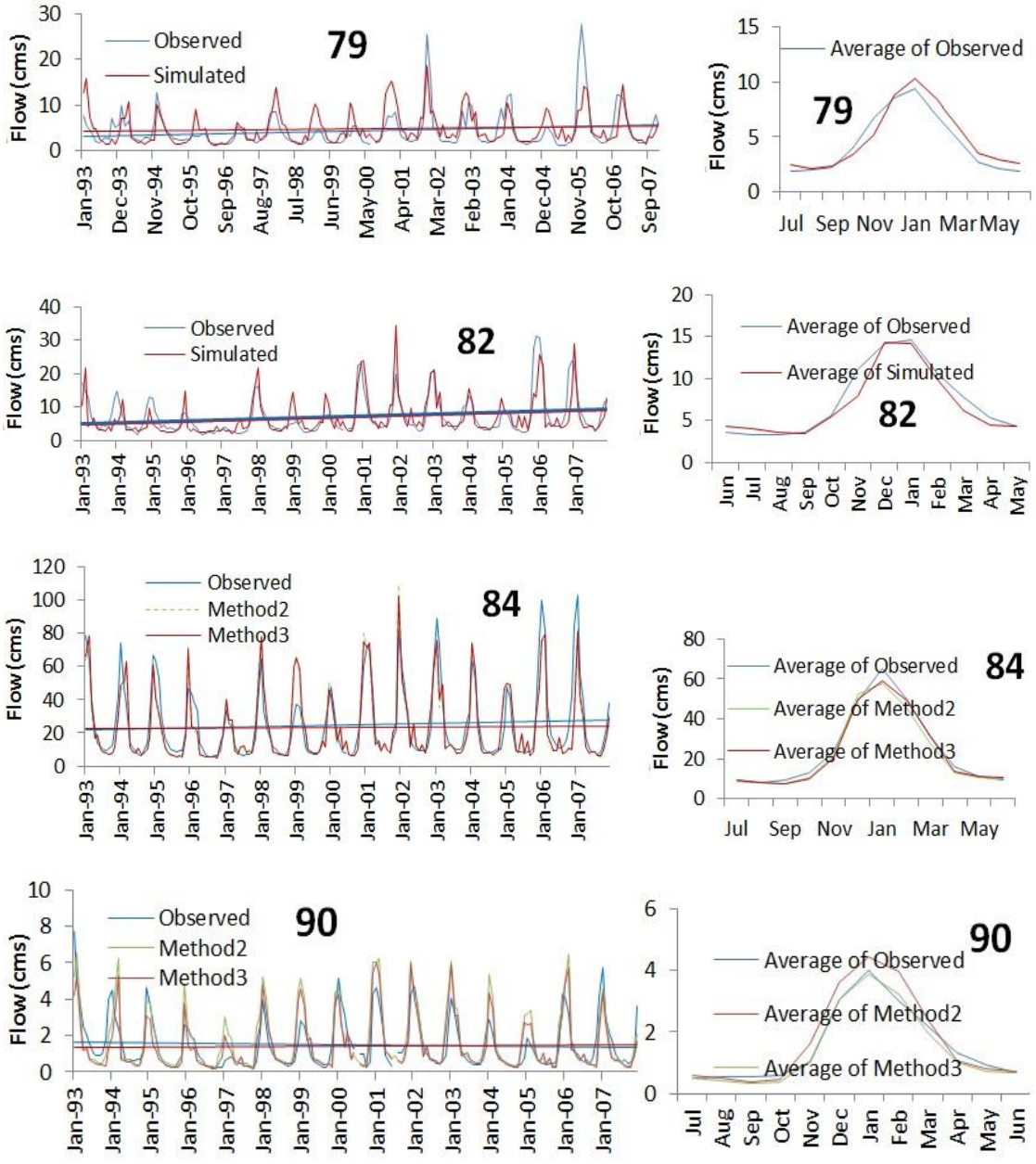

Figure 1. 23. Observed and simulated monthly runoff and mean monthly runoff using SWAT with different melt processes for the calibration period at Mendoza River Basin.

The R^2 and NSE values are generally lower than the values obtained in the Narayani, Vakhsh and Rhone Watersheds. Forecasts of summer runoff take into account

the accumulated snow in the previous winter. Winter precipitation (October to March) inter-annual variability in the Andes is linked to ENSO events which consequently results in a more complex response of streamflow (Waylen and Caviedes, 1990). A cold event of 1996 was linked with scarce snowfall during the winter in the Andes that the1996-1997 summer had below average flows (Figure 1. 23). This La Nina event ended in March 1997 (Compagnucci and Vargas, 1998).

Table 1. 14. Range and mean values of calibration parameters in subbasin-elevation band scale (Method 3), Mendoza River Basin.

90			84			82				79			Other subbasins		
			Ave.	Min.	Max.	Ave.	Min.	Max.		Ave.	Min.	Max.	Ave.	Min.	Max.
SFTMP(1-5)	0.00	SFTMP	2.11	1.00	1.00	2.60	2.00	3.00	SFTMP	2.74	2.00	4.00	2.02	2.00	3.00
SFTMP(3-5)	3.00	SMTMP(1-3)	2.54	2.00	2.00	2.50	2.00	3.00	SMTMP	2.40	1.00	3.80	3.00	2.00	4.00
SFTMP(6-10)	4.20	SMTMP(4-10)	3.30	3.00	3.00	2.70	2.00	4.00	SMFMN(1-6)	2.48	2.30	2.50	2.02	2.00	3.00
SMTMP(1-2)	-0.50	SMFMN(1-6)	2.59	2.30	2.30	2.60	2.00	3.00	SMFMN(7-10)	2.85	2.50	3.00	2.91	2.00	3.00
SMTMP(3-5)	3.70	SMFMN(7-10)	3.88	3.80	3.80	3.20	2.00	3.50	SMFMX(1-6)	3.00	3.00	3.00	2.71	2.00	3.00
SMTMP(6-10)	4.70	SMFMX(1-6)	2.87	2.50	3.50	3.55	2.00	4.50	SMFMX(7-10)	4.00	4.00	4.00	3.02	3.00	4.00
SMFMN(1-5)	2.60	SMFMX(7-10)	4.20	3.60	4.60	3.55	2.00	4.50	TIMP(1-6)	0.52	0.40	0.60	0.27	0.20	1.00
SMFMN(6-10)	3.60	TIMP(1-6)	0.44	0.44	0.44	0.05	0.01	0.10	TIMP(7-10)	0.14	0.005	0.30	0.20	0.01	0.20
SMFMX(1-2)	1.80	TIMP(7-10)	0.14	0.07	0.07	0.05	0.01	0.10							
SMFMX(3-6)	2.10														
SMFMX(7-10)	5.40														
TIMP(1-2)	0.30														
TIMP(3-5)	0.25														
TIMP(6-10)	0.005														
TLAPS	-6.70			-7.3			-7				-6.9			-7	
PLAPS	635		180	80	365		-150				-300		71	21	123
ALPHA_BF	0.017			0.006			0.010				0.010			0.009	

Central Chile

SWAT was calibrated with the observed monthly stream flow from 16 gauge stations at Reaches 5, 6, 7, 9, 14, 37, 38, 39, 40, 55, 59, 66, 76, 86, 100, and 108. Table A. 5 and Table A. 6 (Appendix A) show the calibration parameter values in elevation band scale (Method 3) for drainage area of Reaches 5 and 66. Table 1. 15 gives an average value and range for all the parameters across all subbasins for all of the reaches in the watershed, focusing on the calibration reaches.

SMFMN for snow and glacier ranges between 2 to 7. SMFMX ranges between 2 to 6.25 for snow and 3 to 8 for glaciers. TIMP ranges between 0.01 to 1 with average value of 0.5 for high elevation bands and 0.78 for lower elevation bands.

Model performance measures for Methods 2 and 3 are presented in Table 1. 10. Figure 1. 24 shows the observed and simulated flows at gauges 6, 7, 14, 66, 55, 40, 76 and 86. Subbasins 6 and 66 were selected to compare the model performance of Methods 2 and 3.

Improvement of model performance by Method 3 was negligible when compared to Method 2 in simulation of monthly flow from Reach 6 (Figure 1. 24 and Table 1. 10). Like subbasin 4 and 5 in Rhone River Basin, subbasin 6 and its drainage area is glacier free and melt parameter distribution has no effect on streamflow simulation (Figure 1. 24). The model accuracy improved 47 percent (PBIAS 8.1 in compare with 15.3) in simulation of volume of flow from Reach 66 by Method3. In Figure 1. 24 the simulated peaks by Method3 matched the observed peak flows while Method 2 was unsuccessful to capture the peaks.

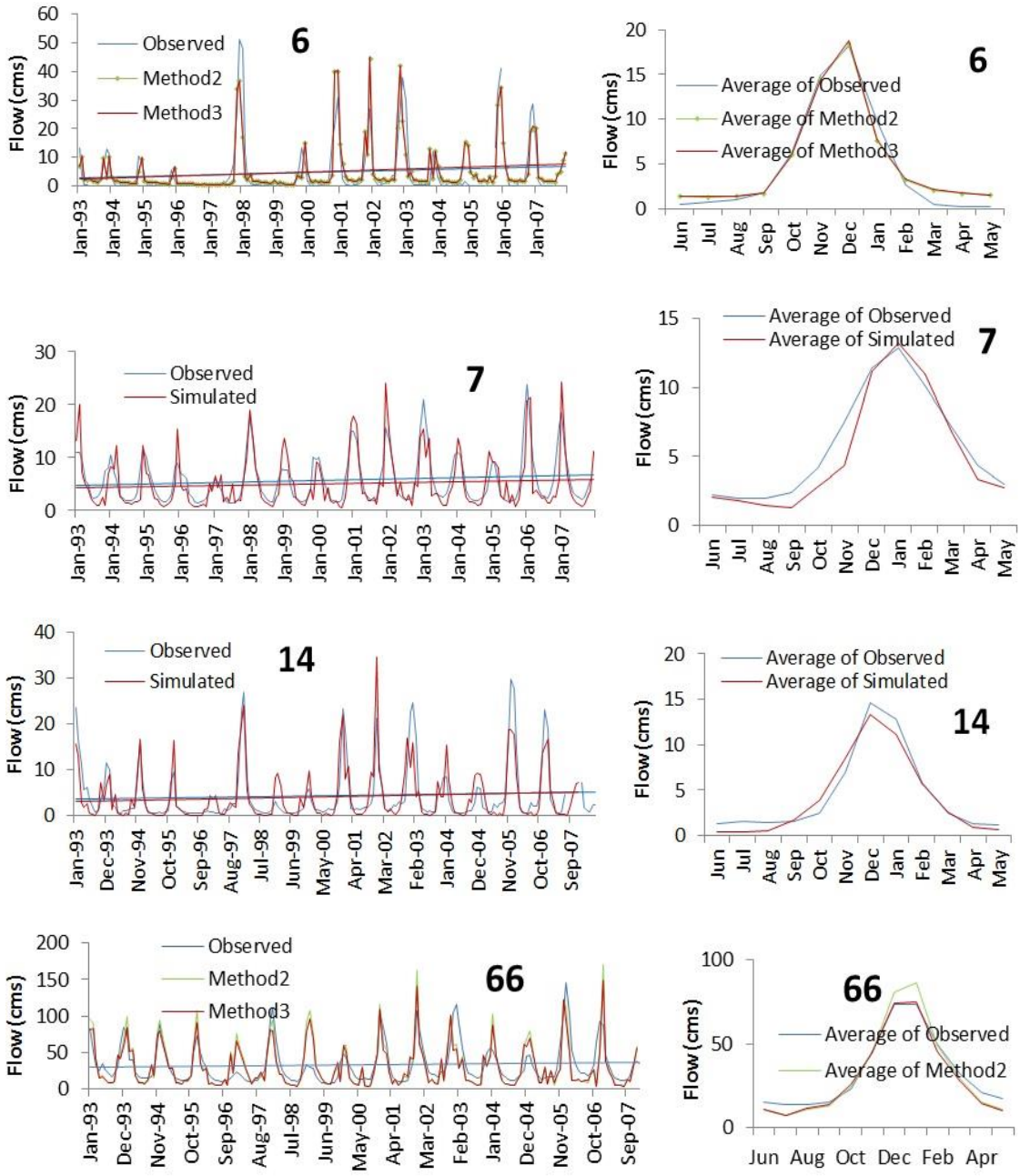

Figure 1. 24. Observed and simulated monthly runoff and mean monthly runoff using SWAT with different melt processes for the calibration period for some of the gauged subbasins of Chilean River Basins.

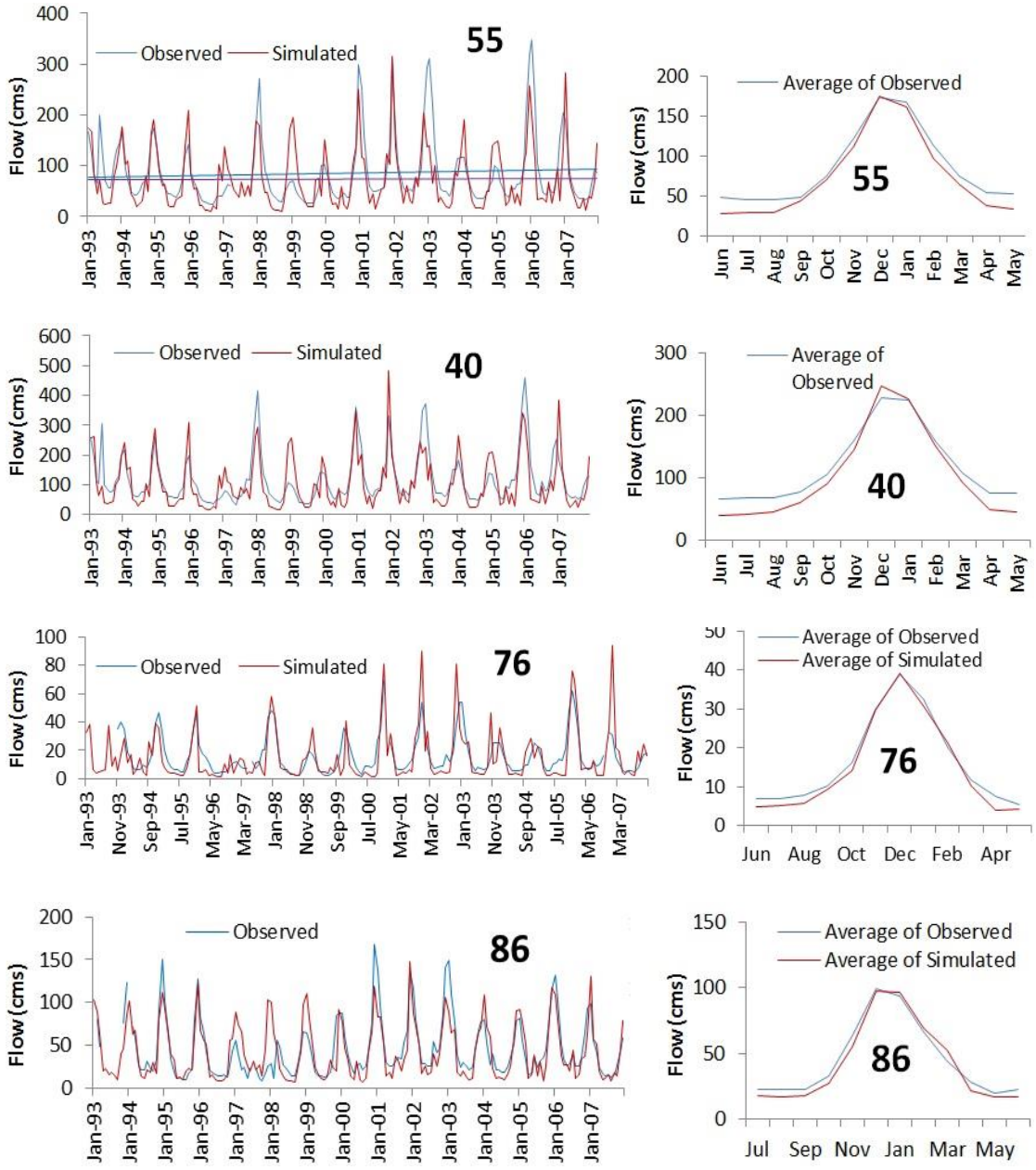

Figure 1. 24. Continued

The comparison between observed and simulated monthly flow during validation period indicates poor to satisfactory simulation with R^2 between 0.30 and 0.64 and NSE between -0.14 and 0.57. The R^2 and NSE values are generally lower than those values

obtained in simulation of monthly flow from the other river basins in this study. Winter precipitation (October to March) inter-annual variability in the Andes is linked to ENSO events and consequently reveals a more complex response of streamflow (Waylen and Caviedes, 1990) which may explain poor model performance in simulation of seasonal flow variability. The major problem in simulation of monthly flows was under prediction of flow during the winter whereas simulated summer flow is in better agreement with observed flow.

Table 1. 15. Range and mean values of calibration parameters in subbasin-elevation band scale (Method3), Central dry Andes of Chile.

Gauged Reach#	37-38-39			55-66-59			76-86-77			108			100			Total basin		
	Ave.	Min.	Max.	Ave.	Min.	Max.	Ave.	Min.	Max.				Ave.	Min.	Max.	Ave.	Min.	Max.
SFTMP	1.0	1.0	1.0	3.0	3.0	3.0	0.88	0.0	3.0	SFTMP	-2.0	SFTMP (1-2)	0.0	0.0	0.0	0.77	-4.6	3.0
SMTMP (1-6)	2.44	0.5	4.0	0.83	0.0	1.0	0.65	0.0	1.0	SMTMP	1.0	SFTMP (3-6)	1.0	1.0	1.0	1.01	-4.6	3.0
SMTMP (7-10)	3.00	0.5	5.0	2.83	2.0	3.0	1.47	0.5	2.0	SMFMX	4.0	SFTMP (7-10)	4.0	4.0	4.0	1.14	-4.6	3.0
SMFMX (1-6)	2.28	2.0	4.5	4.17	4.0	7.0	4.35	4.0	5.0	SMFMN	5.0	SMTMP (1-2)	0.0	0.0	0.0	0.42	-3.0	4.0
SMFMX (7-10)	3.39	2.0	4.5	6.06	6.0	7.0	5.47	4.5	6.0	TIMP	0.50	SMTMP (3-6)	-3.0	-3.0	-3.0	0.90	-1.0	4.0
SMFMN (1-6)	3.06	2.0	4.5	5.83	5.0	6.0	4.82	4.5	5.0			SMTMP (7-10)	-3.0	-3.0	-3.0	1.66	0.5	5.0
SMFMN (7-10)	4.17	3.0	6.0	7.0	7.0	7.0	5.65	4.5	7.0			SMFMN (1-2)	4.0	4.0	4.0	4.07	2.0	6.0
TIMP (1-6)	0.333	0.10	1.0	0.667	0.50	0.70	0.61	0.2	1.0			SMFMN (3-6)	5.0	5.0	5.0	4.06	2.0	6.25
TIMP (7-10)	0.147	0.01	1.0	0.012	0.01	0.05	0.36	0.01	1.0			SMFMN (7-10)	5.0	5.0	5.0	4.93	2.0	7.0
												SMFMX (1-2)	5.0	5.0	5.0	4.68	2.0	6.0
												SMFMX (3-6)	5.5	5.0	6.0	4.64	2.0	6.25
												SMFMX (7-10)	5.5	5.0	6.0	5.38	3.0	8.0
												TIMP(1-2)	0.9	0.8	1.0	0.78	0.1	1.0
												TIMP(3-6)	0.75	0.5	1.0	0.74	0.09	1.0
												TIMP(7-10)	0.51	0.01	1.0	0.50	0.01	1.0

Summary, Conclusions, and Future Works

Treating the glaciered and un-glaciered areas in the watersheds separately, significantly improved the SWAT model performance in simulation of volume and seasonality of runoff in glaciered areas. Spatial and temporal variations of melt rates mainly depend on the spatial and temporal variations of melt factors in hydro-glacial models. While temporal variations of melt factors have been considered in the SWAT model in the past, there has been no consideration of spatial variations in melt factors and lag time factor which are directly influenced by surface type (i.e. snow and ice). In this study, these spatial variations were specifically taken into account.

SWAT performance was evaluated for accuracy in simulation of runoff from glaciated areas with three snow melt algorithms. Different degrees of melt parameter distribution across the basin were considered: lumped (Method 1), subbasin scale (Method 2), subbasin-elevation band scale (Method 3).

The results revealed that the performance of the SWAT model was improved using Method 3 in comparison with the other methods in terms of simulation of runoff seasonality and volume in the five river basins. Method 3 was more advantageous than Method 2 where the glaciers contribution was non-uniform across the subbasins. Analyzing the melt parameter variation for the same elevation band across the subbasins (horizontal variations) showed less variability than the variations across the elevation bands of an individual subbasin (vertical variations) which implies the model well considers the vertical variation of melt vs. its horizontal variations which is dominantly

controlled by solar radiation variations due to aspect and slope. For glacier free areas no improvement were considered.

Model accuracy in simulation of seasonal cycles of runoff was enhanced by determining the melt parameters for glaciers (high altitude elevation bands) and seasonal snow (low altitude elevation bands) separately (Method 3). This could be of considering the late spring flow from melting seasonal snow and late summer flow sources from glacier melt at high altitudes explicitly. It can be concluded that the descending limb of the flow curve in glaciered subbasins is only under the influence of glacier melt at high elevation bands and consequently is adjusted by melt parameters of higher elevation bands. Knowing this, the seasonality of flow can be adjusted with high accuracy.

Model performance using the different melt algorithms also depends on the climate of a river basin. Significance of melt water may be negligible when the melt season coincides with monsoon precipitation, so there was no significance different in the simulation results by the three melt algorithms where monsoons are a factor. For the river basins in the central Andes, applying Method 3 considerably improved the model performance in simulation of runoff volume in comparison with Methods 1 and 2 while seasonality of runoff did not show any improvement. This may be due to high interannual and annual variability of flow in these regions which is more dominated by rainfall-runoff relationships than the snow melt. As a conclusion, considering the spatial variations of associated melt parameters, significantly improves the SWAT performance in simulation of runoff volume and its seasonal variation in highly glaciated river basins.

While the distributed process-based energy budget models have been tested in the SWAT model, no studies have been done to incorporate enhanced temperature-index models to SWAT (Hock, 2003). This method is advantageous when incorporated to a distributed hydrologic model (Hock, 2003). Therefore, incorporating the enhanced temperature-index model to the modified snow algorithm of SWAT can be an objective of the future studies on enhancing the SWAT snow hydrologic process.

CHAPTER II

APPLICATION OF THE SWAT MODEL IN MASS BALANCE MODELLING OF INDIVIDUAL GLACIERS AT THE CATCHMENT SCALE

Overview

The application of a temperature-index melt model was presented coupled with a complex, semi-distributed physically based hydrologic model, Soil and Water Assessment Tool (SWAT), for simulation of mass budget and equilibrium line altitude (ELA) of three glaciers: Rhone and Gries glaciers in the Alps, Switzerland and Abramov glacier in the Pamir Alay in Kyrgyzstan. Generally, there are no data available to calibrate and evaluate the model simulations of glaciered catchments, as they are often located in remote areas. Therefore, the main purpose of this study is glacier mass balance and runoff simulation where limited amount of data is available. Model performance was examined in simulation of annual glacier mass balance when calibrating the model for combination of ELA and runoff data in comparison with applying runoff data alone. The results did not show considerable improvement in runoff simulation whereas the simulated annual mass balance was significantly improved. This demonstrated that even little known information about the glacier ELA or mass balance reduces the uncertainty related to model parameterization significantly while also enhancing the accuracy of mass balance simulation. Thus, even good results in monthly runoff simulation alone do not imply the consistency between simulated and measured

mass balance. The model was then calibrated for only four year mean annual ELAs data and validated for the rest of the ELAs and total available data of annual mass balances. The results revealed that the SWAT model successfully simulates the annual glacier loss, vertical mass balance distribution profile and annual ELAs with light calibration efforts for ungauged catchments with limited available information about the glaciers. The results also revealed that the modelled area of glaciers by elevation bands is not an important source of uncertainty in mass balance simulation.

Introduction

In many parts of the world glacier runoff is the primary water supply for hydropower reservoirs and irrigation systems. Enhanced warming from greenhouse gases can have a significant effect on the water supply from glaciers (Oerlemans, 2001). Assessment of glacier mass loss is required to estimate the contribution of glacier runoff to streamflow and to plan for the water resources in mountainous areas. Many approaches have been applied to estimate the contribution of glacier melt to streamflow but one common problem in applying these methods is limited climate data, continuous observed discharge and glacier mass balance measurements.

In-situ mass balance data are available for only a limited number of glaciers and over short time periods. Therefore, developing a hydrological model with adequate hydrologic components that can be applied to these data scarce catchments has been the objective of many studies (Schäfli et al., 2005; 2010; Konz et al., 2007; Konz and Seibert, 2010; Moore and Demuth, 2001; Micovic and Quick, 2009; Prajka et al., 2007; Martinec and Rango, 1986; Giesen and Oerlemans, 2012; Stahl et al., 2008;

Koboltschnig et al., 2008). In ungauged catchments, glacier mass balances and equilibrium line altitude (ELA) can be used as an additional source of information in glaciered catchments.

According to Konz et al. (2006, 2007) glacier mass balances contain important information that improve the reliability of calibrated model parameters in poorly gauged catchments. Konz and Seibert (2010) also indicated that combining mass balance observations with a few discharge data improved the internal consistency and significantly reduced the uncertainties compared to parameter set selections based on discharge measurements alone. Schäfli et al. (2005) constrained their hydrological model on discharge and three available annual mass balance observations and showed that the resulting model reproduced discharge and the altitudinal mass balance distribution reasonably well.

Stahl et al. (2008) pointed out that including observed mass balance data for parameter tuning could greatly reduce the prediction uncertainty in glacier catchments. Schäfli and Huss (2010) applied a step-wise modification for parameter selection to reproduce the mass balance and discharge using a semi-lumped hydrological model. They demonstrated that information on seasonal mass balance is a pre-requisite to reliably calibrate a hydrological model.

ELA is another important characteristic of glaciers which is used in hydrologic model calibration. The ELA is a theoretical line on a glacier with zero point mass balance at the end of a fixed year (Anonymous, 1969). It separates the ablation area from the accumulation area. The correct simulation of the ELA is therefore a major objective

for hydrological models that are developed for application in climate change impact studies (Schäfli et al., 2005). Ohmura et al. (1992) also indicated that knowledge about the ELA is essential for understanding the relationship between climate changes and glacier variations.

In this study, we developed a model to use sparse points of observation to calibrate and evaluate a modified snow process incorporated into the SWAT model for high mountainous catchments. The reliability of calibration was examined when using observed discharge and when incorporating some information about glacier characteristics (i.e. ELA) along with observed discharge to reproduce glacier mass balances. Using this fact, the model performance was evaluated for its ability to reproduce the mass balance and ELA by calibrating the model using a few mass balance and ELA data for ungauged catchments.

Since the mass balance of an individual glacier may not be representative of larger areas (Huss, 2012) the method was extrapolated from individual glaciers to their neighboring glaciers based on glacier hypsometry and SWAT performance was evaluated through simulation of mass balance in ungauged catchments.

Study Area

This study focuses on the three reference glaciers (Gries, Rhone, and Abramov) in Europe and central Asia where either historical mass balance data by elevation band or runoff data are available. Gries Glacier (46°26' N, 8°20' E) is a small valley glacier 5 km in length (year 2005) situated in the south of the main Alpine crest in Switzerland. In 1973 it had an area of 6.23 km^2 decreasing to 5.26 km^2 in 2008. The glacier has a

northeast exposure and stretches from 2,410 to 3,327 m. Length variation measurements show 2,151 m of retreat from 1847 to 2013.

The Rhone Glacier (46°37' N, 8°24' E) is a medium-sized valley glacier with high precipitation amounts in the accumulation area, a result of regional advection effects and a relatively dry climate at its terminus (Schwarb et al., 2001). The Rhone Glacier is a source of the Rhone River and located in the far eastern Rhone River Basin in Switzerland. The glacier has a southern exposure and stretches from 2,197 to 3,600 m with the area of 16.45 km^2 (year 2000). Length variation measurements show 1,336 m of retreat from 1879 to 2013.

The Abramov is a valley glacier in the country of Kirghizstan (39°40'N, 71°30'E) and located in the north of the Vakhsh River Basin. The glacier is oriented north and stretches from 4,960 to 3,620 m. Its surface area is 26.21 km^2. The glacier has a temperate accumulation zone but cold ice near the surface of the ablation area.

Data

The annual mass balance, annual ELA, and mass balance/altitude profile at benchmark glaciers was extracted from Glaciological reports by VAW/SCAN (the Swiss glacier monitoring network) 'Glacier Mass Balance Bulletin' (GMBB) and 'Fluctuations of Glaciers' (FoG) provided by World Glacier Monitoring Service (WGMS, 2012).

Annual glacier mass balances and ELAs are available for the Rhone Glacier for the years 1979-1980, 1980-1981 and 1981-1982 in FoG reports (version 3) (Zemp et al., 2012). For the Abramov and Gries glaciers the mass balance data is available from 1968-1998 and 1979-2010, respectively (Zemp et al., 2012; Dyurgerov, 2002). Data is

presented in Table B. 1in Appendix B. Published mass balance values include only mass lost by processes on the glacier surface or in the uppermost annual layer of the snow/ice deposited during the hydrological year (October 30-September 1). The annual ELA is generally determined, in the context of mass-balance measurements, by fitting a curve to data representing point mass balance as a function of altitude (Dyurgerov, 2002).

Methodology

Glacier Distribution

Subbasins were divided into 10 elevation bands with 100 m to 200 m intervals depending on the elevation range of the subbasin. Smaller elevation band intervals are able to determine glacier boundaries more accurately. It was assumed that the glacier boundary at a subbasin matches the lowest altitude of the elevation band if more than 50 percent of the elevation band area is covered by a glacier.

To model the glacier areas it was assumed that all zones at altitudes higher than the ELA_0 are permanent snow/ice and seasonal snow is located at lower altitudes by default. According to Ohmura et al. (1992), the equilibrium line represents the lowest boundary of the climatic glacierization. The ELA is determined by climate and the aspect of the glacier. It is not influenced by glacier dynamics, extent and hypsometry; therefore, it can be a representation of the lowest boundary of climatic glacierization (Zemp et al., 2006b). The physical boundary of the glaciers was corrected based on the glacier inventory data, GLIMS glacier outlines and MODIS products. Elevation bands lower than the ELA_0 was considered seasonal snow cover regardless of the extension of

glacier tongues into lower elevations. In the Figure 2. 1 and Figure 2. 2, the dark blue band indicates the ablation zone and higher elevation bands represent the accumulation zone. We did not model the tongue of the glaciers extending into lower altitudes, but the total modeled glacier area is approximately equal the actual glacier area. The elevation band intervals for the Rhone and Gries Glaciers are 200 m and 100 m, respectively. These assumptions have negligible influence on the simulated specific mass balance of the glaciered area of subbasin (Huss et al., 2008). In Figure 2. 3 the black line shows the accumulation boundary of the glaciers at 4,300 m (mean regional ELA_0) and the green line represents the modelled physical boundary of the glaciers at 4000 m.

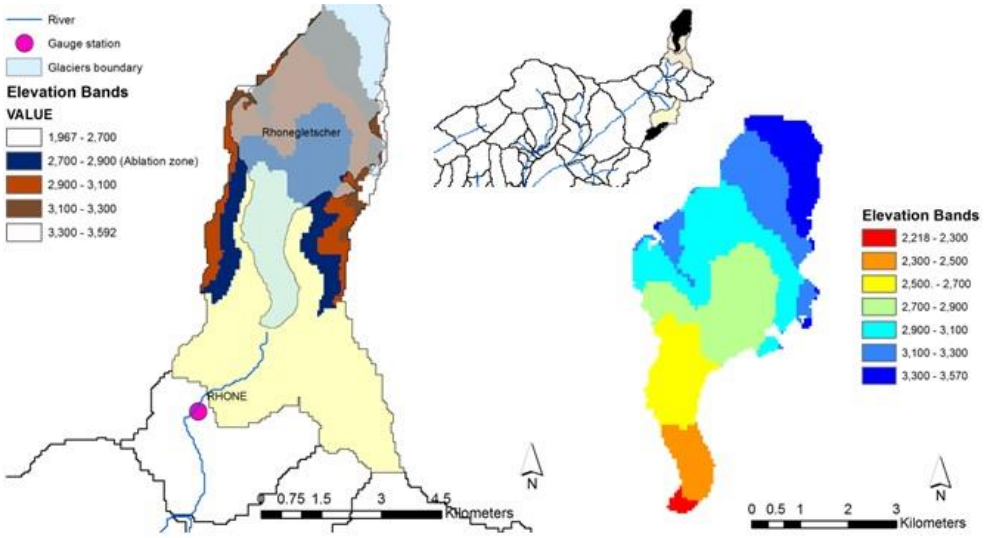

Figure 2. 1. Rhone glaciers outline (WGI) (Right) with the elevation bands, and modelled glacier distribution and elevation bands throughout the catchment area in the Rhone River Basin (Left). In left figure dark blue band shows the ablation zone and higher elevation bands represent accumulation zone.

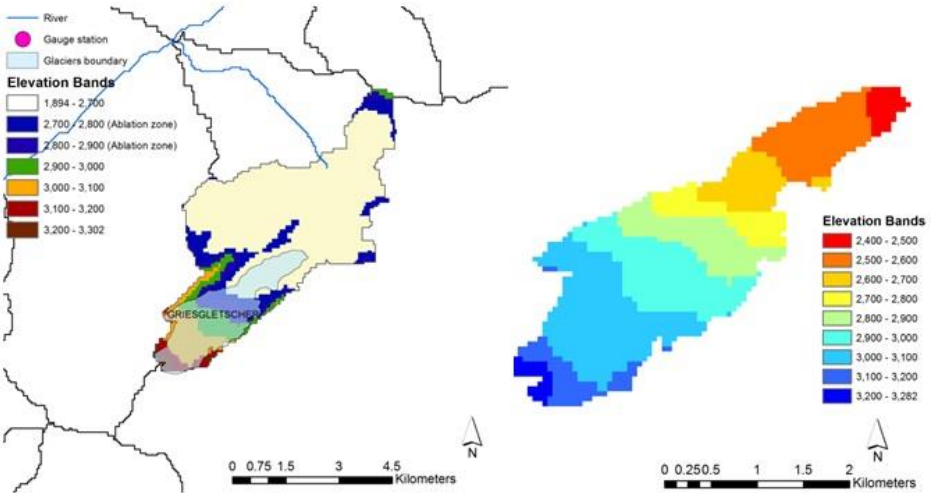

Figure 2. 2. Gries glaciers outline (WGI) (Right) and modelled glacier distribution and elevation bands throughout the catchment area in the Rhone River Basin (Right). In the left figure dark blue band shows the ablation zone and higher elevation bands represent accumulation zone.

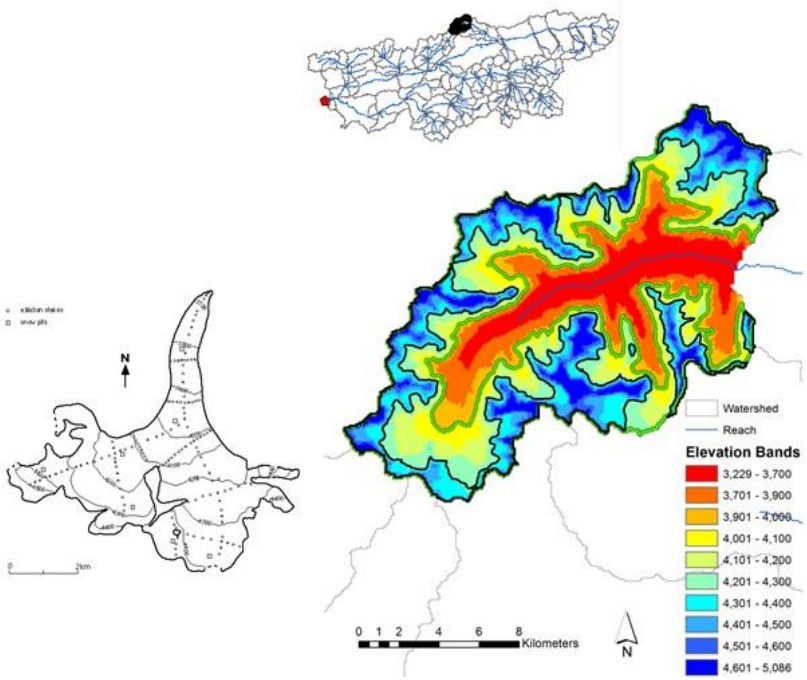

Figure 2. 3. Abramov glaciers outline (WGI) (Left) and modelled glacier distribution and elevation bands throughout the catchment area in the Vakhsh River Basin (Right). Black line shows the accumulation boundary of the glaciers at 4300m (mean regional ELA_0) and green line presents the modelled physical boundary of the glaciers at 4,000m altitude.

Mass Balance and ELA Calculation for Individual Glacier and Range of Glaciers

The mass balance of an individual glacier is calculated using data of area weighted mass balance versus altitude. This was done by multiplying each mass balance versus altitude distribution by the area within the 100m or 200m elevation bands of that individual glacier where:

$$B_n = (1/A)\sum\left(bn_1 * a_1 + bn_2 * a_2 + \cdots + bn_j * a_j\right) \qquad \text{Eq. 2. 1}$$

where B_n (also B_a) are mass balances for the entire glacier, bn_1, bn_2, bn_j are point mass balances for elevation (j) with the area a_j; and A is the surface area of the entire glacier. Annual (B_a) and net (B_n) balances (Mayo et al., 1972) may differ from year to year, although the difference is not likely to be substantial for longer-term averages (Dyurgerov, 2002).

Elevation is the main parameter affecting change in climate and mass balance in mountains **(**Barry, 1992). That is one of the reasons for dividing a glacier area into elevation ranges (usually 100 m, see Appendix B) to make calculations of averages more accurate, given that the variables are homogeneous and isotropic inside a certain elevation range.

In the SWAT model, initial snow storage at the beginning of a simulation period can be set for each individual elevation band. This storage can be permanent snow or glaciers at the end of ablation season. The thickness of initial snow is set for each elevation band as the water volume equivalent; while the lower boundary of the elevation band represents the mean elevation of the snow boundary. This initial storage

is updated on a daily basis for accumulation, sublimation and melting of snow. The mass balance for each HRU is:

$$SNO_i = SNO_{i-1} + R_{day(i-1)} - E_{sub(i-1)} - SNO_{mlt(i-1)} \quad \text{Eq. 2. 2}$$

where SNO is the water content of the snow pack on a given day i (mm H_2O), R_{day} is amount of solid precipitation on a given day, (mm H_2O), E_{sub} is the amount of sublimation on a given day (mm H_2O), and SNO_{mlt} is the amount of snow melt on a given day (mm H_2O). The melt from each elevation band is the area averaged melt from the HRU.

The simulated annual mass balance is calculated from the snow storage change between October 30 and September 1 for glaciered elevation bands. For individual glaciers the mass balance was calculated using the hypsometry of the glacier (Eq. 2. **1**).

For calculation of a mass balance across the range of the glaciers, the area weighted mass balance for the specific altitude of an individual glacier is extended to the same elevation bands over the range of glaciers (Dyurgerov, 2002). To calculate the mass balance for the watershed, all of the area weighted mass balances were summed over the glaciered elevation bands and divided the surface area of the entire watershed.

Annual (end of the hydrological year) ELAs, are measured directly in the field or derived from curves of mass balance versus altitude (Table B. 2, Table B. 3, and Table B. 4 in Appendix B). Here, we derived annual ELA_t values from a regression analysis between the simulated specific mass balances on the elevation bands ($b_{n_{(z)}}$) vs. mean altitude of the elevation bands (z).

Finally, the ELA_0 was calculated from the relationship between the mass balance (B_n) and annual ELAs (Østrem, 1975). The ELA_0 is usually estimated as the altitude at which a curve fitted to an observed relationship between annual ELA and mass balance B_n crosses the axis B_n= 0.

B_{n_t} and the annual ELA_t for year t, can be postulated as follows:

$$B_{n_t} = \alpha(ELA_0 - ELA_t) \quad \text{Eq. 2. 3}$$

where ELA_0 is the balanced-budget ELA, i.e. the ELA when the mean specific balance is zero, and α is the effective balance gradient representing a time and space average of the balance gradient (Braithwaite, 1984). The parameters α and ELA_0 are assumed to be constant for an individual glacier, and are redefined by the equation. These data were used for model validation.

Model Calibration and Validation

Model calibration was performed using minimal data about the glaciers. The model was calibrated first for the watershed of the Rhone Glacier, using monthly flow data from 1993 to 2007. Then SWAT was calibrated with a combination of average annual ELAs (1980- 1983) and flow data (1993-2007). For the Abramov and Gries Glaciers, SWAT was calibrated for mean annual ELA and annual mass balance (1980-1983) (Rabatel et al., 2005). It was assumed that the model was calibrated when there was less than 100 m error between the simulated and measured mean ELA. According to Huss (2012), the mass balance within the 100 m elevation band interval exhibits the

same value everywhere throughout the mountain range, so the absolute error of 100m in ELA is acceptable for mass balance simulation.

ELAs higher than the glacier peak were excluded. For mass balance, an acceptable threshold value of 0.25 for PBIAS was considered (Moriasi et al., 2007). A list of the calibration parameters and their optimum values are presented Table 2. 1. The parameters are sorted from maximum to minimum sensitivity to mass balance change.

The model was validated for mass balance data of the test Rhone watershed. For the Gries and Abramov Glaciers the rest of the available data including the annual mass balance and ELAs were used for model validation (Table B. 1 in Appendix B).

Results and Discussions

Model Calibration and Validation for Test Watershed

SWAT performance in the simulation of glacier mass balance was examined by first calibrating the model with monthly flow data. The results indicated that the model accurately simulated the monthly flow data (R^2=0.83, NSE=0.80). Next, the model was validated using the ELA and mass balance data. The results showed considerably larger simulated mass change (Figure 2. 4) and consequently higher ELA altitude in comparison with the measured ELA. This indicated that calibrating only the monthly flow, regardless of the good results, is not an adequate representation mass balance changes. Investigation of the vertical profile of the mass balance-elevation relationship showed high values of simulated ablation at lower altitudes (2,400 m to 2,900 m) and lower values of simulated accumulation at higher altitudes (over 3,000 m) which

resulted in higher mass loss and consequently higher ELA across the glacier (Figure 2. 5).

To reduce the uncertainty related to glacier change, the average of the mean annual ELA was considered for model calibration along with of monthly flow data. TLAPS, SMTMP, PLAPS, and SFTMP were the most sensitive parameters to ELA variations. However, the model was not calibrated for TLAPS and was calculated using the observed climate data.

The results also revealed that precipitation lapse rate (PLAPS) and snowfall temperature (SFTMP) directly control the amount of accumulation whereas temperature lapse rate (TLAPS) and snowmelt temperature (SMTMP) control the amount of ablation dominantly at lower altitudes. By setting these parameters for elevation bands the ELA was shifted to be matched to the obtained ELA from WGI data sets (Table B. 1 in Appendix B). Increasing the PLAPS from 300 mm to 500 mm and SFTMP from 3 to 4℃ at higher elevation bands resulted in more accumulation at higher altitudes and consequently lowering the ELA. Many researches expressed the relative merits of exponential and power-law relations between accumulation (winter precipitation) and temperature at the ELA (Kotlyakov and Krenke, 1982; Ohmura et al., 1992; Braithwaite and Zhang, 1999, 2000; Braithwaite et al., 2003; Braithwaite and Raper, 2007).

The melt was decreased at lower altitudes by decreasing the SMTMP (2 to 0 and 1) and SFTMP (1 to 0) at lower elevation bands, resulting in further lowering of ELA. Calibrating the ELA resulted in significant improvement in simulated mass balance so that the PBIAS changed from 104 to 9 while the simulated flow did not show

considerable improvement (Figure 2. 6 and Table 2. 2). This demonstrated that even minimal information about the glacier ELA or mass balance reduces the uncertainty related to model parameterization significantly and enhances the accuracy of mass balance simulation; while even good results in monthly runoff simulation alone does not imply consistency between simulated and measured glacier loss.

Table 2. 1. Calibration parameters for catchment area of Rhone glacier (test study area).

	Flow and ELA calibration		Flow calibration	
	Below 2900m	Over 2900m	Below 2900	Over 2900
TLAPS	-7		-7	
SMTMP	0,1	3	2	3
PLAPS	500		300	
SFTMP	0	4	1	3
TIMP	1	0.01	0.6	0.01
SMFMX	2	4	3	5
SMFMN	2	2	1.5	2.5

Table 2. 2. Calibration results for simulated monthly flow and ELA and validation results for specific mass balance of the test study area.

	Flow and ELA calibration		Flow calibration	
	Calibration	Validation	Calibration	Validation
R2	0.83	-	0.86	-
NSE	0.80	-	0.80	-
ME (ELA m)	+74	-	+190	-
PBIAS (Bn)	-	+9	-	+104

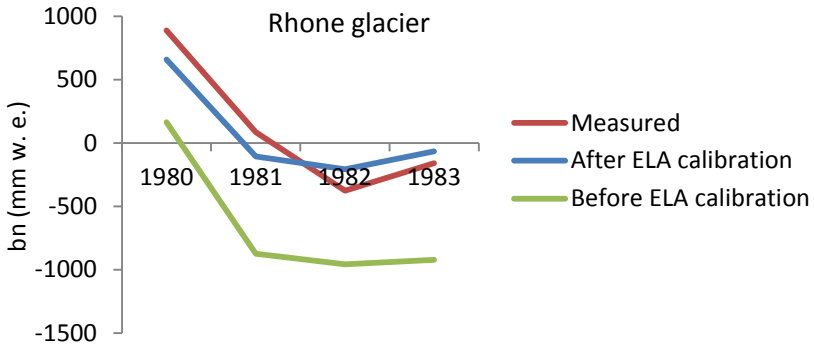

Figure 2. 4. Simulated specific mass balance for Rhone glacier by calibrating the model for monthly flow (green line) and combination of flow and ELA (blue line).

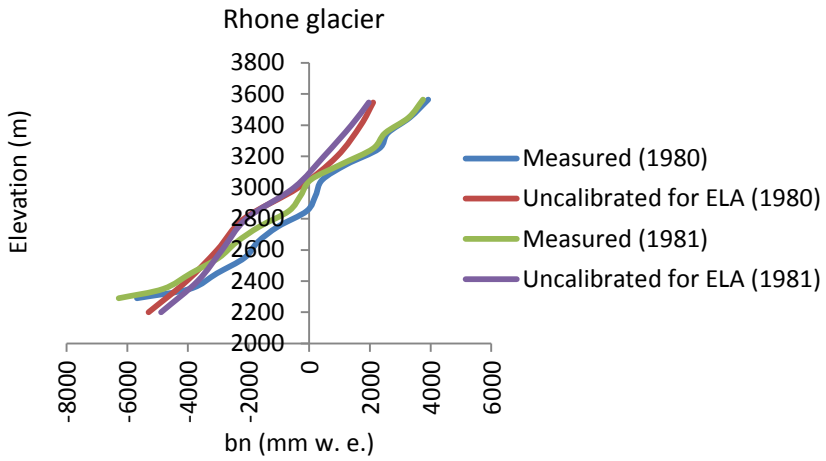

Figure 2. 5. Simulated and measured mass balance profile for Rhone glacier, 1980-1981.

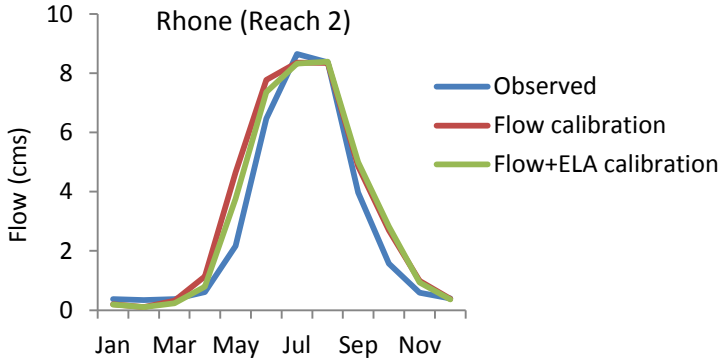

Figure 2. 6. Average monthly flow for calibration period in Rhone River Basin.

Extending the Applied Method to Other Glaciers

This method was extended for predicting the mass balance of the Gries and Abramov Glaciers where there was no observed flow data available. f. In the absence of flow data, four years of mass balance data was used along with the ELA for model calibration. In the hydrological method for calculation of mass balance, usually a combination of ELA with discharge, AAR or mass balance is used for model calibration (Schäfli et al., 2005; Hagg et al., 2004). Moreover, given the high uncertainty in the climate conditions at ELA, calibrating the model only for ELA may not result in accurately simulated mass balance. A period of four years was selected for model calibration to be consistent with the calibration period of ELA for the Rhone Glacier. This also showed the power of the model in mass balance and ELA prediction with minimal data, i.e. four or five years of data is available for model calibration. The same calibration method was applied for the simulations of ELA of the test study area. The default and adjusted parameter values are presented in Table 2. 3. The results revealed that the uncalibrated model generally predicted lower mass loss for both the Gries and Abramov Glaciers (Figure 2. 7).

Calibration and validation results in Table 2. 4 shows for the Gries glacier, the ME for ELA reduced from -43m to +16m and PBIAS reduced from 104 to 23 after calibrating the model. The validation results also shows the very good PBIAS values of 4 with ME 34 m for ELA. For the Abramov Glacier, the ME reduced from -70m to +15m and PBIAS reduced from156 to 68 after calibrating the model. Negative PBIAS indicates the simulated Bn is less than the measured Bn or the model predicts less mass

loss for the glacier. A negative ME indicates the mean simulated ELA is lower than the measured ELA.

According to calibration criteria, the simulation results of specific mass balance of the Abramov Glacier were unsatisfactory; although the total specific mass loss of the glacier (mm w. e.) at the end of the simulation period shows only an 8.4 error (-8.8 m w. e. in comparison with -9.6 m w. e.). The good validation result for the mass balance simulation is due to compensating errors over a relatively long period.

For two anomalous years a profile of the altitude/b_n relationship was constructed for the Gries and Abramov Glaciers. Comparisons of these curves for two years one cold (1980) and one warm (1981) show a difference (Figure 2. 8). The shift between these two curves is clearly visible. Simulated profiles for the Gries Glacier showed only rotation with an increase in ablation below a certain level and an increase in accumulation above this level from the cold year to the warm year. The axis of this rotation is about 200 meters above the ELA, the same result reported by Dyurgerov (2002) for 21 glaciers for two years: 1972, the coldest, and 1990, one of the warmest years during the period of consideration. The simulated profiles of the Abramov Glacier almost match the observed profiles. The altitude-mass balance profiles of the referenced glaciers are transferable to the unmeasured glaciers for estimation of mass balance (Kuhn et al., 2009).

The simulated annual mass balances and ELAs from 1980 to 2007 for Gries and Abramov glaciers are presented in Table 2. 5. All ELA series show great variability from year to year with differences of several hundred meters between maximum and

minimum ELA values corresponding to balance years with highly negative or positive mass balance respectively (Table 2. 5). Unlike the annual ELAs, the variation of balanced-budget ELA (ELA_0) is quite small (Braithwaite and Muller, 1980) and varies with climate change conditions during a long period. Figure 2. 9 shows the balanced-budget ELA at Bn=0 for the Gries and Abramov Glaciers. It was observed that the simulated ELA_0 remained unchanged before and after model calibration as expected. The results show that SWAT constructs the linear relationship between Bn and annual ELAs very well. The measured and extrapolated simulated cumulative specific mass balances until 2007 for the Rhone, Gries and Abramov Glaciers are presented in Figure 2. 10.

Table 2. 3. Calibration parameters for Gries and Abramov glaciers.

		Gries glacier		Abramov glacier	
	Default value	Below 2900m	Over 2900m	Below 4300m	Over 4300m
TLAPS	0	-7.5		-7	
SMTMP	0.5	-1	0	-1	1
PLAPS	0	100		100	
SFTMP	1	0	0.5	2	0.5
TIMP	1	1,0.7	0.1	1,0.5	0.2
SMFMX	4.5	5	7	6	8
SMFMN	4.5	4	5	5	5

Table 2. 4. Calibration and validation results for simulated mass balance and ELA of Gries and Abramov glaciers.

	Abramov glacier			Gries glacier		
	Uncalibrated	Calibration	Validation	Uncalibrated	Calibration	Validation
ME (ΔELA m)	-70	+15	+99	-43	+16	-34
PBIAS (Bn)	-156	-68	+12	-104	+23	-4

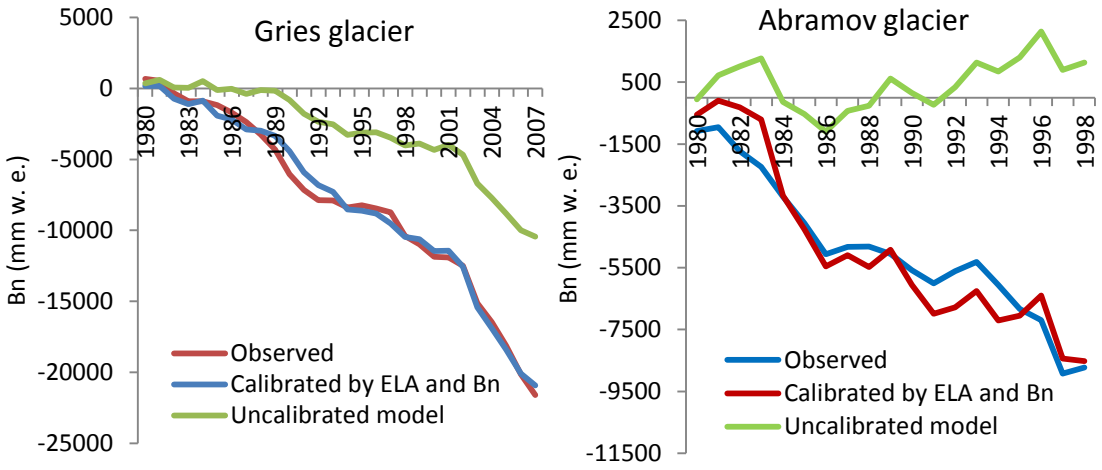

Figure 2. 7. Simulated and measured cumulative specific mass balance for Gries and Abramov glaciers for entire data series from 1979.

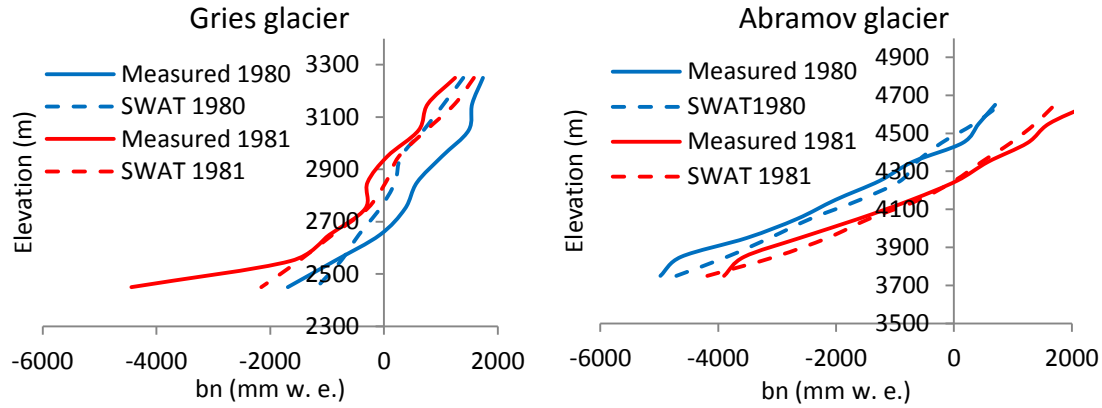

Figure 2. 8. Simulated and measured mass balance profile for Gries and Abramov glaciers, 1980-1981.

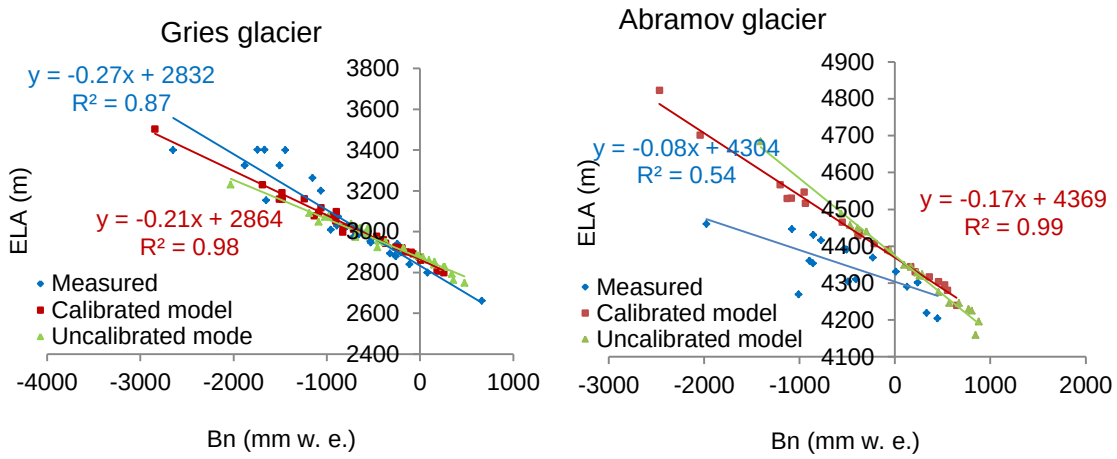

Figure 2. 9. Linear relationship between Bn and annual ELAs.

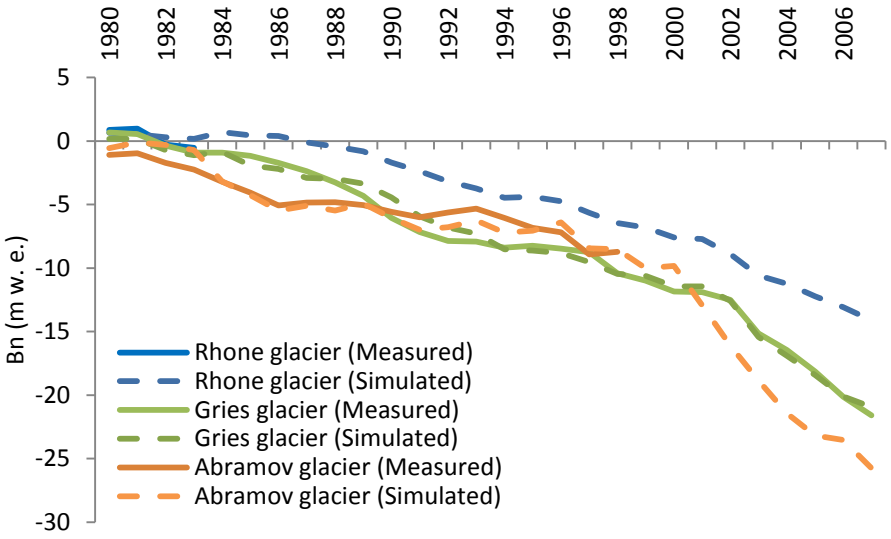

Figure 2. 10. The measured and extrapolated of simulated cumulative specific mass balances until 2007 for Rhone, Gries and Abramov glaciers.

Table 2. 5. The simulated annual mass balances and ELAs from 1980 to 2007 for Gries and Abramov glaciers.

	Gries				Abramov			
	ELA (m)		Bn (mm w. e.)		ELA (m)		Bn (mm w. e.)	
	Measured	Simulated	Measured	Simulated	Measured	Simulated	Measured	Simulated
1980	2660	2807	663	183	4446	4466	-1081	-554
1981	2940	2874	-242	1	4290	4304	129	457
1982	3030	3052	-892	-905	4416	4407	-774	-219
1983	3000	2961	-559	-395	4391	4429	-507	-387
1984	2865	2799	-9	253		>4700	-971	-2468
1985	2878	3118	-261	-1063	4431	4530	-855	-1086
1986	2946	2924	-530	-260	4269	4567	-1010	-1203
1987	2985	3012	-658	-715	4301	4316	240	360
1988	3073	2892	-877	-76	4331	4437	10	-376
1989	3201	2944	-1062	-371	4369	4281	-230	552
1990	3401	3095	-1742	-1087	4393	4530	-530	-1130
1991	3264	3192	-1154	-1481	4304	4517	-488	-937
1992	3028	3099	-780	-900	4204	4331	448	211
1993	2839	2978	-114	-467	4219	4295	333	522
1994	2953	3161	-532	-1243	4353	4546	-859	-954
1995	2799	2899	78	-94	4360	4345	-896	164
1996	2884	2921	-268	-194	4310	4240	-410	647
1997	2893	3018	-323	-714	4460	4701	-1976	-2041
1998	3401	3074	-1667	-941	4330	4391	219	-78
1999	2979	2901	-684	-152		4594		-1485
2000	3009	3022	-958	-827		<3600		178
2001	2897	2860	-207	8		4827		-3111
2002	2975	3061	-713	-1134		4807		-3168
2003	3400	3485	-2649	-2844		4780		-2743
2004	3400	3193	-1445	-1480		4771		-2584
2005	3153	3132	-1652	-1510		4619		-1744
2006	3325	3234	-1880	-1692		4430		-355
2007	3324	2979	-1505	-829		4741		-2226

Extrapolating Glaciers Mass Balances to Modelled Glaciers on a Catchment Scale

The mass balance of glaciers was extrapolated to examine how the mass balance of the catchments was affected by the modeled glaciers contribution. Glaciered areas were separated from glacier free areas using steady state ELA. For the Gries and Abramov Glaciers the steady state ELAs are 2,900 and 4,300m, respectively (Figure 2. 2 and Figure 2. 3). The glacier tongue was not modeled and it was assumed that the

elevation bands with less than 50 glacier cover were glacier free to prevent large amount of ablation from the lower elevation bands. The model was calibrated based on the area weighted mass balances using the real hypsometry (e.g. distribution of area with altitude) of the glaciers. However, the hypsometry and consequently accumulation and ablation area of the modeled glaciers is different from the real hypsometry of the referenced glaciers. According to previous studies, the specific mass balances of the referenced glaciers can be extrapolated to the glaciers range (Huss, 2012; Zhang et al., 2012; Giesen and Oerlemans, 2012; Kuhn et al., 2009). Huss (2012) showed that glaciered surfaces located at a specific range of altitudes exhibit the same mass balance everywhere throughout the mountain range.

The success of a transfer is limited by the local topography (Kuhn et al., 2009). Therefore, assuming that the specific mass balance is constant throughout the catchments, the specific mass balance for the catchments and referenced glaciers should be the same. The topographic data for plotting the modeled glacier hypsometry was extracted from the SWAT topography report. The specific mass balance for the glaciered elevation bands was calculated by Eq. 2. 1. Figure 2. 11 shows the cumulative specific mass balance for the referenced glaciers and catchments. As expected for the small catchment of the Gries Glacier, both curves almost match. For the larger catchment of the Abramov Glacier, the model showed higher loss for the catchment in comparing with the Abramov Glacier loss; its reason is the larger area of the modeled glaciers at lower altitudes (ablation zone) through the watershed in comparison with the ablation area of the Abramov glacier (Figure 2. 12). When the simulated mass balance profile of the

Abramov Glacier is fit to the extracted mass balance profile from the in-situ data one of the important factors for accurate estimation of melt volume is using a finer distribution than elevation bands for modelling the glaciers area.

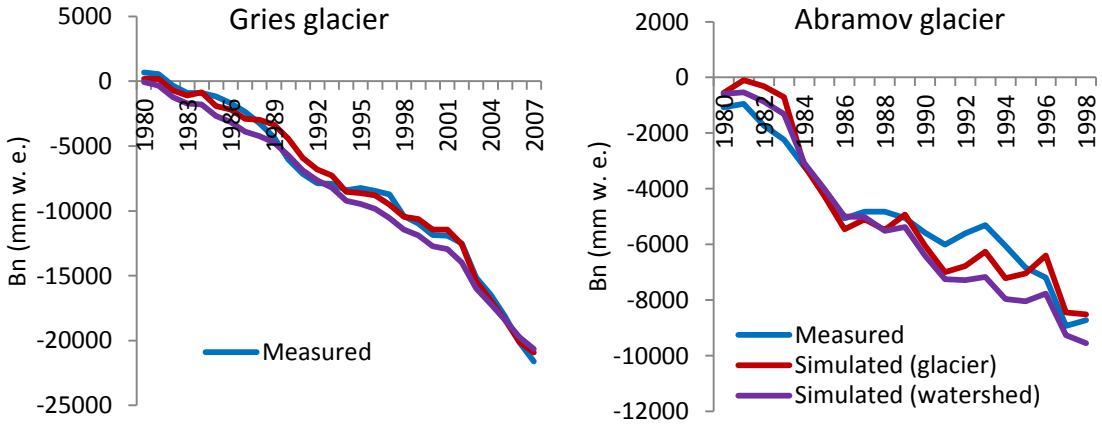

Figure 2. 11. Cumulative specific mass balance for Gries and Abramov glaciers in compare with of modelled glaciers in the catchments.

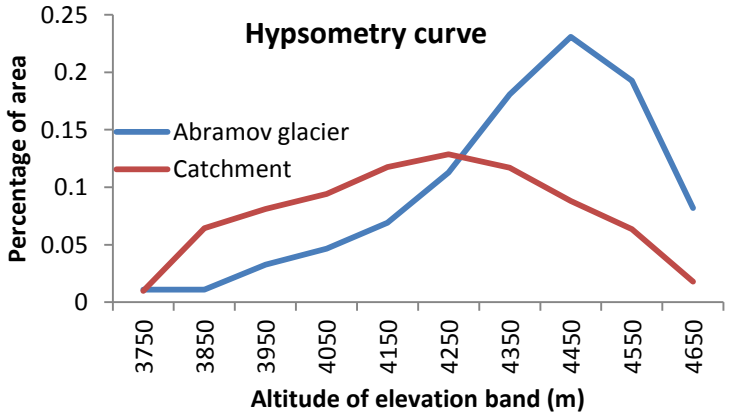

Figure 2. 12. Hypsometry curved for Abramov glacier and the catchment.

Summary, Conclusions, and Future Works

Application of a temperature-index melt model was coupled with a complex semi-distributed physically base hydrologic model, , for simulation of ELA and mass balances for three reference glaciers and their neighboring glacier ranges on a catchment scale. Four years of ELA observations along with observed discharge data provided acceptable mass balance simulations when compared with using only observed discharge in model calibration. The results emphasized the importance of combining even minimal information about the glaciers along with measured discharge data in model calibration for accurate glacier mass balance simulation. This is important for inaccessible glaciers with no mass balance data available.

The model performance in simulation of glacier mass balances of ungauged catchments was also examined by calibrating the model with four years of mass balance and ELA data. The results revealed that SWAT successfully simulates the annual glacier loss, mass balance profile and annual ELAs for ungauged catchments with minimal calibration with limited available in-situ data of glaciers. All ELA series showed great (several hundred of meters) deviation corresponding to balance years with highly negative or positive mass balances, respectively.

The ability of SWAT to predict ELAs implies the applicability of the model on climate change assessment, since ELA is one of the most important indicators of climate change. Although, the model showed very good performance in predicting the ELA variations, which is independent on topography, applying the model for predicting the volume of melt water and consequently the water budget of catchments demands a more

highly spatially distributed model of glaciers. Applying the ELA_0 as a measure of glaciered area is a good representation throughout the catchment in climate change studies but in the case of predicting the total glacier mass loss, the model performance significantly drops in the catchments with heterogeneous topography.

This may result in good model performance in simulations of discharge but the background hydrologic processes related to glacier melt/accumulation might be highly biased relative to the observed data. Therefore, finer discretization between the glaciers and glacier free areas based on HRU divisions is recommended rather using the elevation bands divisions. Another option could be assigning a glacier area percentage for each elevation band.

CHAPTER III

IMPACTS OF CLIMATE CHANGE ON RUNOFF FROM HIGHLY GLACIERIZED RIVER BASINS

Overview

This study assesses the impacts of climate change on river flow from highly glaciered river basins using the SWAT model (Soil and Water Assessment Tool). Analyses are conducted for five river basins that are global in coverage and feature contrasts in climatic and developmental conditions. These include the Narayani (Nepal), Vakhsh (Central Asia), Rhone (Switzerland), Mendoza (Central Andes, Argentina), and Central Dry Andes (Chile). The predicted future climate change by two RCPs (Representative Concentration Pathway) climate change scenarios (RCP4.5 and RCP8.5) and six Coupled Model Intercomparison Project-5 (CMIP5) models are presented. Simulations of mean annual runoff, mean monthly runoff and high (Q5) and low (Q95) monthly runoff and flow duration curves (FDCs) under baseline (1979–2008) and climate change scenarios are presented. Mean annual water yield increased 17 and 40 for Rhone, 50 and 80 for Narayani, 65 and 116 for Vakhsh, 28 and 55 for Mendoza, 17 and 30 for Chile under RCP4.5 and RCP8.5. For GCMs ensemble and RCP8.5, all the glaciers with 100 m w. e. will be disappeared by 2100 across Rhone, Narayani and central Chile River Basins while in Mendoza and Vakhsh at least 41 and 2 of the glaciers will be survived.

Introduction

Glaciers are an important reservoir of water and any changes in their extent/volume influence long-term, downstream water supply in glaciered regions. According to IPCC Fifth Assessment Report (IPCC-AR5), global surface temperature changes at the end of 21st century are likely to exceed 2 ºC for RCP6.0 and RCP8.5 and not to exceed more than 2℃ for RCP4.5 relative to 1850 to 1900. Warming will continue beyond 2100 and glaciers will continue to shrink worldwide, with regional variations.

Massive flooding is predicted in areas where glaciers are receding (IPCC-AR5). Water flow through glaciers affects the quantity and quality of water delivered to areas downstream of glaciered basins. As glacier area is lost, there will be a long term decline in glacier runoff and consequently stream flow during the melt season. Hydrologic systems are affected by increased runoff and earlier spring peak discharges. In particular many glacier- and snow-fed rivers and lakes warm, producing changes in their thermal structures and water quality (Rosenzweig et al., 2007). Alpine glacier retreat during the last two decades caused a 13 increase over the long term average in glacier contribution to August runoff of the four main rivers originating in the Alps (Huss, 2011). Increases in extreme river discharge (peak flows) over the past 30 to 50 years have been observed in parts of Europe (IPCC-AR5).

The development of a hydrologic model with adequate components, and the spatial and temporal resolution needed for assessment of climate change impacts, is a major area of active research. The most common method for assessing the magnitude of this impact is to run a hydrologic model driven by various climate projections from

general circulation models (GCMs) as input forcing data. The simulations of key hydrological indicators, such as river runoff, can then be used to assess the potential impact of climate change. The assessment of hydrologic impact of climate change is particularly challenging in mountainous watersheds due to their extremely variable morphology and topography. Climatic variables such as precipitation and temperature are strongly related to altitude. The presence of glaciers in the watershed will also add to the complexity of the hydrologic system due to temporal and spatial variability of melt.

In this study the Soil and Water Assessment Tool (SWAT) was used to investigate the impact of climate change on the hydrologic regime of snow and glacier driven runoff. SWAT has been widely used in climate change impact assessment studies but few studies have been presented in large complex basins (Mohanty et al., 2012; Bharati et al., 2012; Pradhanang et al., 2011; Jha et al., 2006; Park et al., 2011; Siderius et al., 2013). No study has been conducted on the impact of climate change on glacier change and runoff in multiple large scale river basins with the focus on glaciered catchments.

Therefore, the objectives of this study were: 1) Assess the effect of projected future climate associated with six GCMs and two RCP scenarios on future streamflow volume and seasonal variability at the outlet of five river basins and their catchments with focus on the degree of glacierization, and 2) Test the hypothesis that global mountainous glaciers will vanish by 2100.

Analyses were conducted using five river basins, Narayani (Nepal), Vakhsh (Central Asia), Rhone (Switzerland), Mendoza (Central Andes, Argentina), and Central

Dry Andes (Chile) with total area of 85,000 km^2 , that are global in coverage and feature contrasts in climate and economic development conditions.

Climate Change Scenarios

The future radiative force from greenhouse gases is difficult to quantify because the emissions of these gases depend on many assumptions and uncertain factors such as population growth, the use of carbon fuel as an energy source, technological development, economic development, policy and attitudes towards environment (Nakićenović, 2000; IPCC-TGICA 2007). For this reason, climate scenarios have been developed to investigate the potential consequences of anthropogenic climate change. Using five river basins, simulated flow response for the baseline period was compared to projected future flows associated with several increases in major climate variables from global climate models participating in CMIP5 (Taylor et al., 2012).

In this study, CMIP5 simulations of climate projection are forced with specified concentrations of greenhouse gases and referred to as Representative Concentration Pathways (RCPs).RCPs provide a rough estimate of the radiative forcing in the year 2100 relative to preindustrial conditions (Moss et al., 2010; Taylor et al., 2012). Four RCPs have been produced from the integrated assessment modeling (IAM) scenarios available in the published literature: one high pathway, RCP8.5 (Riahi et al., 2007; Rao and Riahi, 2006), is a business as usual scenario where radiative forcing reaches >8.5 W/m^2 by 2100 and continues to rise for some amount of time; two intermediate "stabilization pathways" , RCP4.5 (Smith and Wigley 2006; Clarke et al., 2007; Wise et al., 2009, Fujino et al., 2006; Hijioka et al., 2008) in which radiative forcing is stabilized

at approximately 6 W/m^2 and 4.5 W/m^2 after 2100; and one pathway, RCP2.6 (van Vuuren et al., 2006, 2007), the lowest RCP which could be considered a moderate mitigation scenario with forcing peaks at approximately 3 W/m^2 before 2100 and declining afterward. In this study, RCP8.5 and RCP4.5 were used to investigate potentially large and moderate future changes in the ST (summer temperature) and WP (winter precipitation). The RCP4.5 and RCP8.5 scenarios are comparable to the SRES B1 and A1F1 scenarios, respectively, used in previous IPCC reports (Taylor et al., 2012).

With the RCP4.5 and RCP8.5 scenarios, a set of downscaled projections from six GCMs from the 14 GCMs commonly used in previous climate change impact studies on hydrologic regimes of a basin (Bradley et al., 2006; Karmacharya et al., 2007; Bharati et al., 2012; Shreshtha and Aryal, 2011), were selected to illustrate a range of changes in a key climate variable in the basins. These models are listed in Table 3. 1. Downscaled 50 km projections over the entire globe were obtained from the Bias-Corrected and Spatially Downscaled (BCSD) archive developed by Reclamation (2013) and were provided through the World Climate Research Programme's Coupled Model Intercomparison Project Phase 5 (CMIP5) multi-model dataset. CMIP5 runs include projections of monthly precipitation, monthly mean temperature, and monthly minimum and maximum temperature. Detailed documentation of the CMIP5model documentation can be found at: http://www.earthsystemgrid.org/search?Type=Simulation2bMetadata and data can be downloaded at:

ftp://gdodcp.ucllnl.org/pub/dcp/archive/cmip5/global_mon/BCSD/

Table 3. 1. List of 14 CMIP5 models.

Model	Resolution (longitude by latitude)	Origin
BCC-CSM1.1	2.815 × 2.815	Beijing Climate Center, China
CanESM2	2.815 × 2.815	Canadian Centre for Climate, Canada
CCSM4	1.25 × 0.9	National Center for Atmospheric Research, USA
CNRM-CM5	1.40 × 1.40	Centre National de Recherches Meteorologiques, France
CSIRO-Mk3.6	1.875 × 1.875	Commonwealth Scientific and Industrial Research, Australia
GFDL-CM3	2.5 × 2.0	Geophysical Fluid Dynamics Laboratory, USA
GISS-E2-R	2.5 × 2.0	NASA Goddard Institute for Space Studies, USA
INM-CM4	2.0 × 1.5	Institute for Numerical Mathematics, Russia
IPSL-CM5A-LR	3.75 × 1.875	Institut Pierre-Simon Laplace, France
IPSL-CM5A-MR	2.5 × 1.25	Institut Pierre-Simon Laplace, France
MIROC5	1.40 × 1.40	Atmosphere and Ocean Research Institute, Japan
MIROC-ESM	2.815 × 2.815	Japan Agency for Marine-Earth Science and Technology, Japan
MPI-ESM-LR	1.875 × 1.875	Max Planck Institute for Meteorology, Germany
MRI-CGCM3	1.125 × 1.125	Meteorological Research Institute, Japan

Projected Climate Change Uncertainty

Uncertainty in projections of future climate conditions stemming from greenhouse gas emissions, are quantified in representative concentration pathways (RCPs). Imperfections in climate models arise from coarse resolution and lack of knowledge about feedback mechanisms and initial conditions (Barsugli et al., 2009). Due to these uncertainties, we selected 12 climate projections (6 GCMs and two scenarios) in this study to capture the possible range of changes in temperature and precipitation in the future. Having a wide range of plausible future climate scenarios is necessary to quantitatively analyze the uncertainty of the results. Techniques of ensembles or model inter-comparisons resulting in a range of climate projections, for example, can be used to quantify the uncertainties or probabilistic aspect of climate

scenarios. Limitation in knowledge and randomness in selection of climate scenarios may misrepresent uncertainty of the climate scenarios that may lead to maladaptation (Hall, 2007).

Generally, selection of models is based on how well they simulate the current climate. Investigation of trends revealed that there is not significance different between the trend of data from GCMs and NCEP/CFSR (National Centers for Environmental Prediction (NCEP) Climate Forecast System Reanalysis (CFSR; Saha, 2010) as input of climate data to SWAT. Although, the Root Mean Square Error (RMSE) between historical GCMs and NCEP/CFSR data was noticeable, it was negligible from one model to another. An RMSE criterion was also rejected for model selection. Therefore, the list of models was narrowed based on range of changes in projected ST and WP relative to the baseline period. The amount and duration of snow accumulation and melt is highly correlated with WP and ST. Therefore, to select an appropriate model, the changes of the projected climate variables related to average WP and ST for a baseline period were analyzed and the models were categorized based on mild, moderate and high increases in projected ST and the change (increase or decrease) in WP.

Climate conditions during the baseline and projection periods are represented as an average for the period 1979-2008 and 2070-2099, respectively, to assess the glaciers condition by 2100. WP and ST changes from the baseline period are presented in Table 3. 2, Table 3. 3 and Table 3. 4 for the Rhone, Narayani, Vakhsh, Mendoza and Central Andes of Chile Watersheds. For example, for the Rhone River Basin, the models were classified into three groups based on a maximum increase in ST of about 7 ºC, a

moderate increase of about 3 ºC which is close to the average ST change of ensemble, and a mild increase of about 2 ºC. Two models from each category were selected based on the percentage of decrease and increase in WP. Therefore, there is a combination of GCMs with a potential range of temperature and precipitation changes.

Future Climate Change

According to the IPCCs AR5, projected rises in global surface temperature by the year 2100 in AR5 should range from about 1.3 ºC for RCP 2.6 to 4.4 ºC for RCP 8.5 and the global mean precipitation will increase by 1 to 3 °C. Mid-latitude and subtropical arid and semi-arid regions will likely experience less precipitation and many moist mid-latitude regions will likely experience more precipitation by the end of this century under the RCP8.5 scenario.

Summer temperature is the main driver of melt (Huss, 2008), so it is important to understand its changes related to the baseline period in each of the climate change scenarios we considered. The greatest increases in ST with a decrease or small increase in WP were observed for the RCP8.5 and GFDL-CM3 in Vakhsh, Narayani and Rhone River Basins, respectively, followed by the IPSL-CM5A-MR in the Mendoza and Chilean River Basins. The predicted temperature changes indicate that the overall climate will become warmer for all climate scenarios and conditions while precipitation changes show high uncertainty due to various climate change conditions. The model ensemble predicts an increase in winter precipitation for the Narayani, Vakhsh and Rhone Watershed and decreased precipitation in the Mendoza and Chilean River Basins.

Overall, the ensemble of models showed mean increase of +2.6 ºC to +6 ºC in ST for the river basins in Northern Hemisphere and increase of +1.8 ºC to +3.4 ºC in ST. It is observed that the river basins in the Northern Hemisphere will experience higher temperature increase in compare to those located in Southern Hemisphere. Future winter precipitation also will be increased +6 to +20 for the river basins in Northern Hemisphere whereas it shows decrease of -7 to -17 for the river basins in Southern Hemisphere (central Chile and Mendoza).

Table 3. 2. Projected changes in summer temperature and winter precipitation for a period of 2079-2099 relative to baseline for 6 GCMs and two RCPs, Rhone River Basin

Rhone	RCP4.5		RCP8.5		Model Classification
GCMs	Summer ΔT	Winter ΔP	Summer ΔT	Winter ΔP	
bcc-csm1-1	2.26	0.12	5.28	7.24	
CanESM2	3.34	22.70	6.80	11.58	
CCSM4	2.55	7.37	4.55	8.65	Moderate (+ΔP)
CNRM-CM5	2.45	16.46	4.23	17.63	
CSIRO-Mk3-6-0	3.58	25.71	6.74	19.45	Extreme (+ΔP)
GFDL-CM3	4.28	-11.19	7.50	7.97	Extreme (-ΔP)
GISS-E2-R	1.81	10.81	3.17	-2.10	Mild (+ΔP)
inmcm4	1.48	-3.13	3.37	-1.62	Mild (-ΔP)
IPSL-CM5A-LR	2.60	9.44	5.77	10.75	Moderate (+ΔP)
IPSL-CM5A-MR	3.17	19.99	5.71	10.52	
MIROC5	2.80	28.15	4.92	15.04	
MIROC-ESM	2.82	11.09	5.61	14.70	
MPI-ESM-LR	2.10	14.23	4.43	7.09	
MRI-CGCM3	1.39	14.73	3.01	12.91	
Mean	2.61	11.89	5.08	9.99	

Table 3. 3. Projected changes in summer temperature and winter precipitation for a period of 2079-2099 relative to baseline for 6 GCMs and two RCPs, Narayani and Vakhsh River Basins.

	Vakhsh					Narayani				
	RCP4.5		RCP8.5			RCP4.5		RCP8.5		Model
GCMs	ΔST	ΔWP	ΔST	ΔWP		ΔST	ΔWP	ΔST	ΔWP	Classification
bcc-csm1-1	2.63	13.97	5.30	14.01		2.02	7.78	3.90	13.39	
CanESM2	4.41	11.60	7.75	26.60		3.26	14.63	5.97	34.26	
CCSM4	2.38	15.37	4.92	19.76		2.12	1.18	4.30	-0.45	
CNRM-CM5	3.02	24.43	4.85	29.90		2.79	0.88	4.38	-3.59	
CSIRO-Mk3-6-0	3.11	24.81	5.26	51.54		2.96	22.33	4.44	26.73	
GFDL-CM3	7.81	12.84	10.94	5.89	Extreme (+ΔP)	5.07	-0.20	7.25	-3.97	Extreme (-ΔP)
GISS-E2-R	2.60	22.74	4.37	35.27		2.00	17.67	3.31	13.67	
inmcm4	2.04	-4.48	3.61	-1.14	Mild (-ΔP)	1.78	13.39	3.47	-13.09	Mild (-ΔP)
IPSL-CM5A-LR	4.11	3.48	7.40	0.10		3.69	-4.28	6.67	-15.42	
IPSL-CM5A-MR	4.22	-3.51	7.96	-8.62	Extreme (-ΔP)	4.17	20.35	7.14	4.66	Extreme (+ΔP)
MIROC5	3.62	16.80	5.98	38.75	Moderate (+ΔP)	2.75	10.15	4.01	34.89	Moderate (+ΔP)
MIROC-ESM	3.44	6.77	6.86	-0.86	Moderate (-ΔP)	3.00	-5.43	5.37	-28.67	Moderate (-ΔP)
MPI-ESM-LR	2.55	5.79	5.10	10.84		2.60	-10.68	5.08	-0.80	
MRI-CGCM3	1.96	35.91	4.14	61.29	Mild (+ΔP)	2.04	-0.62	3.62	15.40	Mild (+ΔP)
Mean	3.42	13.32	6.03	20.24		2.87	6.23	4.92	5.50	

Table 3. 4. Projected changes in summer temperature and winter precipitation for a period of 2079-2099 relative to baseline for 6 GCMs and two RCPs, Mendoza and Chilean Andes River Basins.

	Mendoza				Chile				
	RCP4.5		RCP8.5		RCP4.5		RCP8.5		Model
GCMs	Summer ΔT	Winter ΔP	Summer ΔT	Winter ΔP	Summer ΔT	Winter ΔP	Summer ΔT	Winter ΔP	Classification
bcc-csm1-1	1.44	-12.97	2.95	-24.84	1.32	-10.90	2.84	-24.96	
CanESM2	2.47	6.03	4.32	3.62	2.42	-2.04	4.21	-7.48	
CCSM4	1.97	30.67	3.77	63.56	1.97	13.74	3.66	23.22	Moderate (+ΔP)
CNRM-CM5	3.07	49.62	4.64	37.17	2.92	21.23	4.48	10.51	Extreme (+ΔP)
CSIRO-Mk3-6-0	2.21	-2.10	3.39	-36.95	1.97	-4.22	2.97	-45.27	
GFDL-CM3	2.35	-14.96	3.95	-5.92	2.21	-23.96	3.78	-9.88	
GISS-E2-R	1.03	37.65	2.34	75.66	1.05	31.27	2.40	67.72	Mild (+ΔP)
inmcm4	1.02	-19.37	1.83	-22.49	0.98	-15.83	1.70	-17.94	
IPSL-CM5A-LR	1.68	-43.14	3.31	-48.75	1.71	-41.47	3.26	-49.28	
IPSL-CM5A-MR	2.56	-19.50	4.58	-4.69	2.60	-20.43	4.52	-7.80	Extreme (-ΔP)
MIROC5	1.29	-20.14	2.59	-30.27	1.25	-13.68	2.49	-31.31	
MIROC-ESM	2.04	-36.13	3.75	-51.07	1.95	-38.23	3.63	-55.29	Moderate (-ΔP)
MPI-ESM-LR	1.88	-23.35	4.11	-38.28	1.78	-25.76	3.83	-49.09	
MRI-CGCM3	1.14	-31.20	2.68	-33.50	1.08	-39.74	2.44	-47.88	Mild (-ΔP)
Mean	1.87	-7.06	3.44	-8.34	1.80	-12.14	3.30	-17.48	

Model Setup

In this study, mean monthly precipitation, maximum temperature and minimum temperature from each climate change scenario and the baseline period were disaggregated to daily values using the SWAT weather generator over a 30-year period. Weather generation is a potential tool (and probably the only tool) to produce the synthetic data. Disaggregating temporal data, for example, from annual data to monthly data or monthly to daily, is a complex process. The SWAT weather generator needs statistical data to generate representative daily climate data for the subbasins. To investigate the difference between the simulated flow using the daily NCEP data (i.e. input data for model calibration) and generated daily data for the baseline period using the SWAT weather generator, the model was first run using daily NCEP data and then using the SWAT weather generator.

The results revealed that the uncertainty that arises from using daily data or the SWAT weather generator is negligible in comparison to the uncertainty in the climate models. Weather generators have been widely used in climate change impact studies due to the unavailability of daily climate data at fine spatial resolutions. Aggregating temporal data, from daily to monthly for example, is a straightforward process by calculating the average or sum of the fine resolution data over a coarser temporal resolution. It should be mentioned that the applied projected mean monthly climate variables in the SWAT weather generator including precipitation, maximum and minimum temperature, and the other weather statistics were calculated based on NCEP data. Each GCMs grid covers between 2 to 4 weather stations; so, the projected mean

monthly climates variables were assigned to the nearest NCEP data points (i.e. weather stations) or weather station.

SWAT Responses to Different Climate Change Scenarios

Mean Annual Water Yield and Snowmelt

Figure 3. 1 shows the percentage of changes in simulated mean annual water yield, snow melt and precipitation relative to the baseline for 6 GCMs. Figure 3. 1 is sorted from extreme to mild ST change, and two RCPs and their ensemble. Change of mean annual snow fall and surface runoff are presented in Table C. 1 to Table C. 5 (Appendix C) for all river basins. All are sorted based on predicted extreme to mild increase in ST by GCMs.

Analysis shows an increase in water yield across all 12 climate change scenarios for all of the river basins with large projected differences between GCMs. As expected maximum increase in water yield from the Vakhsh, Narayani and Rhone Watersheds occurred under the projected climate change by RCP8.5/GFDL (+7.25 to +10.94 ΔST and -3.97 to 7.97 ΔWP); for Mendoza and Chile the extreme condition occurred under the climate change by RCP8.5/IPSL-MR (+4.52 to +4.58 ΔST and -4.96 to -7.8 ΔWP). It can be observed that the water yield is highly correlated with snow melt change regardless of increase or decrease in annual precipitation.

An important observation in Figure 3. 1 is a high increase in snowmelt for the Narayani and Vakhsh River Basins with 104 and 106 change, respectively; while, it shows between 20 and 73 for the other river basins. Possible annual water yield for each

river basin respectively are expected to range between +8 to +58 (Rhone), +25 to 129 (Narayani), 23 to 166 (Vakhsh), 20 to 66 (Mendoza) and 10 to 44 (Chile). Possible changes in annual water yield was predicted to be 17 and 40 for Rhone, 50 and 80 for Narayani, 65 and 116 for Vakhsh, 28 and 55 for Mendoza, 17 and 30 for Chile under RCP4.5 and RCP8.5 and GCMs ensemble.

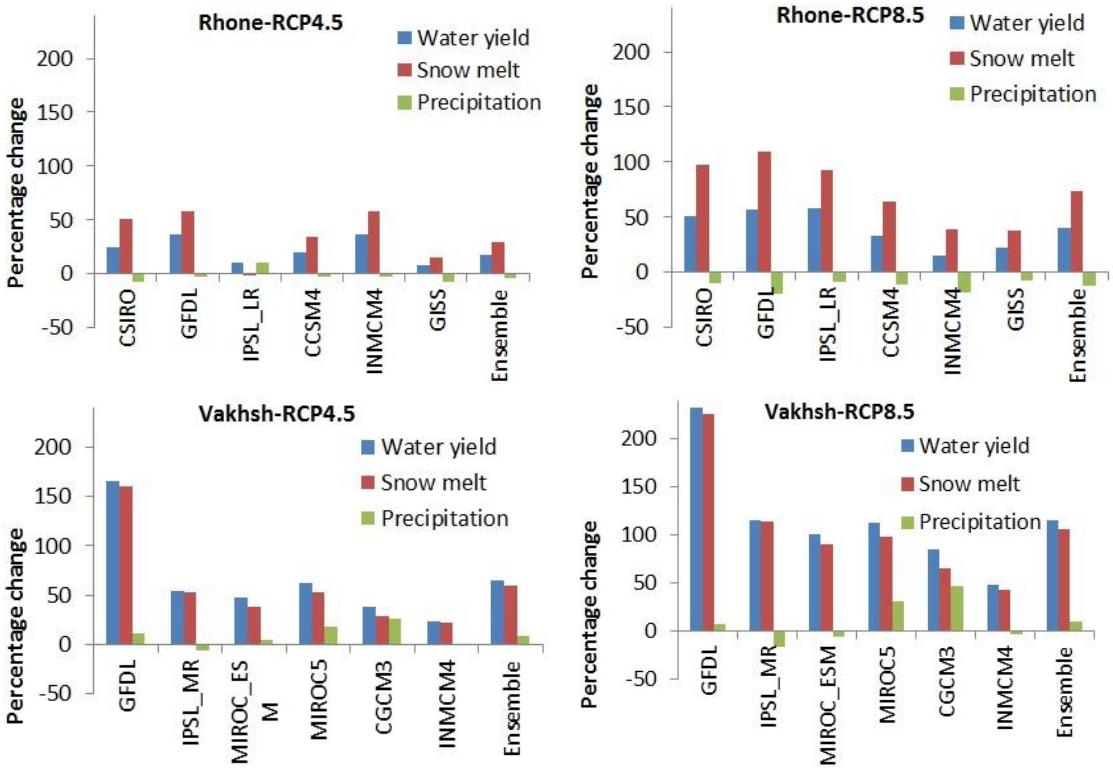

Figure 3. 1. Percentage change in mean specific water yield, snow melt and precipitation relative to baseline period for 6 GCMs and two RCP scenarios for each river basin.

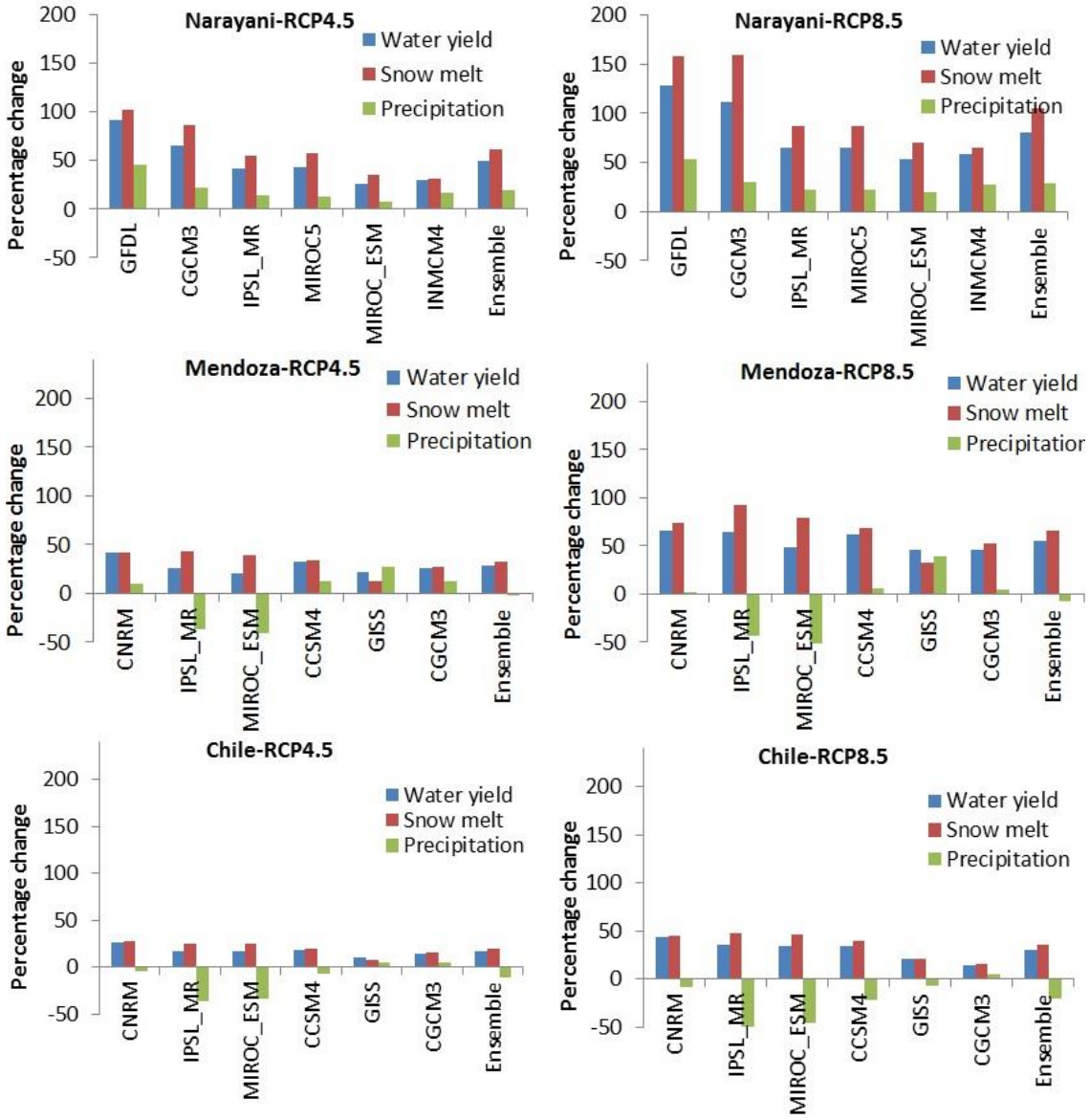

Figure 3. 1. Continued

The Seasonal Cycle

Figure 3. 2 shows the mean monthly streamflow (expressed as a percentage of the mean annual total stremflow) for the five river basin at their main outlets. The ensemble mean, calculated from the mean of the six projections from the GCMs under

the two RCP4.5 and RCP8.5 scenarios, are shown with the inter-GCM range of projections shaded.

For the Mendoza and Chile River Basins, the inter-GCM range is relatively small in comparison to that for other river basins and the ensemble mean for both RCP scenarios is very close to baseline, similar to results reported by Gossling et al. (2011) for the Rio Grande River Basin in South America. The Narayani River Basin shows high inter-GCM ranges only during the summer months which is due to a high increase in projected summer precipitation. Approximately 70 and 81 of increase in annual precipitation is related to the summer precipitation for RCP4.5 and RCP 8.5, respectively while this is not truth for other river basins. For all river basins, the RCP8.5 generated a smoother curve with upward shifting during cold seasons and downward shifting during warm seasons which indicates less snowfall in the winter and consequently less available snow storage for melt in the summer. Also, the ensemble curves show that the peak stream flow moves from July to August for the Rhone, Narayani and Vakhsh River Basins. Similar results were reported for the Mekong River Basin for an ensemble of seven GCMs by Gosling et al. (2011). This implies the decrease in snow fall and consequently reduction or vanishing of the permanent snowpack at lower altitudes and melting of glaciers at higher altitudes. This is less obvious for RCP4.5 but a clear shift is demonstrated under RCP8.5.

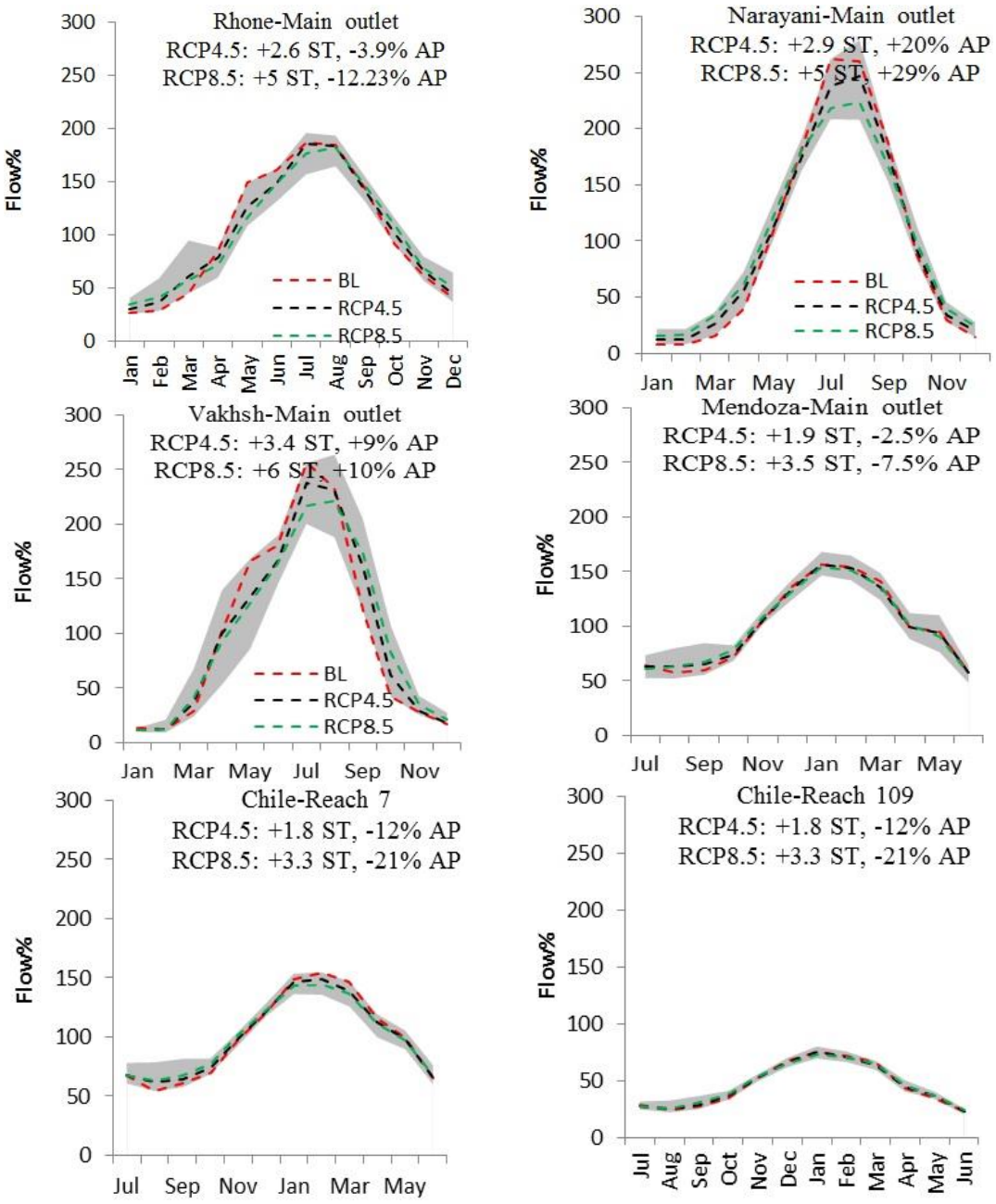

Figure 3. 2. Mean monthly runoff (expresses as percentage of the mean annual total runoff), for the baseline (red line), GCMs ensemble RCP4.5 (black line) and RCP8.5 (green line), the GCMs uncertainty band (grey band).

The change in the seasonal cycle of flow in finer scales can be observed visually in Figure C. 1 to Figure C. 5 in the Appendix C. These figures show the monthly flow pattern for baseline and climate change scenarios from the watersheds with different percentages of glacier area across the five river basins. In low glaciered or glacier free areas, peak summer flow will move from late summer to mid spring (Figure 3. 3-a) with the same pattern by RCP4.5. Under the RCP8.5 the pattern of monthly flow curve is closed to the hydrograph of the rain-fed rivers. This is due to conversion of snow fall to rain fall with warming and consequently rapid increase in stream flow (Figure 3. 3-b and c). In highly glaciered watersheds the temporal pattern of flow remains unchanged but the maximum flow shows considerable increase due to glacier melt (Figure 3. 3-d and e).

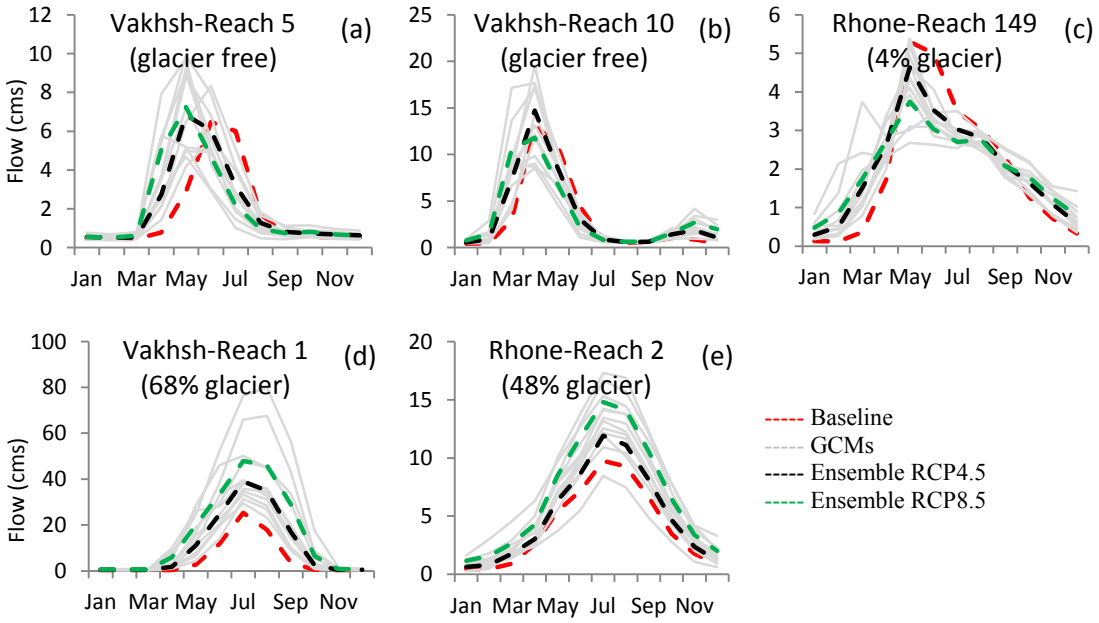

Figure 3. 3. Projected monthly runoff for the watersheds with different percentage of glaciered area for the baseline (red line), GCMs ensemble RCP4.5 (black line), RCP8.5 (green line) and GCMs (grey line).

High and Low Monthly Flow

Figure 3. 4 shows the percentage and magnitude of change from baseline in Q5 (Q5 are high flows that are exceeded 5 of the time) monthly flow for GCMs ensemble and two RCPs for some of the watersheds with different degree of glaciation and whole basin. The percentage of change in Q5 and the change in mean monthly flow is also presented in Table C. 6 to Table C. 10 (Appendix C). The watersheds located at the headwaters were selected based on their percentage of glaciered area and climate type. The flow duration curves for GCMs and ensembles are presented in Figure 3. 5 for the main outlets. In the Chilean River Basins two northern (Reach 7) and southern (Reach 109) watersheds were selected as an example.

The results implied that the projected change of high flow strongly depends on the degree of glaciation of watersheds. With the exception of the Narayani, the projected high flow decreased across the glacier free watersheds and watersheds with very little glaciered area. In the Rhone River Basin, high flow decreased from -17.1 (-29.8) to -1.4 (0.6) for RCP4.5 (RCP8.5) across the watersheds with 3.5 to 5.0 glacier area (Table C. 8 and Figure C. 3 in Appendix C). In the Vakhsh River Basin, this projection ranges from -5.0 (-12.2) to 1.9 (1.0) across the glacier free watersheds for RCP4.4 (RCP8.5). The peak flow from the drainage area to Reach 1 with 68 shows a 101percent increase; whereas it is -10.6 percent for the adjacent glacier free drainage area to Reach 10 with approximately the same size and the same projected climate change (Figure C. 3 in Appendix C). The same responses to climate change scenarios were also observed in the Mendoza and Chilean River Basins with one exception, the drainage area of Reach 2, with only 2 of glacier area, in Chile. Although the percentage change of Q5 shows a

significant increase, the specific Q5 increase (in units of area) are very small (Table C. 10 in Appendix C). This is due to the dry climate of the central Andes; so that, the small monthly flow in this area is very sensitive to any changes in glacier melt in the absence of or with negligible amounts of summer precipitation. In contrast with other regions, peak flow variations across the Narayani River Basin, are not only highly dependent on glaciered area percentage but also varies with coincident summer precipitation changes in mountainous areas.

In contrast with low glaciered watersheds, the peak flow shows significant increase relative to the baseline across highly glaciered watersheds. High flow increased 7.2 (35.2) to 20.3 (69.4) across the Rhone, 33.3 (51.3) to 83.6 (140.4) across the Vakhsh, 22.6 (30.7) to 39.5 (56.1) for the Narayani, 24.2 (43.0) to 41.9 (79.3) across Mendoza, 17.4 (29.2) to 30.5 (67.7) for Chilean watersheds, for RCP4.5 (RCP8.5), respectively.

At the main outlets, Q5 increased 14.5 (30.5) and Q95 increased 51.6 (107.1) for Rhone, Q5 increased 55.1 (89.5) and Q95 increased 66.1 (117.3) for Vakhsh, Q5 increased 41.1 (57.4) and Q95 increased 187.2 (371.1), for RCP4.5 (RCP8.5), respectively.

An increase in high flow implies the potential risk of floods in glaciered watersheds in the future because of the increase in the rapid melt with high air temperatures. Furthermore, because of the increase in the air temperature, the snowfall will decrease, and the rainfall will increase in the future. Such changes may result in an increase in floods during the early spring and significant changes in the hydrological regime in the future. Meanwhile, the risks of droughts may also be increasing during dry

seasons because of the decline in snow storage and consequently less contribution by melt water to runoff.

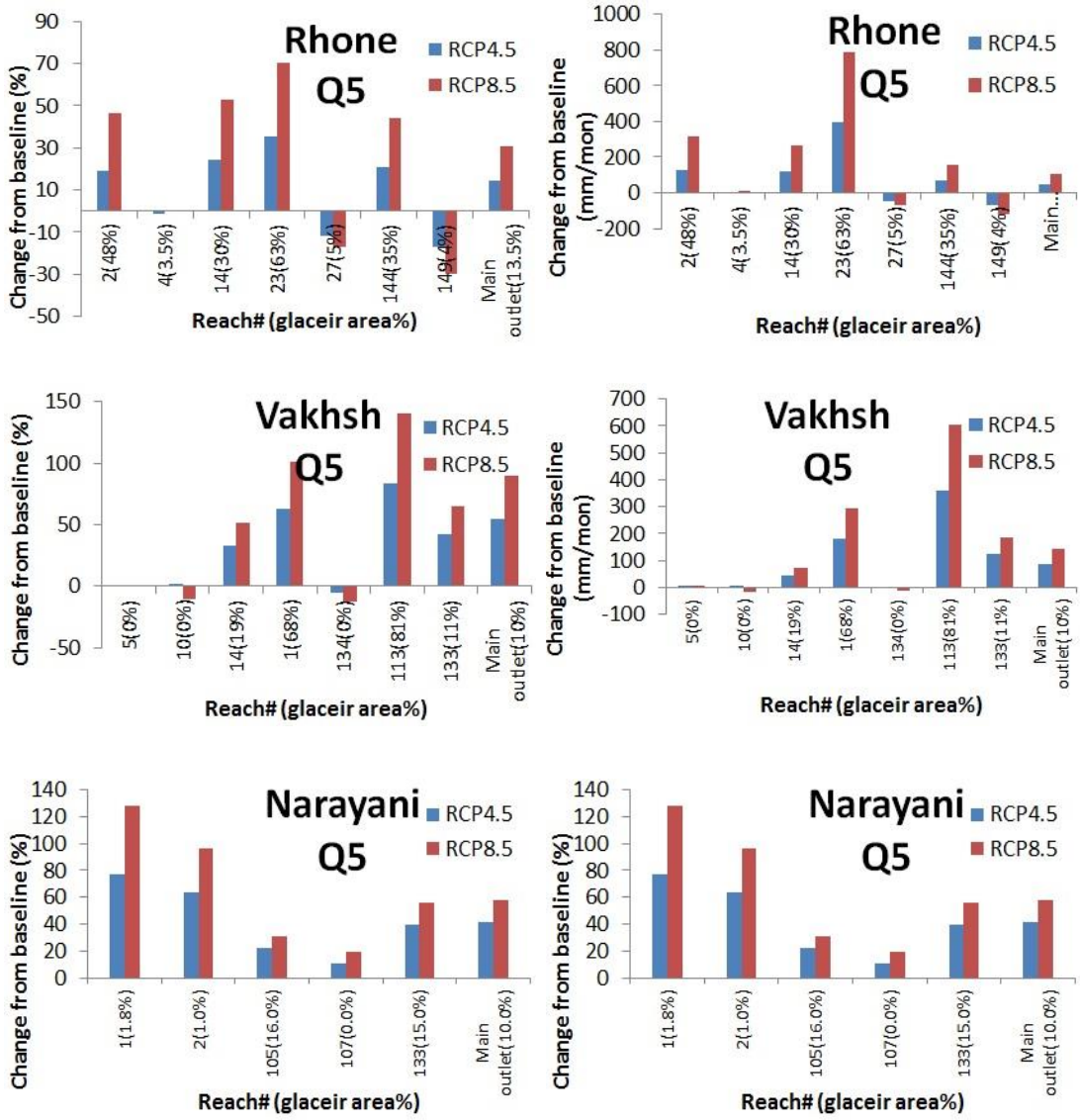

Figure 3. 4. Percentage change in Q5 monthly flow relative to baseline for the glaciated and glacier free watersheds across each river basin.

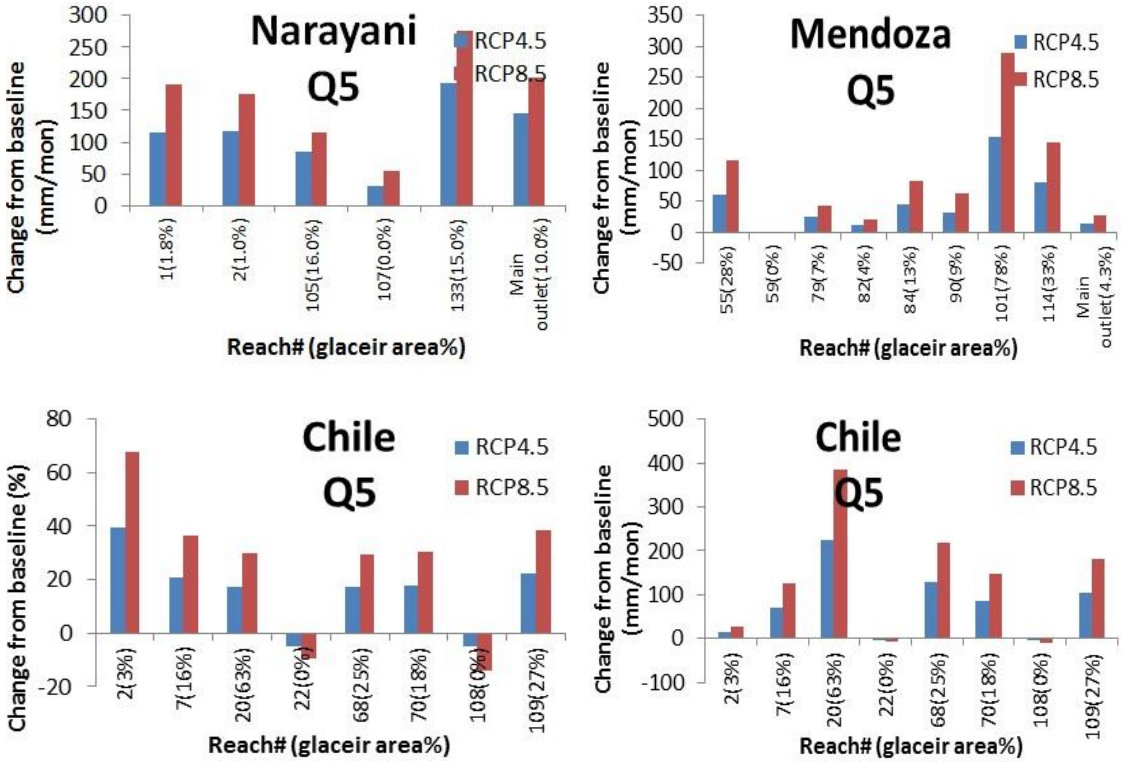

Figure 3. 4. Continued

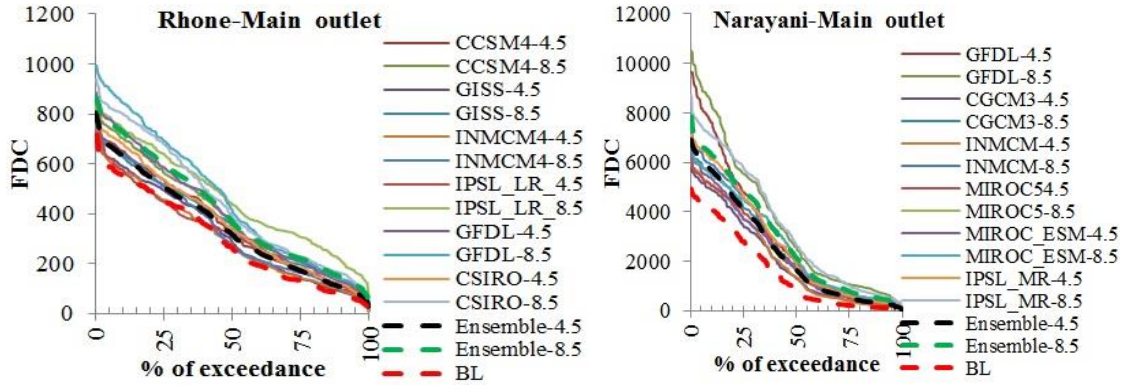

Figure 3. 5. Flow duration curves projections for baseline, GCMs ensembles RCP4.5 and RCP8.5 and 12 climate change scenarios.

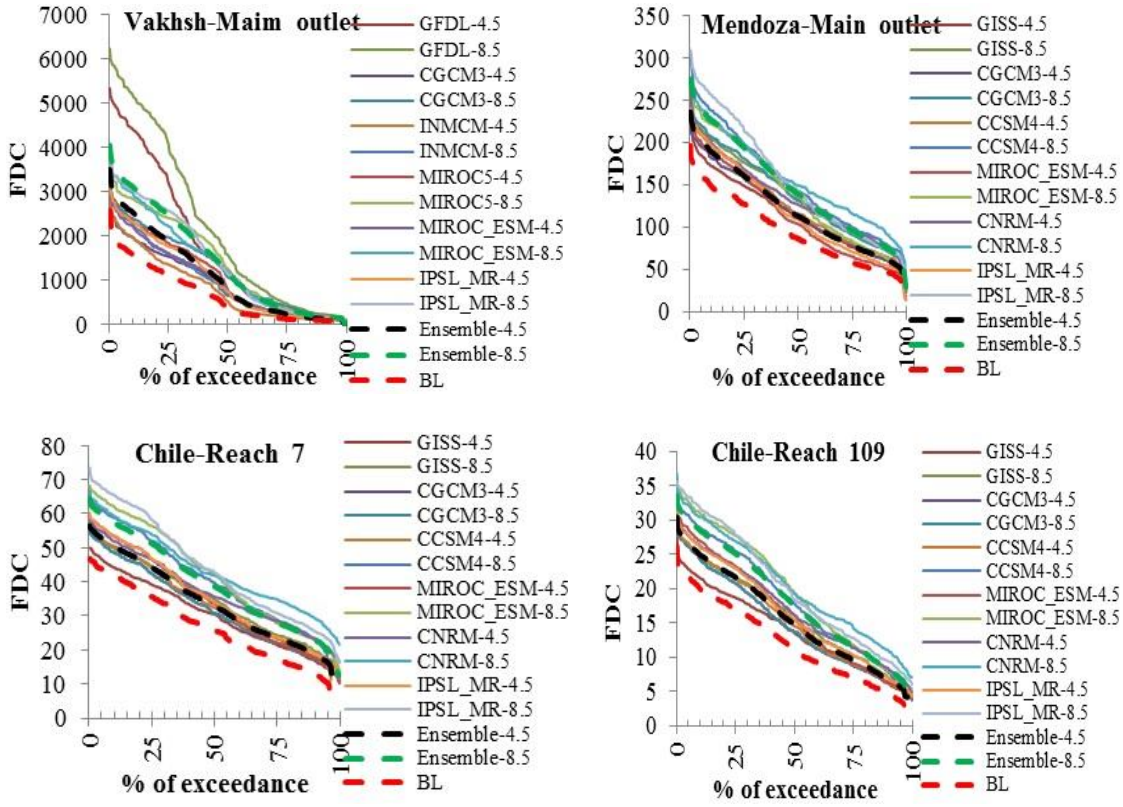

Figure 3. 5. Continued

Glaciers Change under Climate Change Scenarios

The mean specific mass balance for projected climate changes under six GCMs and two RCPs scenarios and their ensembles are presented in Table 3. 5 to Table 3. 9 for five river basins. Assuming that the area of glaciers is constant, the total loss of glaciers thickness by 2100 was calculated as an equivalent of water. The simulated mean annual glacier melt (specific mass balance) was obtained from subtracting the total mean annual melt and sublimation from total mean annual snow fall. The glaciers were divided based on their thicknesses into less than 100 m and greater than 100 m. For the Rhone River

Basin, the ensemble of six GCMSs under the RCP4.5 shows 85 of glaciers with 100 m w.e. thickness will disappear by 2100 whereas 42 of thicker glaciers will vanish. Under RCP8.5 100 of glaciers with 100 m w.e. thickness and less will be disappear and only 30 of thicker glaciers will remain by 2100.

For the Narayani River Basin, all glaciers with 100 m w.e. thickness will vanish under RCP4.5 and RCP8.5 while only 42 and 25 of deeper glaciers will remain under RCP4.5 and RCP8.5, respectively. For the Vakhsh River Basin, 65 and 98 of the glaciers with 100 m w.e. thickness will melt under the projected climate change by RCP4.5 and RCP8.5, respectively, whereas 67 and 51 of the deeper glaciers will remain by 2100. For the Mendoza River Basin, with 2º C warming in the summer (-7 winter precipitation change) under RCP4.5, 46 of the glaciers shallower than 100 m w. e. and 23 of deeper glaciers will disappear by 2100. A 1.4 ºC increase under RCP8.5 accelerates the melting of shallower glaciers up to 13 and deeper glaciers up to 6. In the Central dry Andes of Chile, all shallower glaciers will vanish by 2100 and only 42 and 29 of deeper glaciers will remain by 2100 under the projected climate change by RCP4.5 and RCP8.5, respectively.

It can be concluded that, in the Rhone, Narayani and central Chile River Basins all the glaciers with 100 m w. e. will disappear by 2100 while in Mendoza and Vakhsh at least 41 and 2 of these glaciers will remain under the projected climate changes by RCP8.5. Analysis of the results showed all the glaciers with 45 m w. e. and 55 m w. e. thickness will also be melted across the Mendoza River Basins by RCP4.5 and RCP8.5. This means all the small shallow glaciers in lower altitudes with 5 to 20 m w. e.

thickness will be melted by 2100 across the Mendoza River Basin. No shallower glaciers than 65 m w. e. and 95 m w. e. will survive by 2100 across Vakhsh River Basin by ensemble of GCMs and RCP4.5 and RCP8.5.

Table 3. 5. Glaciers thickness change by 2100 under the climate change scenarios and ensemble of GCMs for Rhone River Basin.

Rhone	RCP4.5					RCP8.5				
	ΔST	ΔWP	mean annual glacier melt (mm w. e.)	Total loss (%)		ΔST	ΔWP	mean annual glacier melt (mm w. e.)	Total loss (%)	
				<100m	>100m				<100m	>100m
CSIRO	3.58	5.71	-1172	100	53	6.74	19.45	-1752	100	79
GFDL	4.28	-11.19	-1315	100	59	7.5	7.97	-2033	100	92
IPSL_LR	2.6	9.44	-527	47	24	5.77	10.75	-1887	100	85
CCSM4	2.55	7.37	-991	89	45	4.55	8.65	-1395	100	63
INMCM4	1.48	-3.13	-808	73	36	3.37	-1.62	-1128	100	51
GISS	1.81	10.81	-824	74	37	3.17	-2.1	-1103	99	50
Base Line	-514	mm w. e.								
Ensemble	2.61	11.89	-939	85	42	5.08	9.99	-1550	100	70

Table 3. 6. Glaciers thickness change by 2100 under the climate change scenarios and ensemble of GCMs for Narayani River Basin.

Narayani	RCP4.5					RCP8.5				
	ΔST	ΔWP	mean annual glacier melt (mm w. e.)	Total loss (%)		ΔST	ΔWP	mean annual glacier melt (mm w. e.)	Total loss (%)	
				<100m	>100m				<100m	>100m
GFDL	5.1	-0.2	-1650	100	74	7.3	-4.0	-2167	100	98
IPSL_MR	2.8	10.2	-1521	100	68	4.0	34.9	-2189	100	98
MIROC_ESM	3.0	-5.4	-1265	100	57	5.4	-28.7	-1504	100	68
MIROC5	2.0	-0.6	-1227	100	55	3.6	15.4	-1504	100	68
CGCM3	4.2	20.4	-1050	95	47	7.1	4.7	-1366	100	61
INMCM4	1.8	13.4	-1002	90	45	3.5	-13.1	-1331	100	60
Base Line	-713	mm w. e.								
Ensemble	2.9	6.2	-1286	100	58	4.9	5.5	-1677	100	75

Table 3. 7. Glaciers thickness change by 2100 under the climate change scenarios and ensemble of GCMs for Vakhsh River Basin.

Vakhsh	RCP4.5					RCP8.5				
	ΔST	ΔWP	mean annual glacier melt (mm w. e.)	Total loss (%)		ΔST	ΔWP	mean annual glacier melt (mm w. e.)	Total loss (%)	
				<100m	>100m				<100m	>100m
GFDL	7.8	12.8	-1985	100	66	10.9	5.9	-1985	100	89
IPSL_MR	4.2	-3.5	-733	66	33	8.0	-8.6	-1245	100	56
MIROC_ESM	3.4	6.8	-613	55	28	6.9	-0.9	-1082	97	49
MIROC5	3.6	16.8	-641	58	29	6.0	38.8	-946	85	43
CGCM3	2.0	35.9	-415	37	19	4.1	61.3	-639	58	29
INMCM4	2.0	-4.5	-468	42	21	3.6	-1.1	-666	60	30
Base Line	-283	mm w. e.								
Ensemble	3.4	13.3	-722	65	33	6.0	20.2	-1094	98	49

Table 3. 8. Glaciers thickness change by 2100 under the climate change scenarios and ensemble of GCMs for Mendoza River Basin.

Mendoza	RCP4.5					RCP8.5				
	ΔST	ΔWP	mean annual glacier melt (mm w. e.)	Total loss (%)		ΔST	ΔWP	mean annual glacier melt (mm w. e.)	Total loss (%)	
				<100m	>100m				<100m	>100m
CCSM4	2.0	30.7	-512	46	23	3.8	63.6	-665	60	30
CGCM3	1.1	-31.2	-470	42	21	2.7	-33.5	-586	53	26
CNRM	3.1	49.6	-555	50	25	4.6	37.2	-687	62	31
GISS	1.0	37.7	-415	37	19	2.3	75.7	-503	45	23
IPSL_MR	2.6	-19.5	-581	52	26	4.6	-4.7	-772	69	35
MIROC_ESM	2.0	-36.1	-560	50	25	3.8	-51.1	-720	65	32
Base Line	-375	mm w. e.								
Ensemble	1.9	-7.1	-516	46	23	3.4	-8.3	-656	59	29

Table 3. 9. Glaciers thickness change by 2100 under the climate change scenarios and ensemble of GCMs for central Chile River Basins.

Chile	RCP4.5					RCP8.5				
	ΔST	ΔWP	Mean annual glacier melt (mm w. e.)	Total loss (%)		ΔST	ΔWP	mean annual glacier melt (mm w. e.)	Total loss (%)	
				<100m	>100m				<100m	>100m
CCSM4	2.0	13.7	-1293	100	58	3.7	23.2	-1643	100	74
CGCM3	1.1	-39.7	-1168	100	53	2.4	-47.9	-1168	100	53
GISS	1.1	31.3	-1074	97	48	2.4	67.7	-1324	100	60
IPSL_MR	2.6	-20.4	-1426	100	64	4.5	-7.8	-1821	100	82
MIROC_ESM	2.0	-38.2	-1402	100	63	3.6	-55.3	-1766	100	79
CNRM	2.9	21.2	-1419	100	64	4.5	10.5	-1736	100	78
Base Line	-934	mm w. e.								
Ensemble	1.8	-12.1	-1297	100	58	3.3	-17.5	-1577	100	71

Projected Equilibrium Line Altitude (Massa Blatten Watershed in Rhone)

There are many studies available on the glaciers of the Rhone River Basin but almost all of them focus on surface mass balance modelling without considering the interactions between ground water, lateral flow, and infiltration for a glacial system of the multiple watersheds.

In this section, the SWAT model was applied for assessment of climate change impact on the regional equilibrium line altitude changes of the glaciers across the Massa Blatten watershed (drainage area of Reach 23, Figure 3. 6) in Rhone, Switzerland. The largest European Alps glacier, Grosser Aletschgletscher, is located in the Massa Blatten watershed. The glacier has lost approximately 16 of its mass during the 20th century. The equilibrium line altitude (ELA) is defined as the altitude where the net mass balance is zero. ELA is an also an index of net mass distribution on the glacier. For example, if the ELA increases, then more of the glacier is in the ablation zone and the glacier retreats. Conversely, if the ELA decreases, all else being equal, the glacier advances. ELA is determined by climate and the aspect of the glacier. It is not influenced by glacier dynamics, extent and hypsometry, and thus reveals a largely unfiltered climatic signal (Huss, 2008). According to previous studies in the Alps (Greene et al., 1999; Maisch, 2000) the ELA sensitivity to temperature rise is on the order of 150 m/°C.

The ELA change relative to a baseline was simulated under the climate change scenario by CCSM4, RCP4.5 for a 2.55 ºC increase in summer temperature and 7.37 increases in winter precipitation. The GCM was selected among 6 GCMs based on the prescribed maximum 2 ºC warming by IPCC.

Huss et al. (2008) suggested a mean ELA of 3003 m and specific net annual mass balance of -460 mm w. e. for Aletschgletscher over the period 1865-2006. For simulation of ELA and the mass balance over the glacier, the glaciered subbasins were divided into 10 elevation bands with 200 m intervals on the glaciers (Figure 3. 6). The elevation bands were set narrower around the regional ELA of the river basin. The specific net annual mass balance (bn) for each elevation band was calculated for a balance year (1 October and 30 September).

Long-term mean ELA was considered as an altitude of zero mass balance over a period of 30 years for baseline and climate change scenarios. The years with negative mass balance at the highest elevation bands were excluded which means that the ELA is higher than the glaciers peak. The results show a 370 m upward shift in long term ELA for 2.5º C warming which is approximately compatible with suggested 150 m shift of ELA for 1°C warming by Greene et al. (1999) and Maisch (2000). The result implies that the SWAT can be used to determine changes in regional ELA due to climate change in future studies.

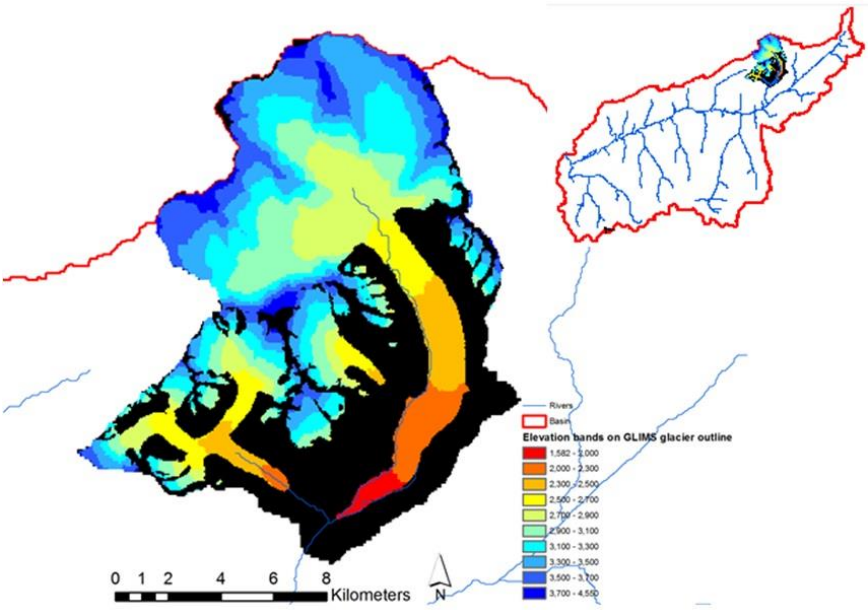

Figure 3. 6. Glaciers outline in Massa Blatten watershed (Drainage area of Reach 23) and location in Switzerland. The elevation band interval is 200m.

Summary, Conclusions, and Future Works

The study has shown the impact of climate change on glacier change and runoff in multiple large-scale river basins with a focus on their glaciered areas**.** Projected climate changes were developed using low representative concentration pathway (RCP4.5 and RCP8.5) and six CMIP5 models. Possible change in annual water yield was predicted to be 17 and 40 for Rhone, 50 and 80 for Narayani, 65 and 116 for Vakhsh, 28 and 55 for Mendoza, 17 and 30 for Chile under RCP4.5 and RCP8.5 and GCMs ensemble. The increase in total water yield exceeded or was in range of the snowmelt increases in all river basins under all climate change scenarios, which indicated that the hydrologic regime of the river basins is highly affected by melt due to

warming. Reduction of snow fall in the future and consequently reduction or vanishing of the permanent snowpack at lower altitudes and melting of the glaciers at higher altitudes postponed peak stream flow from July to August for the Rhone, Narayani and Vakhsh River Basins. In low glaciered or glacier free areas, peak summer flow moved from late summer to mid spring due to conversion of snow fall to rain fall with warming and consequently rapid increase in stream flow.

The results implied that the projected change of high flow is strongly dependent on the degree of glaciation of watersheds. The projected Q5 show decreases across glacier free and low glaciered watersheds, whereas in highly glaciered watersheds, the maximum flow showed considerable increase due to glacier melt. Increasing in high flow implies the potential risk of floods in glaciered watersheds in the future because of the increase in the rapid melt with high air temperatures. Furthermore, because of the increase in the air temperature, the snowfall will decrease, and the rainfall will increase in the future. Such changes may result in an increase in floods during the early spring and significant changes in the hydrological regime in the future. The risks of droughts may also increase during dry seasons because of declining snow storage and consequently less contributed melt water to the runoff in the future. This situation may significantly affect the availability of water resources necessary for agriculture, industrial water use, and so on in these regions.

For GCMs ensemble and RCP8.5, all the glaciers with 100 m w. e. will disappear by 2100 across the Rhone, Narayani and central Chile River Basins. All of the small and

shallow glaciers in lower altitudes with 5 to 20 m w. e. thickness will be melted by 2100 across the Mendoza River Basin.

The SWAT model was also applied for assessment of climate change impact on regional equilibrium line altitude changes of the glaciers across the Massa-Blatten watershed as a test area. The results implied that the SWAT can be used to determine regional changes in ELA due to climate change in the future studies.

REFERENCES

Abbaspour, K. C., Yang, J., Maximov, I., Siber, R., Bogner, K., Mieleitner, J., Zobrist, J., Srinivasan, R. 2007. Spatially-Distributed Modelling of Hydrology and Water Quality in the Prealpine/Alpine Thur Watershed Using SWAT. Journal of Hydrology, 333(2-4): 413-430.

Agrawala, S., Ota, T., Ahmed, A. U., Smith, J., van Aalst, M. 2003. Development and Climate Change in Bangladesh: Focus on Coastal Flooding and the Sunderbans. Organization for Economic Co-Operation and Development (OECD), Paris, France.

Ahl, R. S., Woods, S. W., Zuuring, H. R. 2008. Hydrologic Calibration and Validation of SWAT in a Snow-Dominated Rocky Mountain Watershed, Montana, U.S.A.. Journal of the American Water Resources Association, 44(6): 1411-1430.

Anderson, E. A. 1976. A Point Energy and Mass Balance Model of a Snow Cover. NOAA Tech. Rep. NWS 19, Office of Hydrology, National Weather Service, Silver Spring, MD, 150 pp.

Anderson, E. A. 1973. National Weather Service River Forecast System-Snow Accumulation and Ablation Model. National Oceanographic and Atmospheric Administration, Silver Springs, Md., Tech. Memo NWS_HYDRO-17.

Anonymous, 1969. Mass-Balance Terms. Journal of Glaciology, 52(8): 3-7.

Armstrong, R., Raup, B., Khalsa, S. J. S., Barry, R., Kargel, J., Helm, C., Kieffer, H. 2010. GLIMS Glacier Database. U.S. National Snow and Ice Data Center, Boulder, Colorado, USA: Digital media. Online available from: http://www.glims.org

Arnold, J. G., Muttiah, R. S., Srinivasan, R., Allen, P. M. 2000. Regional Estimation of Base Flow and Groundwater Recharge in the Upper Mississippi Basin. Journal of Hydrology, 227(1-4): 21-40.

Arnold, J. G., Srinivasan, R., Muttiah, R. S., Allen, P. M., Walker, C. 1999. Continental Scale Simulation of the Hydrologic Balance. Journal of American Water Resources Association, 35(5): 1037-1052.

Arnold, J. G., Srinivasan, R., Muttiah, R. S., Williams, J. R. 1998. Large Area Hydrologic Modeling and Assessment: Part I. Model Development. J. American Water Resources Association, 34(1): 73-89.

Bahr, D. B. 1997. Global Distributions of Glacier Properties: A Stochastic Scaling Paradigm. Water Resources Research, 33: 1669-1679.

Baldwin, M., Kellogg, C. E., Thorp, J. 1938. Soil Classification. In Soils and Men: Yearbook of Agriculture. Washington D.C.: U.S. Department of Agriculture. pp. 979-1001.

Barry, R. G. 1992. Mountain Weather and Climate. 2 Ed. Routledge, London and New York, 402 p.

Barsugli, J., Anderson, C., Smith, J. B., Vogel, J. M. 2009. Options for Improving Climate Modeling to Assist Water Utility Planning for Climate Change. Final Report, Water Utility Climate Alliance, San Francisco, Online available from: http://www.wucaonline.org/assets/pdf/actions_whitepaper_120909.pdf

Bharati, L., Gurung, P., Jayakody, P. 2012. Hydrologic Characterization of the Koshi Basin and the Impact of Climate Change. Hydro Nepal: Journal of Water, Energy and Environment, 18-22, 120.

Bradley, R. S., Vuille, M., Diaz, H. F., Vergara, W. 2006. Threats to Water Supplies in the Tropical Andes. Science, 312: 1755–1756.

Braithwaite, R. J. 1984. Calculation of Degree-Days for Glacier Climate Research. Z. Gletscherkd. Glazialgeol., 20: 1–20.

Braithwaite, R. J. 2008. Temperature and Precipitation Climate at the Equilibrium-Line Altitude of Glaciers Expressed by the Degree-Day Factor for Melting Snow. Journal of Glaciology, 54(186): 437-444.

Braithwaite, R. J., Muller, F. 1980. On the Parameterization of Glacier Equilibrium Line Altitude, IAHS Publ. 126 (Riederalp Workshop 1978 –World Glacier Inventory), 263-271.

Braithwaite, R. J., Raper, S. C. B. 2007. Glaciological Conditions in Seven Contrasting Regions Estimated with the Degree-Day Model. Annals of Glaciology, 46: 297-302.

Braithwaite, R. J., Raper, S. C. B. 2009. Estimating Equilibrium-Line Altitude (ELA) from Glacier Inventory Data. Annals of Glaciology, 50(53): 127-132.

Braithwaite, R. J., Zhang, Y. 1999. Modelling Changes in Glacier Mass Balance that May Occur as a Result of Climate Changes. Geografiska Annaler, 81(4): 489–496.

Braithwaite, R. J., Zhang, Y. 2000. Sensitivity of Mass Balance of Five Swiss Glaciers to Temperature Changes Assessed by Tuning a Degree-Day Model. Journal of Glaciology, 46(152): 7–14.

Braithwaite, R. J., Zhang, Y., Raper, S. C. B. 2003. Temperature Sensitivity of the Mass Balance of Mountain Glaciers and Ice Caps as a Climatological Characteristic. Zeitschrift für Gletscherkunde und Glazialgeologie, 38(1): 35-61.

Brenning, A. 2005. Geomorphological, Hydrological, and Climatic Significance of Rock Glaciers in the Andes of Central Chile (33–35 S). Permafrost and Periglacial Processes, 16: 231–240.

Brown, J. F., Loveland, T. R., Merchant, J. W., Reed, B. C., Ohlen, D. O. 1993. Using Multisource Data in Global Land Cover Characteristics: Concepts, Requirements and Methods. Photogrammetric Engineering and Remote Sensing, 59: 977-987.

Clarke, L., Edmonds, J., Jacoby, H., Pitcher, H., Reilly, J., Richels, R. 2007. Scenarios of Greenhouse Gas Emissions and Atmospheric Concentrations. Sub-report 2.1A of Synthesis and Assessment Product 2.1 by the U.S. Climate Change Science Program and the Subcommittee on Global Change Research. Department of Energy, Office of Biological & Environmental Research, Washington, D.C., USA, 154 pp.

Cogley, J. G., Hock, R., Rasmussen, L. A., Arendt, A. A., Bauder, A., Braithwaite, R. J., Jansson, P., Kaser, G., Möller, M., Nicholson, L., Zemp, M. 2010. Glossary of Glacier Mass Balance and Related Terms. IHP-VII Technical Documents in Hydrology No. 86, IACS Contribution No. 2, UNESCO-IHP, Paris. 114 pp.

Compagnucci, R. H., Vargas, W. 1998. Interannual Variability of Cuyo Rivers Streamflow in Argentinean Andean Mountains and ENSO Events. International Journal of Climatology, 18: 1593–1609.

Debele, B., Srinivasan, R. 2005. Comparison of the Performances of Temperature-Index and Process-Based Energy Budget Snowmelt Estimation Approaches in the SWAT Model. Texas A&M University, Spatial Sciences Laboratory, College Station, TX, p 40.

Debele, B., Srinivasan, R., Gosain, A. K. 2010. Comparison of Process-Based and Temperature-Index Snowmelt Modeling in SWAT. Water Resources Management, 24(6):1065–1088.

Di Luzio, M., Srinivasan, R., Arnold, J. G. 2002. Integration of Watershed Tools and SWAT Model into BASINS. Journal of American Water Resources Association, 38(4): 1127-1141.

Dyurgerov, M. B. 2002. Glacier Mass Balance and Regime: Data of Measurements and Analysis, Boulder, CO, University of Colorado. Institute of Arctic and Alpine Research. (INSTAAR Occasional Paper 55).

Dyurgerov, M. B., Meier, M. F., Bahr, D. B. 2009. A New Index of Glacier Area Change: A Tool for Glacier Monitoring, Journal of Glaciology, 55: 710–716.

FAO/IIASA/ISRIC/ISSCAS/JRC. 2012. Harmonized World Soil Database (version 1.2), Food and Agriculture Organization of the United Nations, International Institute for Applied Systems Analysis, ISRIC - World Soil Information, Institute of Soil Science - Chinese Academy of Sciences, Joint Research Centre of the European Commission, Laxenburg

Fontaine, T. A., Cruickshank, T. S., Arnold, J. G., Hotchkiss, R. H. 2002. Development of a Snowfall-Snowmelt Routine for Mountainous Terrain for the Soil Water Assessment Tool (SWAT). Journal of Hydrology, 262(1–4): 209–223.

Fujino, J., Nair, R., Kainuma, M., Masui, T., Matsuoka, T. 2006. Multi-Gas Mitigation Analysis on Stabilization Scenarios Using AIM Global Model. Multigas Mitigation and Climate Policy. The Energy Journal Special Issue.

Giesen, R. H., Oerlemans, J. 2012. Calibration of a Surface Mass Balance Model for Global-Scale Applications. Cryosphere. 6(6): 1463–1482.

Glaciological Reports: The Swiss Glaciers, 1880–2006/07, Tech. Rep. 1–128, Yearbooks of the Cryospheric Commission of the Swiss Academy of Sciences (SCNAT), published since 1964 by Laboratory of Hydraulics, Hydrology and Glaciology (VAW) of ETH Zürich, available at: http://glaciology.ethz.ch/swiss-glaciers/, 1881–2011.

Gosling, S. N., Taylor, R. G., Arnell, N. W., Todd, M. C. 2011. A Comparative Analysis of Projected Impacts of Climate Change on River Runoff from Global and Catchment-Scale Hydrological Models. Hydrology and Earth System Sciences, 15: 279–294.

Greene, A. M., Broeker, W. S., Rind, D. 1999. Swiss Glacier Recession since the Little Ice Age: Reconciliation with Climate Records, Geophys. Res. Lett., 26, 1909–1912.

Gross, G., Kerschner, H., Patzelt, G. 1978. Methodische Untersuchungen Über Die Schneegrenze in Alpinen Gletschergebieten, Z. Gletscherkd. Glazialgeol., 12: 223–251.

Gupta, H. V., Sorooshian, S., Yapo, P. O. 1999. Status of Automatic Calibration for Hydrologic Models: Comparison with Multilevel Expert Calibration. Journal of Hydraulic Engineering, 4(2): 135-143

Hagg, W. J., Braun, L. N., Uvarov, V. N., Makarevich, K. G. 2004. A Comparison of Three Methods of Mass-Balance Determination in the Tuyuksu Glacier Region, Tien Shan, Central Asia. Journal of Glaciology, 50: 505-510.

Hall, J. 2007. Probabilistic Climate Scenarios may Misrepresent Uncertainty and Lead to Bad Adaptation Decisions. Hydrological Processes, 21: 1127 –1129.

Hastenrath, S. 1971. On the Pleistocene Snow-Line Depression in the Arid Regions of the South American Andes. Journal of Glaciology, 10: 225-267.

Hijioka, Y., Matsuoka, Y., Nishimoto, H., Masui, M., Kainuma, M. 2008. Global GHG Emissions Scenarios under GHG Concentration Stabilization Targets. Journal of Global Environmental Engineering, 13: 97-108.

Hock, R. 1999. A Distributed Temperature-Index Ice- and Snowmelt Model Including Potential Direct Solar Radiation. Journal of Glaciology, 45(149): 101–111.

Hock, R. 2003. Temperature Index Melt Modelling in Mountain Areas. Journal of Hydrology, 282(1–4): 104–115.

Huss, M. 2011. Present and Future Contribution of Glacier Storage Change to Runoff from Macroscale Drainage Basins in Europe. Water Resources Research, 47: W07511.

Huss, M. 2012. Extrapolating Glacier Mass Balance to the Mountain Range Scale: The European Alps 1900–2100. Cryosphere, 6(4): 713–727.

Huss, M., Farinotti, D., Bauder, A., Funk, M. 2008. Modelling Runoff from Highly Glacierized Alpine Drainage Basins in a Changing Climate. Hydrological Processes, 22(19): 3888–3902.

Immerzeel, W. W. 2008. Historical Trends and Future Predictions of Climate Variability in the Brahmaputra Basin. International Journal of Climatology, 28: 243–254.

Immerzeel, W. W., Van Beek, L. P. H., Konz, M., Shrestha, A. B., Bierkens, M. F. P. 2011. Hydrological Response to Climate Change in a Glacierized Catchment in the Himalayas, Climatic Change, 110: 721–736.

Ives, J. D., Messerli, B. 1989. The Himalayan Dilemma. Routledge, London.

Jansson, P., Hock, R., Schneider, T. 2003. The Concept of Glacier Storage: A Review, Journal of Hydrology, 282: 116–129.

Jha, M., Arnold, J. G., Gassman, P. W., Giorgi, F., Gu, R. R. 2006. Climate Change Sensitivity Assessment on Upper Mississippi River Basin Streamflows Using SWAT. Journal of the American Water Resources Association, 42(4).

Karmacharya, J., Shrestha, A., Rajbhandari, R., Shrestha, M. L. 2007. Climate Change Scenarios for Nepal based on Regional Climate Model RegCM3, Report, Department of Hydrology and Meteorology, Kathmandu.

Kaser, G., Osmaston, H. 2002. Tropical Glaciers. Cambridge University Press, Cambridge.

Kayastha, R. B., Ageta Yand Fujita, K. 2005. Use of Positive Degree-Day Methods For Calculating Snow And Ice Melting and Discharge in Glacierized Basins in the Langtang Valley, Central Nepal. In De Jong C, Collins D and Ranzi R eds. Climate and hydrology in mountain areas. Wiley, Chichester

Kayastha, R. B., Ageta, Y., Nakawo, M., Fujita, K., Sakai, A., Matsuda, Y. 2003. Positive Degree-Day Factors for Ice Ablation on Four Glaciers in the Nepalese Himalayas and Qinghai-Tibetan Plateau: Bulletin of glaciological research, 20: 7-14.

Kayastha, R. B., Takeuchi, Y., Nakawo, M., Ageta, Y. 2000. Practical Prediction of Ice Melting Beneath Various Thickness of Debris Cover on Khumbu Glacier, Nepal, Using a Positive-Degree Day Factor. In M. Nakao, A. Fountain & C. F. Raymond (Eds.), Debris-covered Glaciers. Washington: IAHS Publication.

Koboltschnig, G. R., Schoner, W., Zappa, M., Kroisleitner, C., Holzmann, H. 2008. Runoff Modelling of the Glacierized Alpine Upper Salzach Basin (Austria): Multi-Criteria Result Validation, Hydrological Processes, 22.

Konz, M., Braun, L., Grabs, W., Shrestha, A., Uhlenbrook, S. 2006. Runoff from Nepalese Headwater Catchments- Measurements and Modelling. IHP/HWRP- Berichte, 4, Koblenz, 160 pp.

Konz, M., Seibert, J. 2010. On the Value of Glacier Mass Balances for Hydrological Model Calibration. Journal of Hydrology, 385: 238–246.

Konz, M., Uhlenbrook, S., Braun, L., Shrestha, A., Demuth, S. 2007. Implementation of a Process-Based Catchment Model in a Poorly Gauged, Highly Glacierized Himalayan Headwater, Hydrology and Earth System Sciences, 11(4): 1323–1339.

Kotlyakov, V. M., Krenke, A. N. 1982. Investigations of the Hydrological Conditions of Alpine Regions by Glaciological Methods. International Association of Hydrological Science Publications, 138: 31–42.

Krenke, A. N., Khodakov, V. G. 1966. The Relationship Between Surface Ice Melting and Air Temperature (In Russian). Data of Glacial Studies 12, 153-164. Moscow, USSR.

Kuhn, M., Abermann, J., Bacher, M., Olefs, M. 2009. The Transfer of Mass-Balance Profiles to Unmeasured Glaciers. Annals of Glaciology, 50: 185–190.

Kull, C., Grosjean, M., Veit, H. 2002. Modeling Modern and Late Pleistocene Glacio-Climatological Conditions in the North Chilean Andes. Climate Change, 52(3): 359–381.

Lang, H. 1986. Forecasting Meltwater Runoff from Snow-Covered Areas and from Glacier Basins. In River Flow Modelling and Forecasting, Kraijenhoff DA, Moll JR (eds). D. Reidel Publishing, Dordrecht, 99–127.

Lehner, B., Reidy Liermann, C., Revenga, C., Vörösmart, C., Fekete, B., Crouzet, P., Döll, P., Endejan, M., Frenken, K., Magome, J., Nilsson, C., Robertson, J. C., Rodel, R., Sindorf, N., Wisser., D. 2011. High-Resolution Mapping of the World's Reservoirs and Dams for Sustainable River-Flow Management. Frontiers in Ecology and the Environment, 9:494-502.

Lliboutry, L. 1986. Rock Glaciers in the Dry Andes. International Symposium ‘Glacier Mass Balance, Fluctuations and Runoff’, Alma-Ata, 30 September–5 October 1985.

Materialy Glyatsiologicheskikh Issledovaniy (Data on glaciological studies), 58: 18–25, 139–144.

Lliboutry, L. 1999. Glaciers of the dry Andes. In Williams RS Jr and Ferrigno JG eds. Satellite Image Atlas of Glaciers of the World: South America. (USGS Professional Paper 1386-I) US Geological Survey, Reston, VA, I119–I147.

Magnusson, J., Farinotti, D., Jonas, T., and Bavay, M. 2011. Quantitative Evaluation of Different Hydrological Modelling Approaches in a Partly Glacierized Swiss Watershed, Hydrological Processes, 25: 2071–2084.

Maisch, M. 2000. The Long-Term Signal of Climate Change in the Swiss Alps: Glacier Retreat since the End of the Little Ice Age and Future Ice Decay Scenarios. Geografia Fisica e Dinammica Quaternaria, 23: 139–151.

Martinec, J., Rango, A. 1986. Parameter Values for Snowmelt Runoff Modelling, Journal of Hydrology, 84: 197.

Masiokas, M. H., Luckman, B. H., Villalba, R., Ripalta, A., Rabassa, J. 2010. Little Ice Age Fluctuation of Glaciar R´Io Manso in the North Patagonian Andes of Argentina, Quaternary Research, 73: 96–106.

Mayo, L. R., Meier, M. F., Tangborn, W. V. 1972. A System to Combine Stratigraphic and Annual Mass Balance Systems: A contribution to the IHD, Journal of Glaciology, 11(61): 3–14.

McKay, M. D., Beckman, R. J., Conover, W. J. 1979. Comparison of Three Methods for Selecting Values of Input Variables in the Analysis of Output from a Computer Code. Technometrics, 21(2): 239-245.

Meier, M. F., Post, A. S. 1962. Recent Variations in Mass Net Budgets of Glaciers in Western North America. Union Geodesiqlle et Geophysique Internationale. Association Internationale d'Hydrologie Scientijique. Colioque d'Obergurgl, p. 63-77.

Micovic, Z., Quick, M. C. 2009. Investigation of the Model Complexity Required in Runoff Simulation at Different Time Scales. Hydrological Sciences Journal, 54: 872–885.

Mohanty, A., Mishra, M., Sharma, D., Ibrahimzada, M. W. 2012. Chapter 3 Assessing the Hydrological Impacts of Climate Change on the Amu Darya River, Afghanistan, in Armando Lamadrid, Ilan Kelman (ed.) Climate Change Modeling For Local Adaptation

In The Hindu Kush-Himalayan Region (Community, Environment and Disaster Risk Management , Volume 11), Emerald group publishing limited, pp 33-52.

Moor, R. D. 1993. Application of a Conceptual Streamflow Model in a Glacierized Drainage Basin. Journal of Hydrology, 150 (1): 151-168.

Moore, R. D., Demuth, M. N. 2001. Mass Balance and Stream-Flow Variability at Place Glacier, Canada, in Relation to Recent Climate Fluctuations. Hydrological Processes, 15.

MOPE. 2000. Implementation of UN Convention to Control Desertification. Ministry of Population and Environment, HMG Nepal, Kathmandu.

Moreiras, S., Lisboa, M. S., Mastrantonio, L. 2012. The Role of Snow Melting Upon Landslides in the Central Argentinean Andes. Earth Surface Processes and Landforms, 37: 1106-1119.

Moriasi, D. N., Arnold, J. G., Van Liew, M. W., Bingner, R.L., Harmel, R.D., Veith, T. L. 2007. Model Evaluation Guidelines for Systematic Quantification of Accuracy in Watershed Simulations. Transactions of the ASABE, 50(3):885–900.

Moss, R. H., Edmonds, J. A., Hibbard, K. A., Manning, M. R., Rose, S. K., van Vuuren, D. P., Carter, T. R., Emori, S., Kainuma, M., Kram, T. 2010. The Next Generation of Scenarios for Climate Change Research and Assessment. Nature, 463:747–756.

Nakićenović, N. 2000. Special Report on Emissions Scenarios: A Special Report of Working Group III of the Intergovernmental Panel on Climate Change, Cambridge University Press, Cambridge, U.K., 599 pp.

Nash, J. E., Sutcliffe, J. V. 1970. River Flow Forecasting Through Conceptual Models, Part I, A Discussion of Principles. Journal of Hydrology, 10: 282–290.

Neitsch, S. L., Arnold, J. C., Kiniry, J. R., Williams, J. R., King, K. W. 2002. Soil and Water Assessment Tool User's Manual. Version 2000. Texas Water Resources Institute, College Station, Texas, USA.

Neitsch, S. L., Arnold, J. G., Kiniry, J. R., Williams, J. R. 2011. Soil and Water Assessment Tool Theoretical Documentation Version 2009, Texas Water Ressources Institute Technical Report 406, Texas A&M University System, College Station (Texas).

Oerlemans, J. 2001. Glaciers and Climate Change. A. A. Balkema Publishers, 148 pp. ISBN 9026518137.

Ohmura, A., Kasser, P., Funk, M. 1992. Climate at the Equilibrium Line of Glaciers. Journal of Glaciology, 38: 397– 411.

Østrem, G. 1975. ERTS Data in Glaciology an effort to Monitor Glacier Mass Balance From Satellite Imagery. Journal of Glaciology, 15: 403–416.

Parajka, J., Blöschl, G., Merz, R. 2007. Regional Calibration of Catchment Models: Potential for Ungauged Catchments, Water Resources Research, 43.

Park, Y. Y., Park, M. J., Ahn, S. R., Park, G. A., Yi, J. E., Kim, G. S., Srinivasan, R., Kim, S. J. 2011. Assessment of Future Climate Change Impacts on Water Quantity and Quality for a Mountainous Dam Watershed Using SWAT. Transactions of the ASABE. 54(5): 1725-1737.

Pellicciotti, F., Brock, B., Strasser, U., Burlando, P., Funk, M., Corripio, J. 2005. An Enhanced Temperature-Index Glacier Melt Model Including the Short Wave Radiation Balance: Development and testing for Haut Glaciered Arolla, Switzerland, Journal of Glaciology, 51: 573–587.

Pradhanang, S. M., Anandhi, A., Mukundan, R., Zion, M. S., Pierson, D. C., Schneiderman, E. M., Matonse, A., Feri, A. 2011. Application of SWAT Model to Assess Snowpack Development and Streamflow in the Cannonsville Watershed, New York, USA. Hydrological Processes, 25: 3268–3277.

Rabassa, J., Clapperton, C. M. 1990. Quaternary Glaciations in the Southern Andes. Quaternary Science Reviews, 9: 153–174.

Rabatel, A., Dedieu, J. P., Vincent, C. 2005. Using Remote-Sensing Data to Determine Equilibrium Line Altitude and Mass-Balance Time Series: Validation on Three French Glaciers, 1994–2002, Journal of Glaciology, 51: 539–546.

Rafferty, J. P. 2011. Rivers and Streams. The Rosen Publishing Group. pp. 217–218. ISBN 1-61530-411-8

Rao, S., Riahi, K. 2006. The Role of Non-CO2 Greenhouse Gases in Climate Change Mitigation: Long-Term Scenarios for the 21st Century. Multigas Mitigation and Climate Policy. The Energy Journal, 3(Special Issue): 177–200.

Raup, B. H., Kieffer, H. H., Hare, T. M., Kargel, J. S. 2000. Generation of Data Acquisition Requests for the ASTER Satellite Instrument for Monitoring a Globally

Distributed Target: Glaciers. IEEE Transactions on Geoscience and Remote Sensing, 38: 1105-1112.

Reclamation, Downscaled CMIP3 and CMIP5 Climate and Hydrology Projections: Release of Downscaled CMIP5 Climate Projections, Comparison with preceding Information, and Summary of User Needs', prepared by the U.S. Department of the Interior, Bureau of Reclamation, Technical Services Center, Denver, Colorado. 47pp, 2013.

Rees, H. G., Collins, D. N. 2006. Regional Differences in Response of Flow in Glacier-fed Himalayan rivers to climatic warming. Hydrological Processes, 20: 2157–2169.

Riahi, K., Grübler, A., Nakicenovic, N. 2007. Scenarios of Long-Term Socio-Economic and Environmental Development under Climate Stabilization. Technological Forecasting *and* Social Change, 74: 887–935.

Richard, L., Tonnel, A. 1985. Contribution a` L'e´Tude Bioclimatique de L'arc Alpin. Doc. Cartogr. Ecol., 28: 33–64.

Rivera, V. M., Wang, X., Wardwell, S., Courage, N. L., Volchuk, A., Keenan, T., Holt, D. A., Gilman, M., Orci, L., Cerasoli Jr, F. 2000. Regulation of Protein Secretion Through Controlled Aggregation in the Endoplasmic Reticulum. Science, 287: 826–830.

Rosenzweig, C., Casassa, G., Karoly, D., Imeson, A., Liu, C., Menzel, A. 2007. Assessment of Observed Changes and Responses in Natural and Managed Systems. In: Climate Change 2007: Impacts, Adaptation and Vulnerability. Contribution of Working Group II to the Fourth Assessment Report of the Intergovernmental Panel on Climate Change (Parry ML, Canziani OF, Palutikof JP, van der Linden PJ, Hanson CE, eds), Cambridge, UK: Cambridge University Press, 79–131.

Saha, S. 2010. The NCEP Climate Forecast System Reanalysis. Bulletin of the American Meteorological Society, 91:1015–1057.

Savoskul, O. S., Smakhtin, V. 2013. Glacier Systems and Seasonal Snow Cover in Six Major Asian River Basins: Hydrological Role under Changing Climate. Colombo, Sri Lanka: International Water Management Institute (IWMI), 53p.

Schäfli, B., Hingray, B., Musy, A. 2007. Climate Change and Hydro-Power Production in the Swiss Alps: Quantification of Potential Impacts and Related Modelling Uncertainties, Hydrology and Earth System Sciences, 11(3):1191–1205.

Schäfli, B., Hingray, B., Niggli, M., Musy, A. 2005. A Conceptual Glaciohydrological Model for High Mountainous Catchments. Hydrology and Earth System Sciences, 11(3): 1191–1205.

Schäfli, B., Huss, M. 2010. Integrating Point Glacier Mass Balance Observations into Hydrologic Model Identification. Hydrology and Earth System Sciences, 15: 1227–1241.

Schaper, J., Martinec, J., Seidel, K., 1999. Distributed Mapping of Snow and Glaciers for Improved Runoff Modelling. Hydrological Processes, 13(12–13): 2023–2031.

Schaper, J., Seidel, K., Martinec, J. 2000. Precision Snow Cover and Glacier Mapping For Runoff Modelling In A High Alpine Basin. In Remote Sensing and Hydrology 2000. Proceedings of the Santa Fe Symposium, IAHS Publ. No. 268.

Schwarb, M., Frei, C., Daly, C., Schär, C. 2001. Mean Seasonal Precipitation Throughout the European Alps 1971–1990. In: Spreafico M, Weingartner R, Leibundgut C (eds) Hydrological atlas of Switzerland. Landeshydrologie und geologie, Bern, Plate 27.

Shreshtha, A. B., Aryal, R. 2011. Climate Change in Nepal and its Impact on Himalayan Glaciers. Regional Environmental Change, 11(1): 65–77.

Siderius, C., Biemans, H., Rao, S., Wiltshire, A., Franssen, W. H. P., Kumar, P., Gosain, A. K., van Vliet, M. T. H., Collins, D. N. 2013. Snowmelt Contributions to Discharge of the Ganges. Science of the Total Environment, 468-469(Suppl.): S93-S101

Singh, I. L. 1985. Rainfall Distribution. In Nepal- Nature's Paradise. T. C. Majupuria, Ed., pp. 56-58. White Lotus Co. Ltd., Bangkok.

Singh, P., Kumar, N. 1996. Determination of Snowmelt Factor in the Himalayan Region. Hydrological Sciences Journal, 41(3): 301–310.

Singh, P., Singh, V.P. 2001. Snow and Glacier Hydrology. Kluwer: The Netherlands.

Smith, S. J., Wigley, T. M. L. 2006. Multi-Gas Forcing Stabilization with the MiniCAM. Energy Journal (Special Issue #3): 373-391.

Srinivasan, R., Ramanarayanan, T. S., Arnold, J. G., Bednarz, S. T. 1998. Large Area Hydrologic Modeling and Assessment: Part II. Model Application. Journal of American Water Resources Association, 34(1): 91-101.

Stahl, K., Moore, R., Shea, J., Hutchinson, D., Cannon, A. 2008. Coupled Modelling of Glacier and Streamflow Response to Future Climate Scenarios. Water Resources Research, 44: W02422.

Stehr, A., Debels, P., Arumi, J. L., Romero, F., Alcayaga, H. 2009. Combining the Soil and Water Assessment Tool (SWAT) and MODIS Imagery to Estimate Monthly Flows in a Data-Scarce Chilean Andean Basin. Hydrological Sciences Journal, 54(6): 1053–1067.

Taylor, K. E., Stouffer, R. J., Meehl, G. A. 2012. An Overview of CMIP5 and the Experiment Design. Bulletin of the American Meteorological Society, 93: 485-498.

USDA, NRCS, 2007 National Soil Survey Handbook, Part 618, Exhibit 8, http://soils.usda.gov/technical/handbook/contents/part618ex.html#ex8

van Vuuren, D. P., Eickhout, B., Lucas, P. L., den Elzen, M. G. J. 2006. Long-Term Multi-Gas Scenarios to Stabilise Radiative Forcing-Exploring Costs and Benefits Within an Integrated Assessment Framework. Multigas Mitigation and Climate Policy. Energy Journal, 3 (Special Issue): 201–234.

van Vuuren, D., den Elzen, M., Lucas, P., Eickhout, B., Strengers, B., van Ruijven, B., Wonink, S., van Houdt, R. 2007. Stabilizing Greenhouse Gas Concentrations at Low Levels: An Assessment of Reduction Strategies and Costs. Climatic Change. Available at http://dx.doi.org/10.1007/s10584-006-9172-9.

Vargas, W. Y., Compagnucci, R. 1985. Relaciones del Régimen de Precipitación Entre Santiago de Chile Y Las Series de la Región Cordillerana, GEOACTA, 13(1): 81-93.

Wang, X., Melesse, A. M. 2005. Evaluation of the SWAT Model's Snowmelt Hydrology in a Northwestern Minnesota Watershed. Transaction of ASAE, 48(4):1359–1376.

Waylen, P. R., Caviedes, C. N. 1990. Annual and Seasonal Streamflow Fluctuations of Precipitation and Streamflow in the Aconcagua River Basin, Chile. Journal of Hydrology, 120: 79-102.

WGMS and NSIDC. 1989. updated 2009. World Glacier Inventory. Compiled and Made Available by the World Glacier Monitoring Service, Zurich, Switzerland, and the National Snow and Ice Data Center, Boulder CO, USA. Digital media.

Williams, V. S. 1983. Present and Former Equilibrium-Line Altitudes near Mount Everest, Nepal and Tibet. Arctic and Alpine Research, 15: 201–211.

Wise, M. A., Calvin, K. V., Thomson, A. M., Clarke, L. E., Bond-Lamberty, B., Sands, R. D., Smith, S. J., Janetos, A. C., Edmonds, J. A. 2009. Implications of Limiting CO2 Concentrations for Land Use and Energy. Science, 324:1183-1186.

Zemp, M., Frey, H., Gärtner-Roer, I., Nussbaumer, S. U., Hoelzle, M., Paul, F., Haeberli, W. 2012. WGMS, Fluctuations of Glaciers 2005-2010 (Vol. X), ICSU (WDS)/ IUGG (IACS)/ UNEP/ UNESCO/ WMO, World Glacier Monitoring Service, Zurich, Switzerland.

Zemp, M., Haeberli, W., Hoelzle, M., Paul, F. 2006a. Alpine Glaciers to Disappear Within Decades, Geophysical Research Letters 33.

Zemp, M., Hoelzle, M., Haeberli, W. 2007. Distributed Modeling of the Regional Climatic Equilibrium Line Altitude of Glaciers in the European Alps. Global and Planetary Change, 56: 83–100.

Zemp, M., Hoelzle, M., Haeberli, W. 2006b. Distributed Modeling of the Regional Climatic Equilibrium Line Altitude of Glaciers in the European Alps, Global Plant. Change, special issue on climate change impacts on glaciers and permafrost.

Zhang, X. S., Srinivasan, R., Debele, B., Hao, F. H. 2008. Runoff Simulation of the Headwaters of the Yellow River Using the SWAT Model with Three Snowmelt Algorithms. Journal of American Water Resources Association, 44(1):48–61.

Zhang, Y., Hirabayashi, Y., Liu, S. 2012. Catchment-Scale Reconstruction of Glacier Mass Balance Using Observations and Global Climate Data: Case Study of the Hailuogou Catchment, South-Eastern Tibetan Plateau. Journal of Hydrology, 146–160.

APPENDIX A

Table A. 1. Calibration parameters for elevation band of the draining subbasins to Reach 123 (Method 3), Narayani River Basin.

Narayani	Reach:123							
Subbasin#	SFTMP	SMTMP	SMFMX (1-6)	SMFMX (7-10)	SMFMN (1-6)	SMFMN (7-10)	TIMP (1-6)	TIMP (7-10)
1	2	2	6	8	4.3	6	0.7	0.06
2	2	2	6	8	4.3	6	0.7	0.06
3	2	2	6	8	4.3	6	0.7	0.06
4	2	0.8	6	8	3.5	6	0.7	0.06
5	2	0.8	6	8	3.5	6	0.7	0.06
6	2	0.8	6	8	3.5	6	0.7	0.06
7	2	2	6	8	4.3	6	0.7	0.06
8	2	0.8	6	8	3.5	6	0.7	0.06
9	2	2	6	8	4.3	6	0.7	0.06
10	2	0.8	6	8	3.5	6	0.7	0.06
11	2	2	6	8	4.3	6	0.7	0.06
12	2	2	6	8	4.3	6	0.7	0.06
13	2	2	6	8	4.3	6	0.7	0.06
14	2	0.8	6	8	3.5	6	0.7	0.06
15	2	0.8	6	8	3.5	6	0.7	0.06
17	2	2	6	8	4.3	6	0.7	0.06
35	2	0	7	9	6	7	0.7	0.05
47	2	0	5	8	4	6	0.7	0.05
48	2	0	5	8	4	6	0.7	0.05
49	2	0	5	8	4	6	0.7	0.05
56	2	0	5	8	4	6	0.7	0.05
57	2	0	5	8	4	6	0.7	0.05
60	2	0	5	8	4	6	0.7	0.05
71	2	0	5	8	4	6	0.7	0.05
72	2	0	5	8	4	6	0.7	0.05
76	2	0	5	8	4	6	0.7	0.05
77	2	0	5	8	4	6	0.7	0.05
91	2	0	5	8	4	6	0.7	0.05
92	2	0	5	8	4	6	0.7	0.05
97	2	0	5	8	4	6	0.7	0.05
98	2	0	5	8	4	6	0.7	0.05
123	2	0	5	8	4	6	0.7	0.05

Table A. 2. Calibration parameters for elevation bands of the draining subbasins to Reach 133 (Method 3), Vakhsh River Basin

Vakhsh	Reach: 133								
Subbasin#	SFTMP	SMTMP (1-3)	SMTMP (4-10)	SMFMX (1-3)	SMFMX (4-10)	SMFMN (1-3)	SMFMN (4-10)	TIMP (1-3)	TIMP (4-10)
91	2.00	0.00	1.00	5.00	7.00	5.00	6.00	0.50	0.20
101	2.00	0.00	1.00	5.00	7.00	5.00	6.00	0.50	0.20
108	1.50	0.00	0.50	5.00	7.00	5.00	6.00	0.70	0.20
111	2.00	0.00	1.00	5.00	7.00	5.00	6.00	0.50	0.20
114	2.00	0.00	1.00	5.00	7.00	5.00	6.00	0.50	0.20
115	2.00	0.00	1.00	5.00	7.00	5.00	6.00	0.50	0.20
116	2.00	0.00	1.00	5.00	7.00	5.00	6.00	0.50	0.20
121	1.50	0.00	0.50	5.00	7.00	5.00	6.00	0.70	0.20
122	2.00	0.00	1.00	5.00	7.00	5.00	6.00	0.50	0.20
123	2.00	0.00	1.00	5.00	7.00	5.00	6.00	0.50	0.20
124	2.00	0.00	1.00	5.00	7.00	5.00	6.00	0.50	0.20
127	2.00	0.00	1.00	5.00	7.00	5.00	6.00	0.50	0.04
128	1.50	0.00	0.50	5.00	7.00	5.00	6.00	0.70	0.04
129	2.00	0.00	1.00	5.00	7.00	5.00	6.00	0.50	0.04
130	2.00	0.00	1.00	5.00	7.00	5.00	6.00	0.50	0.04
132	2.00	0.00	1.00	5.00	7.00	5.00	6.00	0.50	0.04
133	1.50	0.00	0.50	5.00	7.00	5.00	6.00	0.70	0.04
134	1.50	0.00	0.50	5.00	7.00	5.00	6.00	0.70	0.04
136	2.00	0.00	1.00	6.00	8.00	5.00	7.00	0.50	0.03
137	2.00	1.00	1.50	6.00	8.00	5.00	7.00	0.50	0.03
138	2.00	1.00	1.50	6.00	8.00	5.00	7.00	0.50	0.03
139	2.00	1.00	1.50	6.00	8.00	5.00	7.00	0.50	0.03
140	2.00	1.00	1.50	6.00	8.00	5.00	7.00	0.50	0.03
141	2.00	1.00	1.50	6.00	8.00	5.00	7.00	0.50	0.03
142	2.00	1.00	1.50	6.00	8.00	5.00	7.00	0.50	0.03
143	2.00	1.00	1.50	6.00	8.00	5.00	7.00	0.50	0.03

Table A. 3. Calibration parameters for elevation bands of the draining subbasins to Reach 84 (Method 3), Mendoza River Basin

Mendoza	Reach: 84								
Sbbasin#	SFTMP	SMTMP (1-3)	SMTMP (4-10)	SMFMX (1-6)	SMFMX (7-10)	SMFMN (1-6)	SMFMN (7-10)	TIMP (1-6)	TIMP (7-10)
84	1	2	3	2.3	3.8	2.5	4	0.44	0.3
87	1	2	3	2.3	3.8	2.5	4	0.44	0.3
88	2.5	3	3.3	2.3	3.8	2.5	4	0.44	0.1
89	1	2	3	2.3	3.8	2.5	4	0.44	0.3
91	2.5	3	3.3	2.3	3.8	2.5	4	0.44	0.1
92	1	2	3	2.3	3.8	2.5	4	0.44	0.3
93	2.5	3	3.3	2.3	3.8	2.5	4	0.44	0.1
94	1	2	3	2.3	3.8	2.5	4	0.44	0.3
96	2.5	3	3.3	2.3	3.8	2.5	4	0.44	0.1
97	1	2	3	2.3	3.8	2.5	4	0.44	0.3
98	2.5	3	3.3	2.3	3.8	2.5	4	0.44	0.1
99	1	2	3	2.3	3.8	2.5	4	0.44	0.3
100	2.5	2.5	3.5	3	4	3.4	4.5	0.44	0.07
101	2.5	2.5	3.5	3	4	3.4	4.5	0.44	0.07
102	2.5	3	3.3	2.3	3.8	2.5	4	0.44	0.1
103	2.5	3	3.3	2.3	3.8	2.5	4	0.44	0.1
104	2.5	3	3.3	2.3	3.8	2.5	4	0.44	0.1
105	2.5	3	3.3	2.3	3.8	2.5	4	0.44	0.1
106	2.5	2.5	3.5	3	4	3.4	4.5	0.44	0.07
107	2.5	2.5	3.5	3	4	3.4	4.5	0.44	0.07
108	2.5	2.5	3.5	3	4	3.4	4.5	0.44	0.07
109	2.5	2.5	3.5	3	4	3.4	4.5	0.44	0.07
110	2.5	2.5	3.5	3	4	3.4	4.5	0.44	0.07
111	2.5	2.5	3.5	3	4	3.4	4.5	0.44	0.07
112	2.5	2.5	3.5	3	4	3.4	4.5	0.44	0.07
113	2.5	2.5	3.5	3	4	3.4	4.5	0.44	0.07
114	2.5	2.5	3.5	3	4	3.4	4.5	0.44	0.07

Table A. 4. Calibration parameters for elevation bans of the draining subbasins to Reach 79 (Method 3), Mendoza River Basin

Mendoza	Reach: 79							
SUBBASIN	SFTMP	SMTMP	SMFMX (1-5)	SMFMX (6-10)	SMFMN (1-5)	SMFMN (6-10)	TIMP (1-5)	TIMP (6-10)
28	3.4	3.8	2.5	3	3	4	0.5	0.02
31	3.4	3.8	2.5	3	3	4	0.5	0.02
39	3.4	3.8	2.5	2.5	3	4	0.5	0.3
40	4	1	2.3	3	3	4	0.5	0.3
41	3.4	3.8	2.5	2.5	3	4	0.6	0.3
42	4	1	2.5	3	3	4	0.5	0.3
51	2	2	2.5	3	3	4	0.5	0.3
52	2	2	2.5	2.5	3	4	0.6	0.3
56	2	2	2.5	3	3	4	0.4	0.01
60	2	2	2.5	2.5	3	4	0.6	0.01
66	2	2	2.5	3	3	4	0.5	0.01
67	2	2	2.5	3	3	4	0.5	0.01
79	2	2	2.5	3	3	4	0.5	0.01

Table A. 5. Calibration parameters for elevation bans of the draining subbasins to Reach 5 (Method 3), Central dry Andes in Chile.

Chile	Reach: 5									
Subbasin#	SFTMP	SMTMP (1-2)	SMTMP (3-6)	SMTMP (7-10)	SMFMN (1-6)	SMFMN (7-10)	SMFMX (1-6)	SMFMX (7-10)	TIMP (1-6)	TIMP (7-10)
1	-4.00	-0.30	1.00	1.00	4.50	6.50	5.00	7.00	0.700	0.010
2	-4.00	-0.30	1.00	1.00	4.50	6.50	5.00	7.00	0.700	0.010
5	-4.00	-1.00	-1.00		6.00		6.00		1.000	0.000
6	-4.00	-0.30	1.00	1.00	5.00	6.00	5.00	6.70	0.700	0.010
7	-4.60	1.20	2.40	2.40	2.00	5.30	3.00	5.80	0.140	0.014
8	-2.00	-1.00	-1.00	0.00	3.00	4.00	2.00	3.00	0.500	0.400
9	-2.00	-1.00	-1.00	0.00	3.00	4.00	2.00	3.00	0.500	0.010
11	-4.00	-1.00	0.00		4.50		4.50		1.000	0.000
12	-4.00	-1.00	-1.00		4.50		6.00		1.000	0.000
13	-4.60	1.20	2.40	2.40	2.00	5.30	3.00	5.80	0.140	0.014
14	2.00	1.00	1.00	0.00	3.00	4.00	4.00	6.00	0.500	0.500
15	2.00	1.00	1.00	0.00	3.00	4.00	4.00	6.00	0.500	0.500
17	-4.00	-1.00	-1.00		5.00		6.00		1.000	0.000
18	2.00	1.00	1.00	0.00	3.00	4.00	4.00	6.00	0.500	0.500
19	2.00	1.00	1.00	0.00	3.00	4.00	4.00	6.00	0.300	0.500
Ave.	-2.21	-0.03	0.45	0.71	3.73	4.87	4.23	5.66	0.612	0.165
Min.	-4.60	-1.00	-1.00	0.00	2.00	4.00	2.00	3.00	0.140	0.000
Max.	2.00	1.20	2.40	2.40	6.00	6.50	6.00	7.00	1.000	0.500

Table A. 6. Calibration parameters for elevation bans of the draining subbasins to Reach 66 (Method 3), Central dry Andes in Chile.

Chile	Reach: 66								
Subbasin#	SFTMP	SMTMP (1-6)	SMTMP (7-10)	SMFMN (1-6)	SMFMN (7-10)	SMFMX (1-6)	SMFMX (7-10)	TIMP (1-6)	TIMP (7-10)
64	3	1	3	4	6	6	7	0.7	0.01
65	3	1	3	4	6	6	7	0.7	0.01
66	3	1	3	4	6	6	7	0.7	0.01
68	3	1	3	4	6	6	7	0.7	0.01
69	3	1	3	4	6	6	7	0.7	0.01
70	3	1	3	4	6	6	7	0.7	0.01

APPENDIX B

Table B. 1. Published ELA and mass balance data used for model calibration and validation

	Rhone		Gries		Abramov	
	Bn	ELA	Bn	ELA	Bn	ELA
1980	888	2715	665	2660	-1081	4366
1981	87	2875	-123	2940	129	4446
1982	-375	3035	-890	3030	-774	4290
1983	-160	2940	-557	3000	-507	4416
1984			-8	2865	-971	4391
1985			-259	2878	-855	3684
1986			-535	2946	-1010	4431
1987			-659	2985	240	4269
1988			-878	3073	10	4301
1989			-1063	3201	-230	4331
1990			-1743	3401	-530	4369
1991			-1097	3264	-488	4393
1992			-724	3028	448	4304
1993			-32	2839	333	4204
1994			-494	2953	-859	4219
1995			158	2799	-896	4353
1996			-230	2884	-410	4360
1997			-270	2893	-1976	4310
1998			-1660	3401	219	4460
1999			-580	2979		4330
2000			-874	3009		
2001			-50	2897		
2002			-600	2975		
2003			-2630	3400		
2004			-1330	3400		
2005			-1670	3153		
2006			-1995	3325		
2007			-1473	3324		
2008			-1601	3125		
2009			-883	3134		
2010			-803	3085		
Steady state		2918		2853		4354

Table B. 2. Elevation-mass balance data for Rhone glacier

	Elevation	Area km^2	1980-81	1981-82
	3500-3629	0.424	3920	3750
	3400-3500	0.811	3320	3280
	3300-3400	1.139	2590	2500
	3200-3300	1.601	2300	2100
	3100-3200	1.542	1240	1060
	3000-3100	1.803	430	50
	2900-3000	2.615	210	-280
	2800-2900	1.615	-80	-670
	2700-2800	1.378	-1030	-1640
	2600-2700	1.902	-1700	-2400
	2500-2600	1.063	-2130	-2980
	2400-2500	0.589	-3040	-3900
	2300-2400	0.704	-3930	-4810
	2280-2300	0.194	-5680	-6280
SUMMARY	2280-3629	17.38	90	-380

Table B. 3. Elevation-mass balance data for Gries glacier

Elevation (m)	Area (km^2)	1979	1980	1981	1982	1983	1984	1985
3350	0.01	300	1800	1300	300	800	1200	910
3250	0.13	250	1740	1250	250	750	1250	810
3150	0.547	120	1550	770	280	640	1000	700
3050	1.597	-30	1490	610	100	350	780	530
2950	1.004	-650	1020	60	-370	-360	150	260
2850	0.726	-840	580	-290	-590	-680	-20	-120
2750	0.543	-1120	370	-330	-1090	-940	-350	-600
2650	0.984	-1820	-70	-960	-1970	-1500	-820	-1200
2550	0.608	-2230	-870	-1640	-2770	-1800	-1260	-1900
2450	0.184	-2710	-1690	-4440	-5290	-3290	-2110	-2700
Summary	6.337	-860	720	-230	-880	-550	0	-260
Elevation (m)	Area (km^2)	1986	1987	1988	Area (km^2)	1989	1990	1991
3350	0.01	670	550	360	0.01	200	-390	120
3250	0.09	560	430	240	0.09	70	-540	-20
3150	0.43	440	310	110	0.43	-70	-700	-150
3050	1.666	280	160	-50	1.666	-220	-860	-310
2950	1.061	10	-110	-310	1.061	-480	-1120	-570
2850	0.727	-370	-490	-700	0.727	-880	-1520	-960
2750	0.573	-870	-1000	-1220	0.573	-1400	-2080	-1490
2650	0.85	-1490	-1620	-1860	0.85	-2060	-2790	-2160
2550	0.678	-2220	-2370	-2630	0.678	-2850	-3660	-2960
2450	0.164	-3060	-3230	-3520	0.164	-3770	-4670	-3890
Summary	6.249	-530	-660	-880	6.249	-1060	-1740	-1100
Elevation (m)	Area (km^2)	1992	1993	1994	1995	1996	1997	1998
3350	0.01	450	1080	650	1250	890	860	-380
3250	0.09	320	970	530	1150	780	750	-530
3150	0.43	200	860	420	1050	670	630	-680
3050	1.666	40	690	260	870	510	470	-840
2950	1.061	-220	420	-10	600	240	200	-1100
2850	0.727	-610	50	-390	230	-140	-180	-1500
2750	0.573	-1120	-430	-890	-240	-630	-670	-2060
2650	0.85	-1750	-1010	-1510	-810	-1220	-1260	-2770
2550	0.678	-2510	-1690	-2240	-1470	-1920	-1970	-3630
2450	0.164	-3390	-2470	-3090	-2220	-2740	-2790	-4640
Summary	6.249	-720	-30	-500	160	-230	-270	-1660
Elevation (m)	Area (km^2)	1999	2000	2001	2002	2003	2004	2005
3350	0.01	570	2416	3070	2630	-1270	-330	1180
3250	0.206	450	1708	2390	1930	-1300	-450	580
3150	0.692	330	1000	1710	1230	-1450	-490	-20
3050	1.6	170	292	1040	530	-1700	-610	-610
2950	0.994	-90	-416	360	-170	-2080	-850	-1200
2850	0.658	-480	-1124	-320	-880	-2570	-1220	-1790
2750	0.457	-980	-1832	-1000	-1580	-3180	-1700	-2370
2650	0.619	-1610	-2540	-1670	-2280	-3900	-2310	-2940
2550	0.805	-2350	-3248	-2350	-2980	-4730	-3050	-3510
2450	0.153	-3210	-3956	-3030	-3680	-5690	-3900	-4080
Summary	6.194	-580	-847	-50	-600	-2630	-1330	-1670
Elevation (m)	Area (km^2)	2006	2007					
3350	0.004	604	622					
3250	0.081	171	242					
3150	0.287	-325	-174					
3050	1.454	-805	-549					
2950	0.945	-1440	-1047					
2850	0.609	-1961	-1438					
2750	0.364	-2451	-1786					
2650	0.367	-3416	-2586					
2550	0.769	-4300	-3370					
2450	0.172	-4994	-3906					
Summary	5.084	-1995	-1473					

Table B. 4. Elevation-mass balance data for Abramov glacier

AREA	0.685	2.092	4.337	5.192	4.067	2.538	1.557	1.05	0.736	0.249
Altitude	4650	4550	4450	4350	4250	4150	4050	3950	3850	3750
1979	1510	1160	630	40	-420	-1300	-2070	-2940	-3810	-4000
1980	700	420	150	-700	-1260	-2010	-2660	-3510	-4630	-4980
1981	2300	1610	1250	580	50	-720	-1620	-2610	-3560	-3900
1982	1325	690	390	-280	-900	-1740	-2490	-3380	-4490	-4850
1983	1090	980	440	-80	-640	-1290	-2020	-2730	-3780	-4170
1984	2500	2190	1910	1480	1400	1170	850	600	430	330
1985	850	520	320	-190	-960	-1740	-2600	-3730	-5030	-5330
1986	160	110	-30	-510	-1190	-1800	-238	-320	-393	-417
1987	1090	1490	1210	700	170	-650	-1230	-2380	-3580	-3670
1988	1270	1560	1340	650	-280	-1130	-2000	-3070	-4220	-4210
1989	990	910	690	200	-380	-1090	-1770	-2570	-3290	-3420
1990	1070	990	750	170	-700	-1650	-2490	-3560	-4450	-4590
1991	800	1480	1280	900	300	-630	-1460	-2390	-3430	-4580
1992	900	1790	1790	1620	1160	320	-460	-1380	-2440	-3640
1993	940	1550	1580	1460	1040	240	-510	-1420	-2480	-3710
1994	220	1030	900	590	10	-920	-1760	-2730	-3820	-5020
1995	700	560	650	630	100	-1090	-1780	-2790	-3770	-5280
1996	780	860	880	910	440	-690	-1230	-2110	-2750	-4270
1997	60	480	210	-280	-1080	-2110	-2920	-3780	-4700	-5940
1998	1580	1820	1750	1550	990	160	-810	-1930	-3310	-4190
1999	1580	1820	1750	1550	990	160	-810	-1930	-3310	-4190

APPENDIX C

Table C. 1. Percentage of changes in simulated hydrologic components for a period of 2070-2099 relative to baseline period (1979-2008) for Rhone River Basin.

Rhone	CSIRO		GFDL		IPSL_LR		CCSM4		INMCM4		GISS		Ensemble	
	RCP 4.5	RCP 8.5	RCP 4.5	RCP 8.5	RCP 4.5	RCP 8.5	RCP 4.5	RCP 8.5	RCP 4.5	RCP 8.5	RCP 4.5	RCP 8.5	RCP 4.5	RCP 8.5
Precipitation	-7.93	-9.83	-2.80	-18.93	10.14	-9.02	-3.00	-10.71	-2.80	-17.91	-7.87	-6.98	-3.92	-12.23
Snow fall	-17.39	-28.41	-28.12	-54.52	-4.00	-62.04	-17.04	-30.49	-28.12	-30.51	-23.87	-30.00	-17.86	-39.33
Snow/glacier melt	50.81	98.00	58.05	109.49	-0.77	92.11	34.41	64.10	58.05	39.50	15.25	37.61	29.25	73.47
Sublimation	11.56	22.73	12.49	23.20	-6.83	12.08	7.27	12.87	12.49	9.26	3.44	7.05	5.36	14.53
Surface runoff	37.39	78.06	50.37	90.52	0.22	78.07	28.30	48.90	50.37	23.98	11.23	28.63	22.50	58.03
Total water yield	25.08	51.30	36.04	57.16	9.95	58.16	20.35	33.37	36.04	15.02	8.47	22.60	17.38	39.60

Table C. 2. Percentage of changes in simulated hydrologic components for a period of 2070-2099 relative to baseline period (1979-2008) for Narayani River Basin.

Narayani	GFDL		IPSL_MR		MIROC5		MIROC_ESM		CGCM3		INMCM4		Ensemble	
	RCP 4.5	RCP 8.5	RCP 4.5	RCP 8.5	RCP 4.5	RCP 8.5	RCP 4.5	RCP 8.5	RCP 4.5	RCP 8.5	RCP 4.5	RCP 8.5	RCP 4.5	RCP 8.5
Precipitation	45.69	53.87	22.33	30.32	14.40	22.48	13.33	22.48	7.24	19.97	17.02	26.95	20.00	29.35
Snow fall	-41.67	-62.36	-42.03	-67.25	-27.04	-30.77	-32.38	-30.77	-19.51	-31.47	-16.23	-37.95	-29.81	-43.43
Snow melt	101.73	158.40	86.50	159.86	54.87	86.60	58.22	86.60	35.60	70.17	30.79	64.95	61.28	104.43
Sublimation	14.60	22.54	11.71	22.96	8.45	15.23	9.40	15.23	5.69	12.88	3.40	8.14	8.87	16.16
Surface runoff	117.62	169.80	84.24	148.07	51.65	81.94	51.75	81.94	31.26	66.14	35.97	71.27	62.08	103.19
Total water yield	91.48	128.72	65.73	111.85	41.93	64.54	43.42	64.54	25.43	53.89	30.18	57.91	49.70	80.24

Table C. 3. Percentage of changes in simulated hydrologic components for a period of 2070-2099 relative to baseline period (1979-2008) for Vakhsh River Basin.

Vakhsh	GFDL		IPSL_MR		MIROC_ESM		MIROC5		CGCM3		INMCM4		Ensemble	
	RCP 4.5	RCP 8.5	RCP 4.5	RCP 8.5	RCP 4.5	RCP 8.5	RCP 4.5	RCP 8.5	RCP 4.5	RCP 8.5	RCP 4.5	RCP 8.5	RCP 4.5	RCP 8.5
Precipitation	11.70	7.90	-6.54	-15.90	4.94	-5.50	17.44	30.50	25.75	46.99	-1.31	-3.15	8.66	10.14
Snow fall	-13.91	-29.31	-17.69	-35.27	-12.18	-33.81	0.87	2.49	14.44	20.32	-6.80	-16.06	-5.88	-15.27
Snow melt	160.95	225.87	52.18	114.12	38.47	90.92	52.38	97.67	29.00	65.38	21.55	43.21	59.09	106.19
Sublimation	26.85	33.30	10.31	17.79	10.46	18.19	8.83	16.65	7.57	15.37	6.00	11.72	11.67	18.84
Surface runoff	249.47	361.13	72.41	167.17	56.24	137.39	76.39	144.53	39.02	93.96	29.09	60.22	87.10	160.73
Total water yield	166.30	232.85	54.51	115.22	47.71	101.49	61.91	113.01	37.99	85.14	23.28	47.81	65.28	115.92

Table C. 4. Percentage of changes in simulated hydrologic components for a period of 2070-2099 relative to baseline period (1979-2008) for Mendoza River Basin.

Mendoza	CNRM		IPSL_MR		MIROC_ESM		CCSM4		GISS		CGCM3		Ensemble	
	RCP 4.5	RCP 8.5	RCP 4.5	RCP 8.5	RCP 4.5	RCP 8.5	RCP 4.5	RCP 8.5	RCP 4.5	RCP 8.5	RCP 4.5	RCP 8.5	RCP 4.5	RCP 8.5
Precipitation	9.81	2.55	-37.01	-43.06	-40.45	-55.35	12.67	6.57	27.37	39.35	12.70	4.85	-2.48	-7.52
Snow fall	-26.73	-45.11	-58.51	-77.14	-53.52	-73.24	-12.63	-43.89	8.70	-2.06	7.80	-17.37	-22.48	-43.14
Snow melt	41.94	73.95	43.53	92.03	38.76	78.86	33.32	67.96	12.71	33.15	27.68	52.85	32.99	66.47
Sublimation	-0.89	-3.83	-14.41	-17.23	-13.48	-17.83	2.31	-3.69	4.75	6.14	5.11	2.26	-2.77	-5.70
Surface runoff	66.20	121.63	63.11	153.45	54.19	120.66	54.57	115.77	27.47	64.92	45.55	87.86	51.85	110.72
Total water yield	42.05	66.37	26.25	64.28	19.99	48.27	33.19	61.52	22.39	45.79	26.37	46.51	28.37	55.46

Table C. 5. Percentage of changes in simulated hydrologic components for a period of 2070-2099 relative to baseline period (1979-2008) for central Chile River Basins.

Chile	CNRM		IPSL_MR		MIROC_ESM		CCSM4		GISS		CGCM3		Ensemble	
	RCP 4.5	RCP 8.5	RCP 4.5	RCP 8.5	RCP 4.5	RCP 8.5	RCP 4.5	RCP 8.5	RCP 4.5	RCP 8.5	RCP 4.5	RCP 8.5	RCP 4.5	RCP 8.5
Precipitation	-4.25	-8.26	-36.51	-49.30	-33.32	-46.16	-7.02	-21.39	5.27	-6.69	4.75		-11.85	-21.17
Snow fall	-33.54	-50.47	-52.18	-72.63	-43.08	-61.77	-25.31	-50.17	-8.18	-33.01	-2.17		-27.41	-45.04
Snow melt	26.80	45.24	24.41	47.54	24.13	45.52	19.61	39.02	7.99	20.53	15.11		19.68	35.49
Sublimation	3.35	5.24	1.40	3.46	2.55	4.33	3.70	4.87	1.08	2.95	3.29		2.56	4.02
Surface runoff	34.14	59.79	23.52	54.24	23.90	51.43	23.27	47.69	11.70	25.85	19.39		22.65	43.07
Total water yield	26.58	43.64	16.79	35.77	16.14	33.46	18.07	33.73	9.83	20.11	14.73		17.02	30.24

Table C. 6. Percentage of changes in simulated high flow, low flow and mean monthly flow for a period of 2070-2099 relative to baseline period (1979-2008) for Rhone River Basin.

Rhone		CCSM4		GISS		INMCM4		IPSL_LR		GFDL		CSIRO		Ensemble	
Reach#		RCP 4.5	RCP 8.5	RCP 4.5	RCP 8.5	RCP 4.5	RCP 8.5	RCP 4.5	RCP 8.5	RCP 4.5	RCP 8.5	RCP 4.5	RCP 8.5	RCP 4.5	RCP 8.5
2	Q5	26.6	40.8	11.4	22.8	15.6	31.1	-15.5	51.3	41.7	70.3	34.0	63.7	19.0	46.7
	Mean	34.4	58.5	19.3	40.1	15.8	35.3	-19.2	95.2	56.2	97.4	41.4	81.4	24.6	68.0
4	Q5	1.6	-0.4	-4.8	-1.7	-8.9	-7.7	-1.2	0.7	6.7	9.9	-1.7	2.7	-1.4	0.6
	Mean	12.5	17.2	2.5	12.7	-2.3	2.3	18.8	34.2	22.5	28.3	11.5	25.7	10.9	20.1
10	Q5	12.9	14.8	-0.4	-0.2	0.1	4.3	-2.1	24.6	19.6	45.8	13.3	32.5	7.2	20.3
	Mean	26.8	44.6	10.0	26.6	5.8	20.8	32.9	74.7	47.5	80.5	33.2	69.8	26.1	52.8
14	Q5	28.5	45.5	14.3	27.0	17.1	32.2	-4.2	60.1	48.9	80.5	37.5	68.0	23.7	52.2
	Mean	31.6	53.5	17.1	36.8	13.4	31.3	-6.1	86.7	52.8	88.3	38.4	75.4	24.5	62.0
23	Q5	39.3	65.3	16.1	31.5	24.0	47.4	7.3	68.9	64.8	106.7	59.3	96.8	35.2	69.4
	Mean	48.4	86.5	27.3	54.6	25.0	56.8	8.6	128.3	81.1	146.6	66.7	126.8	42.8	99.9
27	Q5	-9.7	-19.4	-12.1	-17.6	-17.7	-23.2	-14.1	-16.8	-10.6	-15.5	-17.6	-19.6	-13.7	-18.7
	Mean	7.5	6.4	-1.0	6.1	-5.9	-5.5	7.9	18.6	13.9	9.6	3.5	10.7	4.3	7.6
144	Q5	13.8	37.7	-0.2	10.3	3.7	16.9	35.2	52.0	40.1	80.1	27.4	62.5	20.0	43.3
	Mean	33.1	60.4	14.6	36.2	10.4	32.2	74.5	101.0	62.2	112.6	46.9	97.6	40.3	73.3
149	Q5	-11.8	-26.0	-15.7	-25.1	-12.1	-27.3	-27.5	-40.3	-20.7	-35.1	-14.6	-25.3	-17.1	-29.8
	Mean	1.7	-0.7	-3.8	-0.5	-8.7	-10.4	20.4	9.4	5.6	0.1	-0.3	4.7	2.5	0.5
101	Q5	17.1	26.4	6.3	14.3	3.6	15.4	6.3	34.2	32.4	52.5	21.4	40.3	14.5	30.5
	Q95	46.7	93.9	22.1	84.3	35.0	57.9	67.1	194.3	86.3	94.8	52.7	117.3	51.6	107.1
	Mean	20.0	32.6	8.1	22.1	3.9	14.1	10.3	57.1	35.5	55.7	24.5	50.3	17.0	38.6

Table C. 7. Percentage of changes in simulated high flow, low flow and mean monthly flow for a period of 2070-2099 relative to baseline period (1979-2008) for Vakhsh River Basin.

Vakhsh		GFDL		CGCM3		INMCM		MIROC5		MIROC_ESM		IPSL_MR		Ensemble	
Reach#		RCP 4.5	RCP 8.5	RCP 4.5	RCP 8.5	RCP 4.5	RCP 8.5	RCP 4.5	RCP 8.5	RCP 4.5	RCP 8.5	RCP 4.5	RCP 8.5	RCP 4.5	RCP 8.5
5	Q5	18.5	16.3	25.0	39.9	-18.2	-19.7	9.2	31.2	-6.8	-18.6	-20.6	-43.2	1.2	1.0
	Mean	27.4	26.7	35.1	64.0	-4.4	-6.1	26.1	37.5	12.2	-6.3	-13.5	-30.3	13.8	14.3
10	Q5	-15.2	-27.4	21.6	38.7	-2.1	-27.1	35.2	22.2	-6.6	-31.5	-21.7	-38.4	1.9	-10.6
	Mean	16.6	8.9	35.0	66.6	-0.4	-4.1	27.3	43.7	11.1	-6.8	-12.5	-24.6	12.8	14.0
14	Q5	83.7	110.5	30.1	49.8	4.5	6.3	45.2	72.3	17.5	30.0	19.1	39.2	33.3	51.3
	Mean	124.0	165.3	39.5	89.2	15.4	31.2	49.8	90.6	39.9	72.8	39.6	82.5	51.4	88.6
1	Q5	181.4	228.0	22.4	63.5	28.9	52.5	39.3	62.6	44.0	96.0	60.7	104.0	62.8	101.1
	Mean	382.6	497.1	144.1	218.9	139.6	185.1	182.1	257.5	182.8	292.4	217.6	343.6	208.1	299.1
113	Q5	257.1	337.5	22.9	59.0	36.1	70.6	64.3	107.8	57.0	133.1	64.3	134.2	83.6	140.4
	Mean	404.0	592.5	47.4	126.1	53.8	110.0	121.9	244.9	96.7	247.8	132.5	307.2	142.7	271.4
134	Q5	-5.7	-24.6	23.0	25.7	-16.6	-29.3	16.3	19.6	-19.0	-31.1	-27.7	-33.2	-5.0	-12.2
	Mean	1.7	-14.9	30.7	59.8	-8.6	-16.6	23.2	32.9	-4.8	-25.1	-21.9	-38.1	3.4	-0.3
133	Q5	130.1	163.6	16.7	34.5	17.6	31.3	30.0	44.6	27.2	54.4	31.3	58.5	42.1	64.5
	Mean	142.9	197.5	30.6	69.6	22.0	45.0	51.9	90.4	42.7	91.1	50.9	103.0	56.8	99.4
109	Q5	165.6	215.0	22.1	47.4	22.7	43.9	42.4	66.8	36.4	80.8	41.4	83.0	55.1	89.5
	Q95	168.4	235.7	38.5	86.3	23.5	48.3	62.7	114.3	48.2	102.6	55.0	116.5	66.1	117.3
	Mean	38.6	54.0	8.8	19.8	5.4	11.1	14.4	26.2	11.1	23.5	12.6	26.7	15.1	26.9

Table C. 8. Percentage of changes in simulated high flow, low flow and mean monthly flow for a period of 2070-2099 relative to baseline period (1979-2008) for Narayani River Basin.

Narayani		GFDL		CGCM3		INMCM		MIROC5		MIROC_ESM		IPSL_MR		Ensemble	
Reach#		RCP 4.5	RCP 8.5	RCP 4.5	RCP 8.5	RCP 4.5	RCP 8.5	RCP 4.5	RCP 8.5	RCP 4.5	RCP 8.5	RCP 4.5	RCP 8.5	RCP 4.5	RCP 8.5
1	Q5	212.1	280.6	21.3	47.6	25.7	53.2	39.2	86.0	43.3	86.0	118.6	214.0	76.7	127.9
	Mean	173.9	280.2	25.6	65.3	34.8	69.1	53.4	118.5	47.5	118.5	118.4	258.3	75.6	151.7
2	Q5	182.4	204.0	18.6	45.0	21.6	49.4	30.8	70.8	38.2	70.8	87.6	135.8	63.2	96.0
	Mean	160.5	227.6	26.8	65.5	36.5	70.6	54.7	112.5	49.9	112.5	104.8	195.7	72.2	130.7

Table C. 8. Continued

Narayani		GFDL		CGCM3		INMCM		MIROC5		MIROC_ESM		IPSL_MR		Ensemble	
Reach#		RCP 4.5	RCP 8.5	RCP 4.5	RCP 8.5	RCP 4.5	RCP 8.5	RCP 4.5	RCP 8.5	RCP 4.5	RCP 8.5	RCP 4.5	RCP 8.5	RCP 4.5	RCP 8.5
1	Q5	212.1	280.6	21.3	47.6	25.7	53.2	39.2	86.0	43.3	86.0	118.6	214.0	76.7	127.9
	Mean	173.9	280.2	25.6	65.3	34.8	69.1	53.4	118.5	47.5	118.5	118.4	258.3	75.6	151.7
2	Q5	182.4	204.0	18.6	45.0	21.6	49.4	30.8	70.8	38.2	70.8	87.6	135.8	63.2	96.0
	Mean	160.5	227.6	26.8	65.5	36.5	70.6	54.7	112.5	49.9	112.5	104.8	195.7	72.2	130.7
105	Q5	63.3	75.7	5.2	17.1	14.8	28.6	8.2	16.6	19.7	16.6	24.2	29.5	22.6	30.7
	Mean	152.4	254.6	40.3	83.6	38.6	80.9	52.9	92.5	58.6	92.5	117.0	242.7	76.6	141.1
107	Q5	54.5	66.6	-9.8	-0.3	4.0	17.1	-3.6	10.0	6.7	10.0	12.9	10.9	10.8	19.1
	Mean	81.5	109.5	17.3	40.4	25.9	49.4	30.4	47.5	32.2	47.5	50.7	73.5	39.7	61.3
133	Q5	87.9	106.1	20.3	35.5	20.9	40.2	23.8	38.6	30.2	38.6	53.6	77.6	39.5	56.1
	Mean	0.7	1.0	0.0	0.2	0.2	0.4	0.1	0.2	0.1	0.2	0.3	0.4	0.2	0.4
159	Q5	90.0	110.6	20.4	39.0	28.1	49.0	25.9	36.0	30.6	36.0	51.4	74.0	41.1	57.4
	Q95	219.7	546.6	116.0	249.0	117.8	243.4	199.8	342.6	233.9	342.6	236.2	502.2	187.2	371.1
	Mean	91.9	129.7	25.5	54.1	30.3	58.2	42.1	64.8	43.6	64.8	66.0	112.3	49.9	80.7

Table C. 9. Percentage of changes in simulated high flow, low flow and mean monthly flow for a period of 2070-2099 relative to baseline period (1979-2008) for Mendoza River Basin.

Mendoza		GISS		CGCM3		CCSM4		MIROC_ESM		CNRM		IPSL_MR		Ensemble	
Reach#		RCP 4.5	RCP 8.5	RCP 4.5	RCP 8.5	RCP 4.5	RCP 8.5	RCP 4.5	RCP 8.5	RCP 4.5	RCP 8.5	RCP 4.5	RCP 8.5	RCP 4.5	RCP 8.5
55	Q5	11.2	31.5	28.8	53.1	33.5	67.4	44.1	79.1	40.8	70.3	47.1	95.6	34.2	66.2
	Mean	18.5	43.0	30.6	61.2	38.6	79.4	42.3	88.0	54.4	92.9	48.8	104.9	38.9	78.2
59	Q5	69.5	90.6	5.7	-5.7	25.8	26.6	-71.5	-77.0	11.8	-5.1	-52.4	-37.1	-1.9	-1.3
	Mean	72.0	115.2	16.7	4.9	38.6	34.8	-62.9	-69.7	20.5	6.1	-49.6	-42.8	5.9	8.1
79	Q5	11.4	28.7	21.3	39.2	28.0	53.1	32.1	54.3	33.9	53.0	37.0	70.3	27.3	49.8
82	Q5	34.7	38.4	40.6	41.8	19.8	40.4	12.5	36.1	31.0	47.8	19.1	53.6	26.3	43.0
	Mean	22.2	36.5	26.8	40.6	24.0	42.1	10.1	32.9	34.9	55.7	13.9	44.1	22.0	42.0
84	Q5	8.1	25.0	22.5	38.5	28.4	53.2	32.4	55.1	30.4	48.8	36.6	75.0	26.4	49.3
	Mean	15.5	37.0	25.9	51.3	34.0	67.4	33.3	68.4	44.6	74.9	38.8	83.1	32.0	63.7
90	Q5	20.2	46.3	29.9	60.4	43.9	90.9	45.3	81.6	55.4	80.7	56.7	115.8	41.9	79.3

Table C. 9. Continued

Mendoza		GISS		CGCM3		CCSM4		MIROC_ESM		CNRM		IPSL_MR		Ensemble	
Reach#		RCP 4.5	RCP 8.5	RCP 4.5	RCP 8.5	RCP 4.5	RCP 8.5	RCP 4.5	RCP 8.5	RCP 4.5	RCP 8.5	RCP 4.5	RCP 8.5	RCP 4.5	RCP 8.5
90	Mean	27.7	64.0	40.3	85.3	56.5	120.3	51.8	116.0	78.5	133.4	66.4	154.9	53.5	112.3
101	Q5	7.8	26.0	28.5	50.7	31.1	59.9	43.9	72.9	34.9	61.6	45.6	87.6	31.9	59.8
	Mean	14.6	43.3	32.4	68.4	44.2	91.9	55.0	106.3	56.1	100.2	60.9	122.2	43.9	88.7
114	Q5	7.0	21.0	19.2	34.4	25.7	47.8	30.4	49.7	28.6	44.8	34.4	67.2	24.2	44.2
	Mean	12.6	31.6	20.9	44.6	30.2	61.3	32.5	63.9	40.4	65.9	38.0	77.6	29.1	57.5
86	Q5	13.7	32.5	20.5	36.0	28.3	54.4	24.3	44.5	31.0	47.5	29.2	65.5	24.5	46.7
	Q95	28.8	56.8	30.0	57.3	43.6	76.3	13.3	38.8	59.4	94.1	22.8	63.0	33.0	64.4
	Mean	22.8	46.6	26.9	47.4	33.9	62.7	20.5	49.4	42.8	67.7	26.7	65.6	28.9	56.6

Table C. 10. Percentage of changes in simulated high flow, low flow and mean monthly flow for a period of 2070-2099 relative to baseline period (1979-2008) for central Chile River Basins.

Chile		GISS		CGCM3		CCSM4		MIROC_ESM		CNRM		IPSL_MR		Ensemble	
Reach#		RCP 4.5	RCP 8.5	RCP 4.5	RCP 8.5	RCP 4.5	RCP 8.5	RCP 4.5	RCP 8.5	RCP 4.5	RCP 8.5	RCP 4.5	RCP 8.5	RCP 4.5	RCP 8.5
2	Q5	55.1	81.1	29.8	29.8	49.1	80.5	7.8	42.2	71.4	95.4	23.6	77.1	39.5	67.7
	Mean	40.3	81.3	58.0	58.0	59.3	97.0	15.9	62.2	75.0	123.1	22.7	85.7	45.2	84.5
7	Q5	6.4	19.1	17.7	17.7	19.7	39.2	27.7	47.4	25.1	41.3	27.7	54.1	20.7	36.5
	Mean	12.4	28.4	19.4	19.4	26.3	52.2	28.0	55.7	37.2	61.2	30.7	63.3	25.6	46.7
20	Q5	6.2	16.5	13.8	13.8	15.6	30.4	24.2	40.6	21.2	36.3	23.1	41.6	17.4	29.9
	Mean	9.9	22.6	14.1	14.1	19.6	38.6	24.5	45.5	26.8	44.1	25.5	47.7	20.1	35.4
22	Q5	8.6	4.8	23.4	23.4	9.6	-0.5	-33.3	-46.0	-3.8	-1.4	-35.0	-37.0	-5.1	-9.4
	Mean	10.6	17.9	4.0	4.0	13.8	28.9	-12.5	-6.0	21.2	35.8	-8.4	2.1	4.8	13.8
68	Q5	4.8	14.2	13.5	13.5	16.0	31.1	24.4	38.4	23.6	38.4	22.2	39.6	17.4	29.2
	Mean	8.2	20.0	13.4	13.4	19.1	36.9	21.9	39.1	28.2	44.0	23.8	41.7	19.1	32.5
70	Q5	5.8	15.4	13.0	13.0	16.7	32.6	23.6	38.8	24.6	39.6	22.1	41.6	17.6	30.2
	Mean	8.0	18.8	12.6	12.6	17.9	34.9	19.2	37.0	26.9	43.8	21.1	39.2	17.6	31.1
108	Q5	5.4	-9.7	9.0	9.0	-7.5	-13.8	-15.0	-19.0	-2.6	-6.7	-18.9	-43.4	-4.9	-13.9
	Mean	4.3	-18.6	12.1	12.1	-14.7	-30.7	-36.5	-44.5	-12.5	-18.3	-40.7	-57.5	-14.7	-26.2
109	Q5	4.6	20.0	20.0	20.0	22.2	40.9	31.1	49.9	27.1	47.5	27.7	53.1	22.1	38.6
	Mean	11.9	29.6	19.4	19.4	26.5	52.3	31.4	59.7	38.5	65.8	32.4	62.6	26.7	48.2

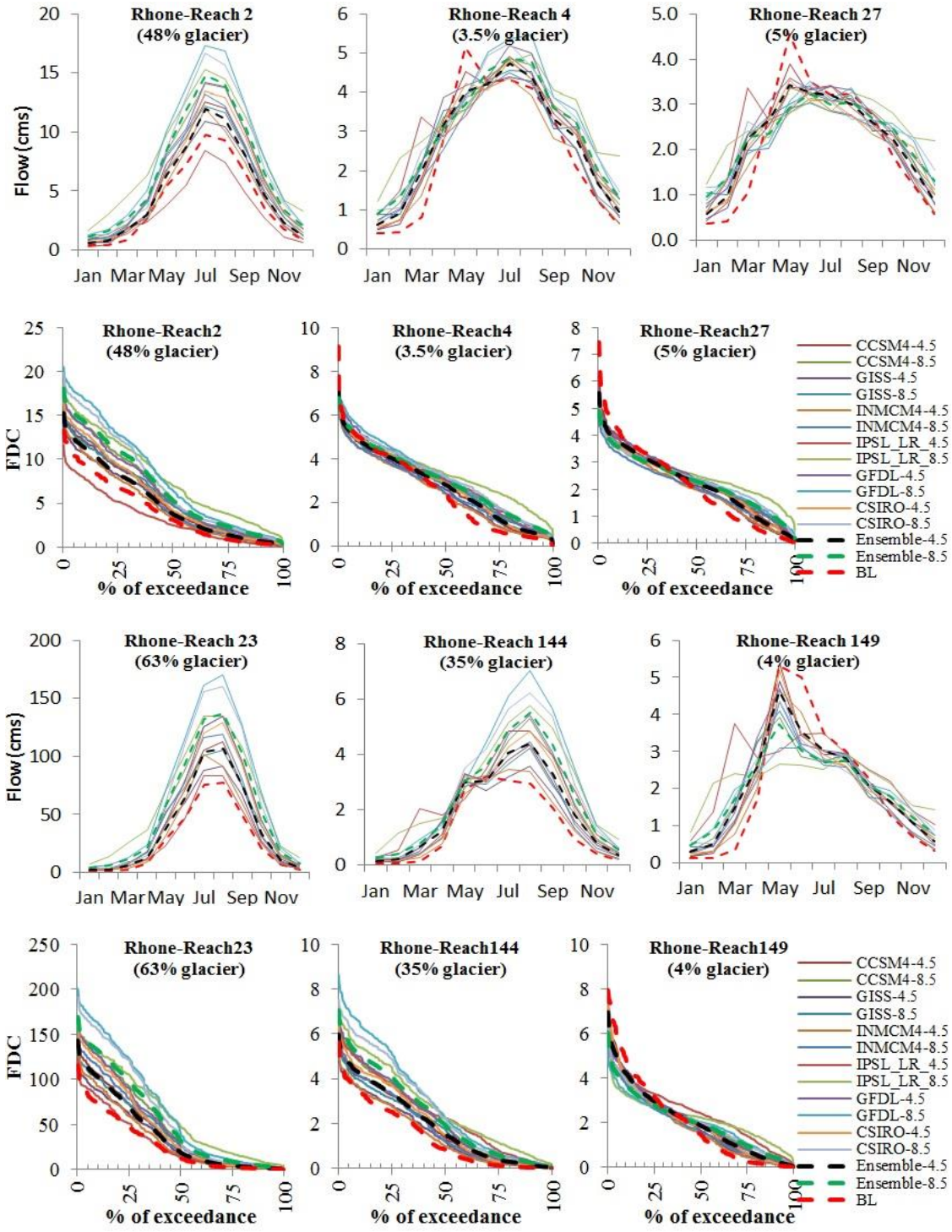

Figure C. 1. Projected monthly runoff and CDF for the watersheds across the Rhone River Basin with different percentage of glacierized area for the baseline (red line), GCMs ensemble RCP4.5 (black line), RCP8.5 (green line) and GCMs.

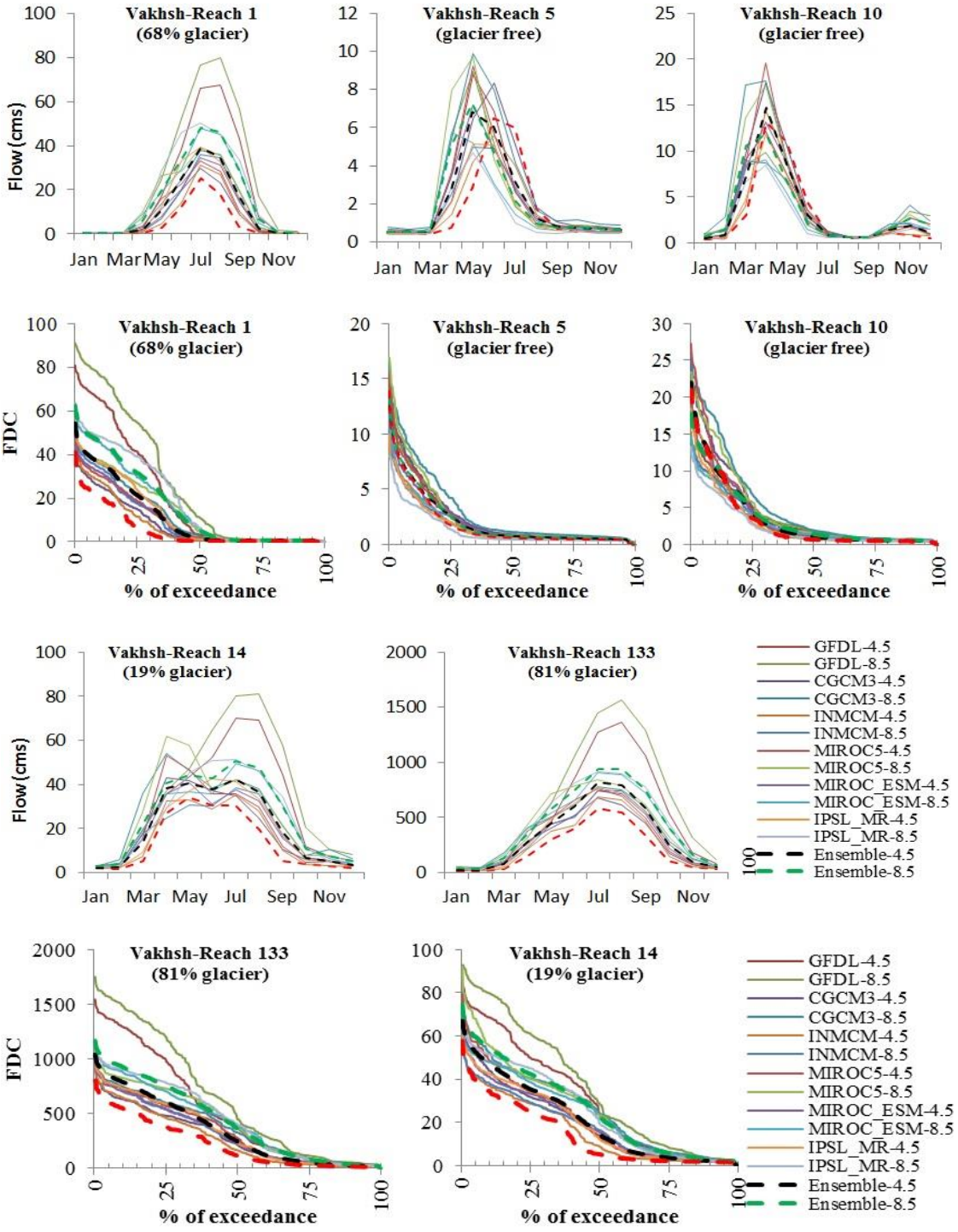

Figure C. 2. Projected monthly runoff and CDF for the watersheds across the Vakhsh River Basin with different percentage of glaciered area for the baseline (red line), GCMs ensemble RCP4.5 (black line), RCP8.5 (green line) and GCMs.

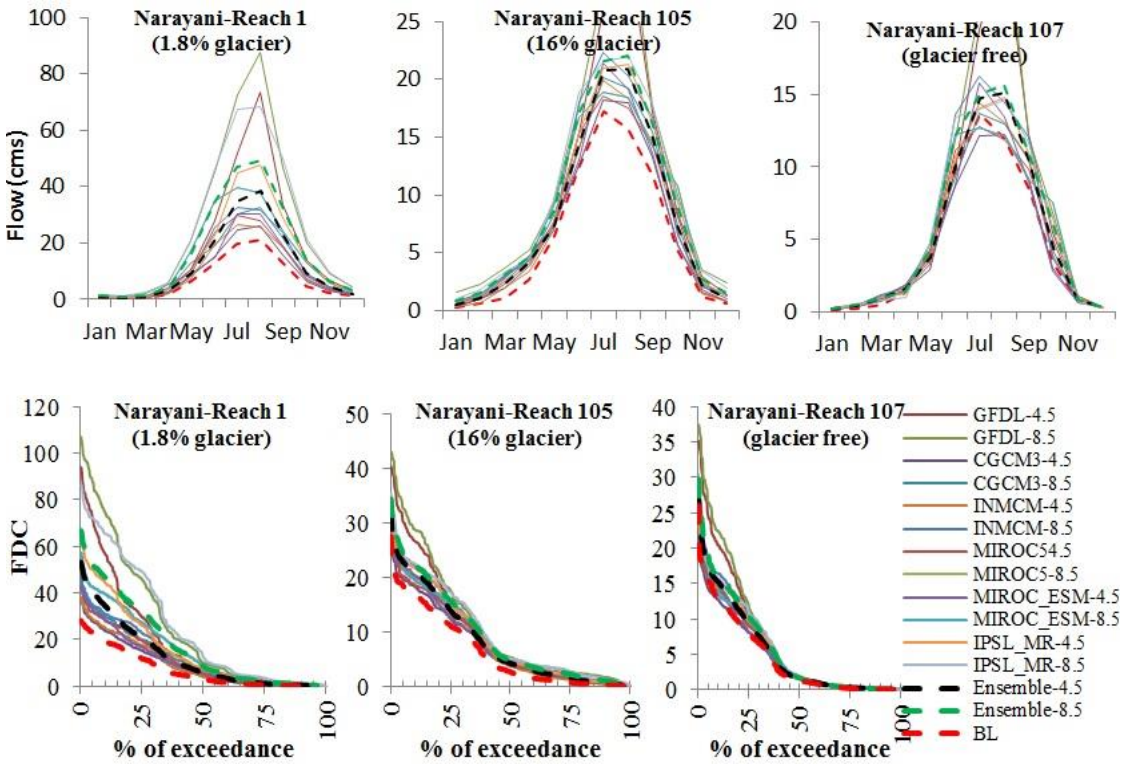

Figure C. 3. Projected monthly runoff and CDF for the watersheds across the Narayani River Basin with different percentage of glaciered area for the baseline (red line), GCMs ensemble RCP4.5 (black line), RCP8.5 (green line) and GCMs.

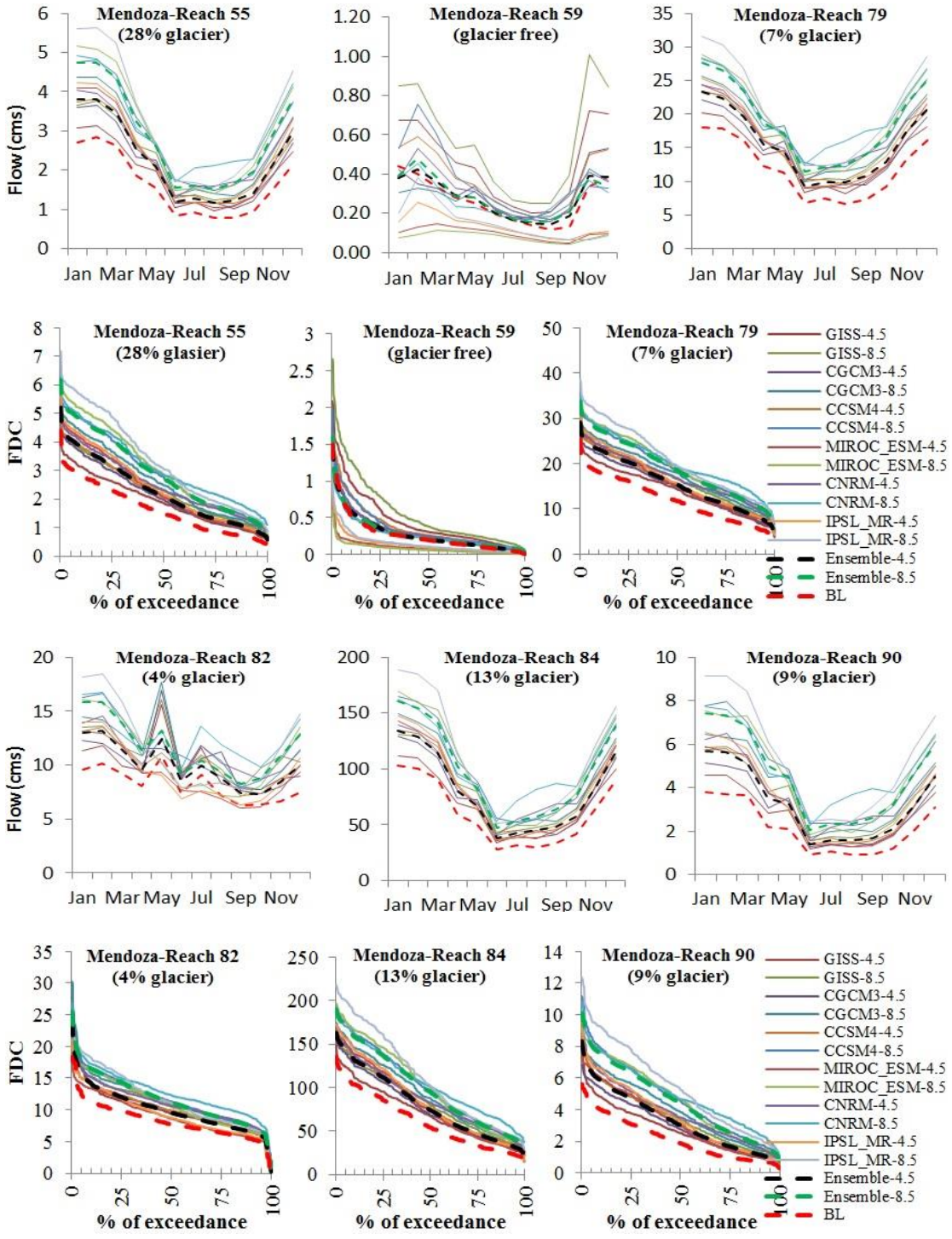

Figure C. 4. Projected monthly runoff and CDF for the watersheds across the Mendoza River Basin with different percentage of glaciered area for the baseline (red line), GCMs ensemble RCP4.5 (black line), RCP8.5 (green line) and GCMs.

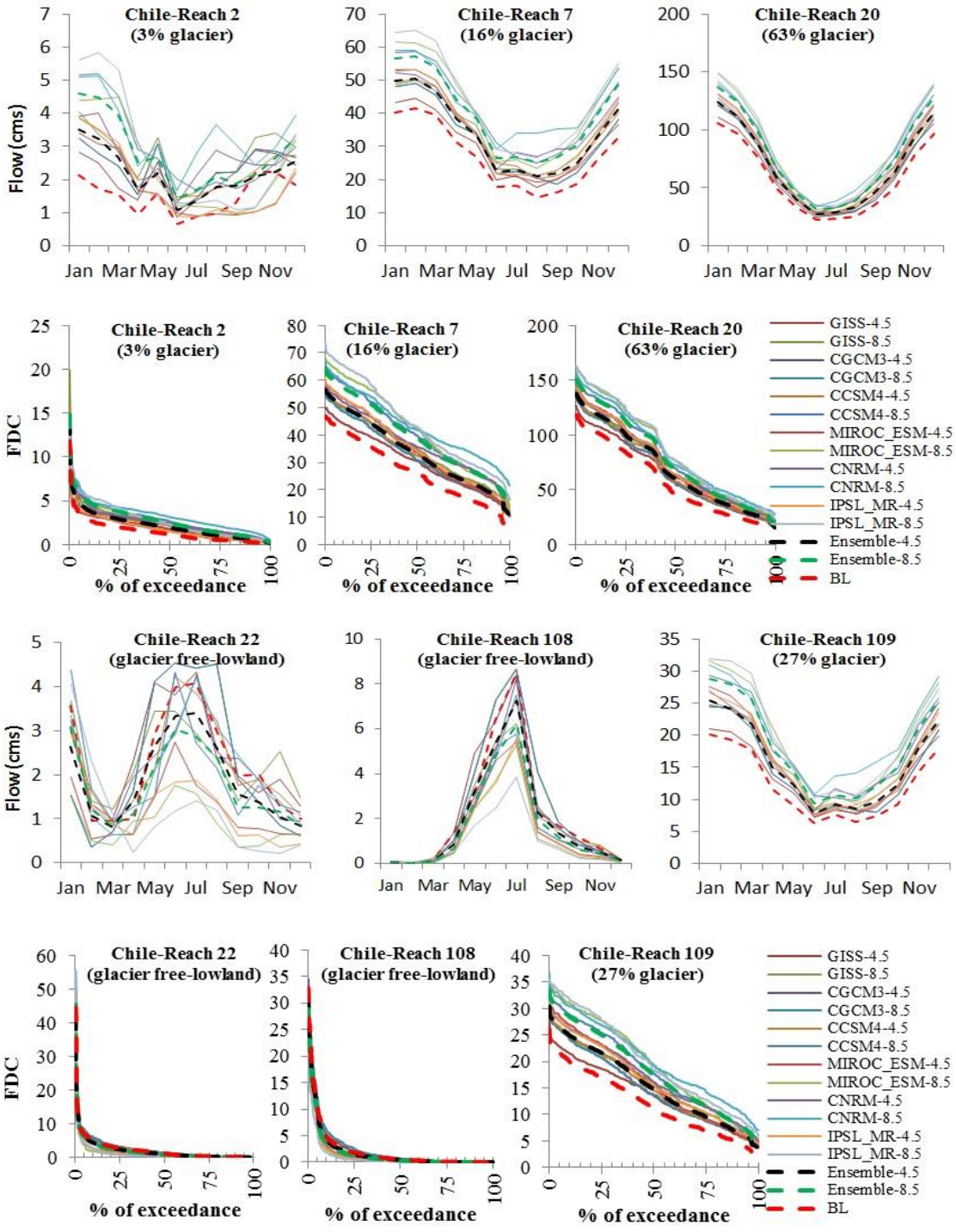

Figure C. 5. Projected monthly runoff and CDF for the watersheds across the Dry Andes at Central Chile with different percentage of glaciered area for the baseline (red line), GCMs ensemble RCP4.5 (black line), RCP8.5 (green line) and GCMs.